SILVER ION AND/OR GRAPHENE OXIDE INCORPORATED ELECTROSPUN MATRICES FOR GUIDED NEURITE EXTENSION

PRIMA S.

PHD. THESIS

2024

SREE CHITRA TIRUNAL INSTITUTE FOR MEDICAL SCIENCES AND TECHNOLOGY, THIRUVANANTHAPURAM

An Institution of National Importance established by an Act of the Indian Parliament (Act No.52 of 1980)

Dept. of Science and Technology, Govt. of India

www.sctimst.ac.in

SILVER ION AND/OR GRAPHENE OXIDE INCORPORATED ELECTROSPUN MATRICES FOR GUIDED NEURITE EXTENSION

A THESIS SUBMITTED BY

PRIMA S.

To

SREE CHITRA TIRUNAL INSTITUTE FOR MEDICAL SCIENCES AND TECHNOLOGY, THIRUVANANTHAPURAM

IN PARTIAL FULFILMENT OF THE REQUIREMENTS

FOR THE AWARD OF

DOCTOR OF PHILOSOPHY

2024

DECLARATION

I, Prima S., hereby certify that I had personally carried out the work depicted in the thesis titled, "SILVER ION AND/OR GRAPHENE OXIDE INCORPORATED ELECTROSPUN MATRICES FOR GUIDED NEURITE EXTENSION" under the direct supervision of Dr. P. Ramesh, Scientist, Division Polymeric Medical Devices, Biomedical Technology Wing, Sree Chitra Tirunal Institute for Medical Sciences and Technology, Thiruvananthapuram, Kerala, India. No part of this thesis has been submitted for the award of any other degree or diploma prior to this date.

Prima S.

Date: 29/08/2024

श्री चित्रा तिरुनाल आयुर्विज्ञान एवं प्रौद्योगिकी संस्थान, त्रिवेंद्रम, जैवचिकित्सकीय प्रौद्योगिकी स्कंध
पूजप्पुरा, तिरुवनन्तपुरम- 695012, केरल ,भारत
SREE CHITRA TIRUNAL INSTITUTE FOR MEDICAL SCIENCES AND TECHNOLOGY, TRIVANDRUM
BIO MEDICAL TECHNOLOGY WING
POOJAPPURA, THIRUVANANTHAPURAM – 695 012, KERALA, INDIA
(एक राष्ट्रीय महत्व का संस्थान, विज्ञान एवं प्रौद्योगिकी विभाग, भारत सरकार)
(An Institution of National Importance, Department of Science and Technology, Government of India)
टेलीफॉन नं./Telephone No.: 0471- 2340801/ 2520450, फैक्स/Fax: -0471-2341814
ई-मेल / E-mail: sct@sctimst.ac.in वेबसाइट / Website: www.sctimst.ac.in

Dr. Ramesh P.
Scientist G (Senior Grade)
Division of Polymeric Medical Devices
Email: rameshp@sctimst.ac.in

CERTIFICATE BY THE RESEARCH GUIDE

This is to certify that Ms. Prima S., Division of Polymeric Medical Devices of this institute has fulfilled the requirements prescribed for the Ph.D. degree of the Sree Chitra Tirunal Institute for Medical Sciences and Technology, Thiruvananthapuram.

The thesis entitled; "Silver Ion and/or Graphene Oxide Incorporated Electrospun Matrices for Guided Neurite Extension" was carried out under my direct supervision. No part of the thesis was submitted for the award of any degree or diploma prior to this date.

Ramesh P.

Date: 29/8/2024

APPROVAL OF THE THESIS

The thesis entitled

Silver Ion and/or Graphene Oxide Incorporated Electrospun Matrices for Guided Neurite Extension

Submitted by

Prima S.

for the degree of

Doctor of Philosophy

of

SREE CHITRA TIRUNAL INSTITUTE FOR MEDICAL SCIENCES AND TECHNOLOGY, THIRUVANANTHAPURAM

is evaluated and approved by

…… ……

Dr. P. Ramesh

(Name and signature of the guide) (Name and signature of examiner)

Dedicated to

GOD ALMIGHTY AND MY FAMILY

TABLE OF CONTENTS

Contents

ACKNOWLEDGEMENT

A thesis, even though submitted by a single person is a collective effort of several individuals. So, here I consider this part of my thesis to acknowledge the support and help I received from the individuals throughout this journey to complete my task and to submit the thesis.

First and foremost, I express my sincere gratitude and respect to my Guide Dr. P. Ramesh, Scientist G, Division of Polymeric Medical Devices, SCTIMST for his continuous advice and encouragement throughout my study. It would have been difficult to complete this endeavour without his timely appropriate suggestions for work and life.

I would take this opportunity to thank CSIR, India for the financial assistance that helped me to complete this research work.

I express my gratitude to the Head of, the BMT wing and the Director of SCTIMST for providing the facilities for the research works. I would like to thank the Dean, Registrar, Deputy Registrar, and all the staff of the academic section for their help.

I thank all my Doctoral Advisory Committee members, Dr. P. R. Anilkumar (co-guide), Dr. Roy Joseph, Dr. A. Maya Nandkumar, and Dr. Anugya Bhatt for their timely suggestions.

I sincerely thank Dr. Renjith, Mr. Willi Paul, Ms. Nimi, Dr. Sasikala, and Dr. Radhakumari of Central Analytical Facility (BMT Wing, SCTIMST) for providing facilities such as FTIR, and Raman analysis. I take this opportunity to thank Dr. Manoj Komath, Dr. Nishad, Dr. Remya, and Mr. Suresh of the Division of Bioceramics for the SEM, ICP-OES, and XRD analysis of my samples. I would like to acknowledge Dr. Anil Kumar P.R, Dr. Naresh Kasoju, Mr. Vinodkumar and students of Division of Tissue Culture for providing fluorescent imaging facilities.

I am thankful to Dr. Rekha M. R. and the students of Division of Biosurface Technology for providing me with the facility for sonication. I am grateful to Dr. P. V. Mohanan and Dr. Megha of the Division of Toxicology for providing the C6 cell lines whenever requested.

I also acknowledge Dr. Prabha D. Nair, Dr. Lynda V. Thomas, and students of the Division of Tissue Engineering and Regenerative Technology for providing the facility for cell cryopreservation.

I express my sincere gratitude which is difficult to express in words to my team of Division of Polymeric Medical Devices, Dr. Gijo Raj, Ms. Jasmin Joseph, and Dr. Chandrasekhar for their sincere support during my tenure. I express my gratefulness to my fellow lab mates, Dr. Resmi R., Dr. Parvathy, Dr. Medha Surendranath, Ms. Athira M, Ms. Athira K. R., Ms. Swetha P. V., Ms. Sarah., Ms. Theerdha, Ms. Prathyusha, Mr. Saravana Perumal, Mr. Ansar, Mr. Nikhil Prasad, Ms. Sruthi S, Mr. Rahul R. K., Ms. Sithara, Ms. Aleesha, Ms. Reshmi, Dr. Gopika V Gopan, Dr. Dhanya C. S, Ms. Gopika Ramesh, Dr. Anand, and Ms. Arya for encouraging me in my works and keeping a pleasant lab atmosphere.

I would like to extend my thanks to the Central Laboratory for Instrumentation and Facilitation (CLIF), Kerala University for carrying out the XPS analysis of my samples. I also thank Dr. Jackson James and Dr. Riya (Neuro stem cell biology lab, RGCB, TVM) for providing N2a and PC12 cell lines whenever requested.

I would like to give special gratitude to Mr. Prasannakumar D. and Ms. Sumam K. (parents), Mr. Priyadarsan P. (Brother), and Mr. Praveen C. (Husband) for their faith in me and my goals and immense support given to me in my weakest and strongest life events. I also express gratitude soaked with motherly love for my son (Master Sathwik Praveen) for his interesting nature which gave me some relief during this tough journey. I also thank all my friends, mentors, and well-wishers (inside and outside the campus) for their support.

I bow before the **GOD,** the supreme power, whom I felt throughout the easy and difficult events and the one who strengthened my consciousness by providing me the strength, courage, and health to complete the task.

Prima S.

LIST OF FIGURES

LIST OF TABLES

LIST OF ABBREVIATIONS

$AgNO_3$	Silver nitrate
AgNP	Silver nanoparticle
AO	Acridine orange
ATR	Attenuated Total Reflectance
BSA	Bovine serum albumin
CNS	Central nervous system
DAPI	4`, 6-diamidino-2-phenylindole
DMEM	Dulbecco Modified Eagles Medium
DRG	Dorsal root ganglion
ECM	Extracellular matrix
EDX	Energy dispersive X-ray
ePTFE	Polytetrafluoroethylene
EtBr	Ethidium bromide
EVAL or EVOH	Ethylene vinyl alcohol copolymer or poly(ethylene-co-vinyl alcohol)
FA	Focal adhesion
FBS	Fetal bovine serum
FDA	Food and Drug Administration
FDA	Fluorescein diacetate
FTIR	Fourier Transform Infrared
GelMA	Gelatin methacrylyol
GO	Graphene oxide
IC50	Half-maximum inhibitory concentration
ICP-OES	Optical Emission Spectroscopy with Inductive Coupled Plasma
IPA	Isopropyl alcohol (isopropanol or 2-propanol
MTT	3-[4,5-dimethylthiazol-2-yl]-2,5 diphenyl tetrazolium bromide
N2a	Neuro2a

NGC	Nerve guidance conduit
NGF	Nerve growth factor
NS	Nervous system
NW	Nerve wrap
PBS	Phosphate buffer saline
PC12	Pheochromocytoma cell12
PCL	Polycaprolactone
PDMS	Polydimethylsiloxanes
PFA	Paraformaldehyde
PGA	Polyglycolic acid
PI	Propidium iodide
PLCL	Poly DL-lactide-co-caprolactone
PLGA	Poly(lactic-co-glycolic acid)
PLLA	Poly(L-lactic acid)
PMMA	Polymethyl methacrylate
PNI	Peripheral nerve injury
PNS	Peripheral nervous system
PPy	Polypyrrole
PVA	Polyvinyl alcohol
PVC	Polyvinyl chloride
PVDF	Polyvinylidene fluoride
RPMI	Roswell Park Memorial Institute
SEM	Scanning Electron Microscopy
SC	Schwann cells
TCP	Tissue culture plate
UHMWPE	Ultra-high molecular weight polyethylene
UTM	Universal Testing Machine
XPS	X-ray Photon Spectroscopy
XRD	X-ray Diffraction

SYNOPSIS

The peripheral nervous system (PNS), unlike the central nervous system, is not protected in bony cases. This exposes the PNS to traumatic conditions that occur due to crutch-palsy, compressions, fractures, joint dislocations, self-inflicting injuries, gunshots, etc. The spontaneous regenerative capacity of PNS after injuries is a relief. However, the regenerative success is determined by the severity of the injury. The severity of the injury depends on whether the axon alone or the connective tissues are involved in the injury. According to the severity of the injury, the peripheral nerve injury (PNI) was classified by Seddon (1943) and Sunderland (1951) as neuropraxia (axonal conduction block), axonotmesis (axon or myelin sheath severed), neurotmesis (epineurium or perineurium or endoneurium severed). Successful regeneration of neurons, functional restoration of the nerve, and reinnervation of the target tissue spontaneously occur only if the injury is neuropraxia and axonotmesis. If a nerve undergoes neurotmesis (grade III, IV, V, or VI), it is difficult for a successful regeneration due to the loss of intactness of the connective tissues. Proper guidance is lost when the connective tissue intactness is poor. It will mislead the proximal stump axonal sprouts from reaching the distal stump. This delays nerve regeneration and can cause neuroma formation and reinnervation of the target tissue and its normal functioning.

Besides surgical reconnection and nerve autografting (gold standard), surgeons need synthetic origin nerve repair scaffolds that could successfully replace the autograft. Such nerve repair scaffolds are known as nerve guidance conduits or nerve wraps (NGC/NWs). Using an accurate NGC/NWs to bridge the proximal and distal stumps

of an injured nerve could avoid donor-site morbidity that occur at the autograft donor site. The ongoing research on NGC/NWs is to construct them with some surface features that promote or enhance nerve regeneration. One such surface feature is structures that provide guidance cues to the proximal axonal sprouts to reach the distal stump. This enables the neuron to extend via contact guidance. The substrates with aligned fibers, grooves, ridges, channels, etc. are mostly fabricated to provide discernible indicators that guide the neurites to reach the targets. Among these, the aligned fibrous scaffolds are outstanding because of their resemblance with the extracellular matrix (ECM). The aligned fibers can act as one of the best physical guidance cues for a regenerating axon. Besides guiding an axon, the fiber alignment is also essential for the de-differentiated Schwann cells at the injury site to align and migrate to form Bungner's band and support the regenerating axon. Cellular alignment and migration occur due to cytoskeletal polarisation induced by the interaction and adhesion of these cells to the aligned fibers. The integrin protein bound to the fiber surface activates the focal adhesion kinase (FAK) pathway and Rho GTPase family proteins and causes cytoskeletal reorganization and migration.

The construction of an aligned fibrous scaffold becomes an easy task by employing electrospinning as the fabrication technique. Electrospinning is a versatile technique used for fabricating fibroporous matrices (membranes/mats) by collecting fibers ejected from a charged polymer solution on a charged collector. The matrices obtained have a high surface area-to-volume ratio, nano-to-micro-sized fibers, and pores. The manipulation of electrospinning parameters enables the fabrication of random or aligned fibers according to the need.

Ethylene vinyl alcohol copolymer or poly(ethylene-co-vinyl alcohol) abbreviated as EVAL or EVOH is a semicrystalline polymer with randomly arranged ethylene and vinyl alcohol units. EVAL is synthesized by hydrolyzing poly(ethylene-co-vinyl acetate). The vinyl alcohol units make EVAL slightly hydrophilic and ethylene units prevent it from dissolving in water. Studies have shown that substrates suitable for neuronal cultures can be developed from EVAL. The easiness in spinnability of EVAL makes it a considerable polymer for electrospinning.

The increase in conductivity of the polymer solution induces fiber alignment by reducing the jet whipping and thus stabilizes the jet. Conductivity increases by the incorporation of inorganic salts into the polymer solution. Uniaxially aligned yarns were generated from EVAL in the study of Mayuri et al. by incorporating $AgNO_3$ in the polymer solution. It is known from the study of Alon et al. that silver-sputtered and silver nanoparticle-coated substrates induce a large number of neurites from the soma.

Graphene oxide (GO), a hydrophilic, non-conductive graphene derivative is widely used as a bioactive nanomaterial. The presence of GO in scaffolds initiates cell adhesion, growth, proliferation, migration, etc. in neuronal and non-neuronal cells. Schwann cell functions are enhanced when interacting with GO. GO is a filler material that improves the mechanical properties of polymer scaffolds.

- The above-mentioned knowledge led to a hypothesis,

  “Would electrospun matrices with aligned fibers fabricated from Ethylene vinyl alcohol copolymer be a suitable substrate for neuronal alignment?”

- The following objectives were postulated to test the hypothesis:

1. To fabricate electrospun matrices incorporated with silver ions and/or graphene oxide.
2. To evaluate the physico-chemical properties of the matrices.
3. To evaluate the cell-material interactions *in vitro*.
    - Evaluation of cytotoxic effects of the matrices *in vitro.*
    - Evaluation of guided neurite extension based on cell and neurite response on fibers of the matrices.

The study was designed to prepare three different systems and their evaluation. Each system contained EVAL as the polymer matrix and these matrices were also incorporated with either silver ions or GO or both. The systems are (1) EVAL incorporated with GO (EVAL-GO), (2) EVAL incorporated with Ag^+ (EVAL-Ag), and (3) EVAL incorporated with Ag^+ and GO (EVAL-Ag-GO). Electrospinning was the fabrication technique used to construct the matrices in all these systems. Several compositions were tried for these systems as part of optimization. Physico-chemical characterizations were done to study the material properties of the fabricated matrices. Cytotoxic evaluations were done with L-929 fibroblast cells to sort out the nontoxic matrices. Cellular and neurite responses on these matrices were evaluated via *in vitro* cell-material interaction studies with Neuro2a (N2a), C6 glioma, and PC12 cells.

The entire study is presented in 5 chapters. Chapter 1 introduces the peripheral nervous system (PNS), peripheral nerve injuries (PNIs), and treatment methods. It also details the relevance of a nerve repair scaffold in treatment and electrospinning as a fabrication technique to construct the scaffold. The introduction also elaborates on the importance of anisotropic substrates such as aligned fibers in neurite extension and

nerve regeneration. This chapter also deals with the electrospinning of ethylene vinyl alcohol copolymer (EVAL).

Chapter 2 deals with a vast literature review on the peripheral nervous system (PNS), peripheral nerve injuries (PNIs) and their classification, treating approaches to PNIs, nerve guidance conduits (NGC) or nerve wraps (NW) and their evolution, techniques in the fabrication of nerve repair scaffolds, the importance of anisotropic substrates in nerve repair, fabrication of anisotropic substrates (aligned fibers) via electrospinning, polymers used in the construction of NGC/NWs, influence of EVAL, Ag^{+}, and GO in fabricating electrospun fibroporous substrates and in cellular and neurite responses on these matrices, and cells used in the neurite extension studies.

Chapter 3 includes the materials used in the study and the methods executed for achieving the objectives. Chapter 3 is divided into different sections. All the materials used in the study are included in section 3.1. Section 3.2 included the methods of the study. The synthesis of GO is described in section 3.2.1. The physico-chemical characterizations are done after GO synthesis and are detailed in section 3.2.2. It includes Raman spectroscopy, Fourier transform infrared spectroscopy (FTIR), and X-ray diffraction (XRD) analysis done to confirm the oxidation of graphite to form GO. The physico-chemical characterizations carried out are as follows. UV-Visible spectroscopy analysis, and X-ray photon spectroscopy (XPS) analysis for evaluating the oxidation state of silver and its complexation with -OH of EVAL. A viscosity analysis of the solutions was done. Solution conductivity was analyzed to assess the influence of silver and GO in the solution. Fourier transform infrared (FTIR) spectroscopy was done to analyze the functional groups. Raman spectroscopy was

used to analyze the presence of GO in the matrices. Energy dispersive X-ray spectroscopy (EDX) was done to find the presence of silver in the matrix. Scanning electron microscopy (SEM) was used to analyze the morphology and arrangement of the fibers in the matrices. The Universal testing machine (UTM) was used for mechanical testing to evaluate the tensile properties of the matrices. Optical Emission Spectroscopy with Inductive Coupled Plasma (ICP-OES) was used for analyzing the silver content in the matrices and the extracts. The cytotoxic evaluations and cell-material interactions included in section 3.2.3 are direct contact test and MTT assay for evaluating the viability of L-929 fibroblast cells upon interacting with the EVAL systems. Live/dead assay was carried out to assess the viability of N2a and C6 cells after interacting with the EVAL systems. The F-actin staining and immunostaining of cells were done to evaluate the cellular and neurite response on the fibers of the matrices. The spatial response of PC12 cells on EVAL-Ag and EVAL-Ag-GO matrices in the presence of nerve growth factor (NGF) was also studied.

Chapter 4 presents the results and elaborately discusses the findings. EVAL-neat is the bare material in the study. EVAL-neat has neither Ag^{+} nor GO in the solution or matrix. The incorporation of GO in EVAL led to the formation of EVAL-GO matrices. The presence of GO in these matrices was evident from Raman spectra and imaging. The random fiber orientation of EVAL-GO matrices was evident from SEM images and fiber orientation analysis with ImageJ software. The influence of GO in the system was figured out from FTIR analysis. The significant reduction in fiber diameter of EVAL-GO matrices was evaluated with ImageJ software using the SEM images. The decrease in fiber diameter also increased the mechanical properties of EVAL-GO matrices. However, the random arrangement of the fibers in EVAL-GO matrices gives

it less preference for constructing nerve repair scaffolds (NGC/NWs). In contrast to EVAL-GO, the EVAL-Ag and EVAL-Ag-GO systems had aligned fibers. The involvement of Ag^{+} in the EVAL led to an increase in the conductivity of the solution. The conductivity of the polymer solution reduces the jet whipping and produces aligned fibers. The fiber alignment was evident from the SEM images and the ImageJ software-assisted fiber orientation analysis also confirmed the fiber alignment. The fiber diameter of EVAL-Ag and EVAL-Ag-GO significantly increased than EVAL-neat. The presence of silver was evident in the EDX analysis of the EVAL-Ag matrix. The UV-Vis and XPS spectral analysis results of EVAL-Ag and EVAL-Ag-GO systems indicated that the silver is not reduced to Ag^{0} and no nanoparticles are formed. The silver was in an Ag^{+} state in the matrices. The increase in D band and G band intensities in EVAL-Ag-GO matrices confirmed the incorporation of GO. The GO also contributed to the peak shifts of -OH around 3300 cm^{-1} in EVAL. EVAL-Ag and EVAL-Ag-GO matrices also showed improved mechanical properties. The fiber alignment and fiber diameter influenced the cells and neurites to align on these fibers. The effect of fiber alignment of EVAL-Ag and EVAL-Ag-GO matrices in cells was presented via F-actin staining and immunostaining of cells. Fluorescence images of C6, N2a, and PC12 cells adhered to the aligned fibers showing that they extend their filopodia/neurites in an aligned manner. The fiber alignment, fiber diameter, better mechanical properties, and biocompatibility of EVAL-Ag and EVAL-Ag-GO matrices make them considerable for constructing NGC/NWs.

Chapter 5 summarises the results of the study. The study suggests that the EVAL-Ag and EVAL-Ag-GO matrices with aligned fibers are suitable for constructing NGC/NWs.

The extended future work plan of the study is proposed. Citations are listed in the bibliographic section.

CHAPTER 1: INTRODUCTION

Peripheral nerve injuries (PNIs) are now common traumatic conditions that occur due to nerve compression, crutch palsy, gunshot, self-inflicting injuries, surgical procedures, etc. The peripheral nervous system (PNS) is more prone to injuries since they are not enclosed in a bony structure like the central nervous system (brain and spinal cord). The central nervous system (CNS) is not easily injured because the brain and spinal cord are protected by the skull and vertebral column respectively.

Seddon (1943) and Sunderland (1951) have classified the PNIs according to the severity of the injury. The PNIs are classified into neuropraxia, axonotmesis, and neurotmesis based on injured tissues. Neuropraxia is the conduction block in the axons, axonotmesis is the condition where the axon is cut and neurotmesis occurs due to the cut occurred in the connective tissues (epineurium, perineurium, and endoneurium). However, the PNS can regenerate its own in a post-injury situation. This ability is lacking in CNS. The glial cells in the CNS decelerate the recovery by forming scar tissues. In PNS the Schwann cells (SC) (glial cells) accelerate the recovery. Soon after an injury in PNS, the myelin sheath around the injured axon dedifferentiates into Schwann cells and proliferates. These dedifferentiated Schwann cells participate in "Wallerian degeneration" to remove all the axonal debris formed in the distal axonal stump. Then they form "Bands of Bungner" that secrete nerve growth factors and basal lamina to attract proximal axonal sprouts and guide them to the distal stump. These events occur spontaneously for recovery. However, it occurs only if the connective tissue surrounding an axon is intact. If the connective tissues are also severed (neurotmesis), the proximal axonal sprouts will be misled, and regeneration delays

eventually lead to neuroma formation. As a result of neuroma formation, the reinnervation of the target tissue does not occur and it faces functional impairment.

In neurotmesis, recovery is possible only via surgical intervention. The treatment approach can be (1) surgical reconnection for gaps < 5 mm or sometimes < 3 cm, (2) placing an autograft (gold standard) to bridge the proximal and distal stumps if the gap is up to ~ 5cm, (3) connecting the proximal and distal stumps using a nerve guidance conduit or nerve wrap (NGC/NWs). NGC/NWs are nerve repair scaffolds constructed using various fabrication techniques to replace the autograft treatment method. Using an NGC/NWs could prevent donor site morbidity resulting from the surgery done to get a donor nerve in autograft treatment. Other shortcomings of gold standard treatment are limitations in tissue availability and mismatch between donor and acceptor nerve regarding their shape and size.

Developing nerve repair scaffolds (NGC/NWs) that could replace an autograft could avoid donor site morbidity. Research has been focused on constructing either biological or synthetic NGC/NWs. Several features can be included in the construction of NGC/NWs to make it similar to an autograft. Incorporating the NGC/NWs with cells that support regeneration, features that provide topographical cues (physical guidance cues) for the proximal axonal sprouts, intra-luminal channels, nerve growth factors (NGCs), electrical conductivity, and more. Among the features mentioned previously, topographical cues on the constructs can act similarly to the environment provided by the basal lamina laid by the Schwann cells during spontaneous regeneration. The topographical cues on the substrates can guide or orient the proximal axonal sprouts to reach the destination.

Anisotropic substrates offer better guidance in the form of topographical cues which provide physical guidance to an extending neurite. The neurites consider the topographical guidance cues through physical contact and navigate on the fibers to reach the destination. The process by which a neurite is guided according to a topographical cue through physical contact is known as contact guidance. Parallelly arranged grooves, ridges, and aligned fibers are continuous topographic cues that guide neurites. Substrates with aligned fibers can resemble the basal lamina produced by Schwann cells in the regeneration scenario. The aligned topography of a fibrous substrate enables an adhering cell on the fibers to extend its neurites in an aligned manner through contact guidance.

Fabrication of aligned fibers is achieved easily via the electrospinning technique. Electrospinning is a versatile technique used to fabricate fibroporous membranes by ejecting a polymer solution from a syringe with a conductive needle and collecting them as a polymer fiber on a conductive collector. Nano to micro-sized fibers with a high surface area-to-volume ratio can be generated via electrospinning. Random and aligned fibers are generated through electrospinning according to the parameters used. Collection of fibers using parallel electrodes, rotating wire drum, wire wounded drum collector, disc collector, mandrels rotating at very high velocity, etc. helps to generate aligned fibers. These methods have limitations such as less fiber yield during collection, difficulty in obtaining continuous fibers, and usage of extra accessories while spinning for making fiber alignment. All these make the process more challenging.

Increasing the polymer solution conductivity helps to generate aligned fibers with a high fiber yield and continuity on a rotating collector. Here fiber alignment is possible even at lower collector rotating velocities. The high solution conductivity reduces the whipping motion of the ejected fibers and results in the collection of aligned fibers on a rotating collector. As the solution conductivity increases the repulsion of surface charges on the fibers also increases. The fibers are stabilized by stretching them in a straight path. This leads to the collection of aligned fibers.

Aligned fibrous matrices fabricated from electrospinning through simple approaches would help to construct nerve repair scaffolds (NGC/NWs) easily. Besides the topography provided by the aligned fibers, the scaffold fabricated must be non-cytotoxic, biocompatible, and provide a micro-environment for proper cell-material interactions regarding cellular and neurite alignment.

Three materials were mainly considered in the present study. They are:

(1) Ethylene vinyl alcohol copolymer or poly(ethylene-co-vinyl alcohol) (EVAL or EVOH)
(2) Silver nitrate ($AgNO_3$)
(3) Graphene oxide (GO)

The reasons why they were considered in the study are described in the following paragraphs.

Ethylene vinyl alcohol copolymer or poly(ethylene-co-vinyl alcohol), abbreviated as EVAL or EVOH (Kenawy et al., 2003) is the polymer chosen in this study for fabricating the scaffold. EVAL is the term opted in the entire thesis. Ethylene units and

vinyl alcohol units with random arrangement constitute the EVAL. It is a semicrystalline polymer obtained through the hydrolyzation of poly(ethylene-co-vinyl acetate). According to the vinyl alcohol content (55-70 mol %), commercially available EVAL has different compositions (Aucejo et al., 1999; Kenawy et al., 2003). EVAL's melting point (Tm) ranges from 170-190 ºC, and the vinyl alcohol content determines it. The glass transition temperature (T_g) ranges from 45-50 ºC. The polymer could interact or absorb water due to -OH via hydrogen bonding (Aucejo et al., 1999). However, the presence of ethylene repeat units makes it water-insoluble. The hydroxyl functionalities in the polymer provide secondary functionalization opportunities (Kenawy et al., 2003).

The studies of Young et al. claim that EVAL membranes (porous) are suitable for neuronal cultures (Young et al., 2001). Mayuri et al. have shown that it is possible to generate aligned fiber yarns from EVAL by increasing the conductivity of the polymer solution (Mayuri and Ramesh, 2016). Dimethyl sulfoxide or a mixture of isopropyl alcohol (isopropanol or 2-propanol; IPA) and water are the solvents usually considered for dissolving EVAL. Kenawy et al. propose that the dissolution of EVAL in IPA:water mixture would help to make a disinfected polymer scaffold. They have also shown that these membranes support smooth muscle cells and fibroblasts (Kenawy et al., 2003). The easiness of EVAL solution preparation and electrospinning makes it more convenient to generate fibro-porous membranes for developing neural repair scaffolds.

$AgNO_3$ is an inorganic compound with a silver ion (Ag^+) and a nitrate ion (NO_3^-). A study done by Alon et al. by sputtering and coating Ag, and AgNPs respectively on glass substrates based on neuronal growth showed that these substrates induced more

neurite outgrowth from the soma (Alon et al., 2014). By incorporating silver ions in the polymer solution Mayuri et al. have generated uniaxially aligned yarns via electrospinning. The incorporation of silver ions increased the conductivity of the solution, stabilized the jet, and allowed it to be on a straight path (Mayuri and Ramesh, 2016).

GO is a graphene-derivative nanomaterial that induces neuronal and Schwann cell proliferation (Chiacchiaretta et al., 2018; Wang et al., 2019; Zhang et al., 2016). GO has been widely used in tissue engineering and bioprinting (Kang et al., 2017). The hydrophilic groups, large surface area, topographical features, and other physico-chemical properties are some of the considerable features of GO in the research world (Rahman et al., 2023). The incorporation of GO in polyurethane electrospun fibrous matrices improved the mechanical properties (Thampi et al., 2015). The interaction of neuronal and non-neuronal cells increases cell adhesion, growth, proliferation, migration, etc. (Thampi et al., 2020; Wang et al., 2019; Zhang et al., 2020). In the *in vitro* and *in vivo* studies of Qian et al., they found the GO/PCL scaffolds performed similarly to nerve autografts. A long nerve defect was morphologically and functionally restored by using these scaffolds (Qian et al., 2018). Neural repair scaffolds with gelatin methacrylyol/polycaprolactone hybrid nanofibers constructed by Fang et al. containing reduced GO performed well as a nerve repair scaffold (Fang et al., 2020).

This thesis evaluates three systems. They are (1) the EVAL-GO system, in which the EVAL is incorporated with GO, (2) the EVAL-Ag, in which the EVAL is incorporated with Ag^{+} and (3) the EVAL-Ag-GO system, in which the EVAL is incorporated with

Ag^+ and GO. The method of solution preparation, electrospinning, physico-chemical characterizations, and cell-material interaction studies are detailed in this thesis. The systems were physico-chemically characterized using Scanning Electron Microscopy (SEM), Fourier Transform Infrared (FTIR) Spectroscopy, UV-Visible Spectroscopy, Raman Spectroscopy and imaging, Energy dispersive X-ray Spectroscopy (EDX), Viscosity analysis, Conductivity analysis, X-ray Diffraction (XRD) analysis, X-ray Photon Spectroscopy (XPS), and Mechanical testing using Universal Testing Machine (UTM). The cell material-interaction studies based on viability assessment and cellular/neurite response on the EVAL systems were analyzed with L-929 fibroblast, Neuro2a, C6 glioma, and PC12 cell lines. Direct contact test, MTT assay, and Live/Dead assay were done to evaluate the viability of the cells. F-actin and immunostaining were done to evaluate the cell-material interactions.

CHAPTER 2: REVIEW OF LITERATURE

2.1. Nervous System

The nervous system (NS) in the human body, is comprised of the central nervous system (CNS) and peripheral nervous system (PNS). Along with the endocrine system, the nervous system controls and coordinates the entire bodily functions. Control and coordination are achieved by sending, receiving, and sorting electrical impulses. The CNS involves the brain and spinal cord, whereas the PNS consists of nerves, which arise from the brain (cranial nerves) and spinal cord (spinal nerves). The nerves of PNS either start or reach CNS. Thereby the PNS is classified as the afferent system (sensory), which conducts messages to the CNS from various body parts, and the efferent system (motor), which conducts messages to various body parts from the CNS. The efferent system is again classified into the autonomic system (involuntary) and somatic system (voluntary). The autonomic system gives rise to sympathetic, parasympathetic, and enteric systems (Hall and Guyton, 2011; Sherwood, 2010; Tortora and Derrickson, 2018).

Nerves or nerve fibers are the signal-conducting systems of PNS. Nerves are long fibers made up of nerve cells or neurons, connective tissues, and blood vessels. The neurons are the functional units in the nervous system which is responsible for signal or impulse conduction. They carry signals to and from the brain and spinal cord. A typical neuron has a cell body (cyton or soma), dendrites, axons, axonites, and synapses. The cell body and dendrites are embedded within the spinal cord or ganglion. The axons arising from the hillock of the cell body are seen within the nerve fibers and the axonites end up either in postsynaptic ganglion or at various organs. Neurons are

also associated with glial cells, a kind of non-neuronal cells that support neurons. The Schwann cells are the glial cells, which surround the axons of peripheral neurons. They form a structure called the myelin sheath around the neurons of PNS. The glial cells found in CNS are oligodendrocytes, astrocytes, ependymal cells, and microglia (Hall and Guyton, 2011).

Neurons of PNS are surrounded by connective tissues such as mesoneurium, epineurium, perineurium, and endoneurium (Figure 1). From a surgical standpoint, the first portion of a nerve that is encountered is the mesoneurium. It is a connective tissue that glides around a nerve. Mesoneurium is continuous with the other connective tissue known as epineurium, which is seen just inner to it. The epineurium is again a loose connective tissue, which is seen as two layers called extrinsic epineurium and intrinsic epineurium. The extrinsic epineurium is the outermost and is a sheet-like covering around the whole nerve. The intrinsic epineurium is a fibrous tissue part in which the nerve fascicles are embedded (Evans, 2001; Grinsell and Keating, 2014; Sunderland, 1990). Blood vessels (vasa nervorum) are also seen in the intrinsic epineurium. Vasa nervorum enters the epineurium at various levels and communicates with a complex longitudinal anastomotic network of arterioles and venules (Chhabra et al., 2014; Ishibe et al., 2011). 70% of a nerve cross-section is extrinsic and intrinsic epineurium together. Fascicles are embedded within the intrinsic epineurium. The fascicles seen within the intrinsic epineurium will be several in number according to the nerve type, region, etc. Each fascicle is surrounded by a connective tissue that is a tough lamellar structure known as perineurium. Like epineurium, perineurium also appears as two different portions. The outer portion of the perineurium is a sheet and it surrounds each fascicle. The inner portion embeds the endoneurial tubes. The perineurial compartment

also consists of blood vessels. Each fascicle encloses several numbers of endoneurium with axons. Each endoneurium surrounds an axon of a neuron whose cell body is either in a ganglion or is synapsed with a pre-synaptic or post-synaptic neuron. The axons within the endoneurium may or may not be surrounded by myelin sheaths made up of Schwann cells (Evans, 2001; Grinsell and Keating, 2014; Sunderland, 1990).

A neuron is comprised of a dendrite, cell body, axon hillock, axon, axonites, and synapses. Dendrites are small spine-like structures from the cell body that help a neuron receive electrical signals from another. The signals collected by the dendrites are sent to the cell body. The cell body is the neuronal part where the nucleus, endoplasmic reticulum (Nissl granules), and mitochondria are located. So, the cell body is the site where proteins, hormones, and neurotransmitters are produced in a neuron. The cell body then narrows and initially forms an axon hillock and then an axon. Whenever a neuron receives an inhibitory or excitatory input, the axon hillock is the portion where the input is summed up and a decision is taken. The decision might be whether or not to send an action potential through the axon. If the decision is to send the action potential, then the electrical signals are transmitted to the axon. The axon then sends the signal to a space called a synapse, where a neuron communicates with other neurons or an organ. When the action potential reaches the synaptic knob (end of the axon), a series of events occur to release neurotransmitters into the synapse. The post-synaptic neuron or the effector organ responds according to the neurotransmitter released into the synapse by the presynaptic neuron (Anderson et al., 2015).

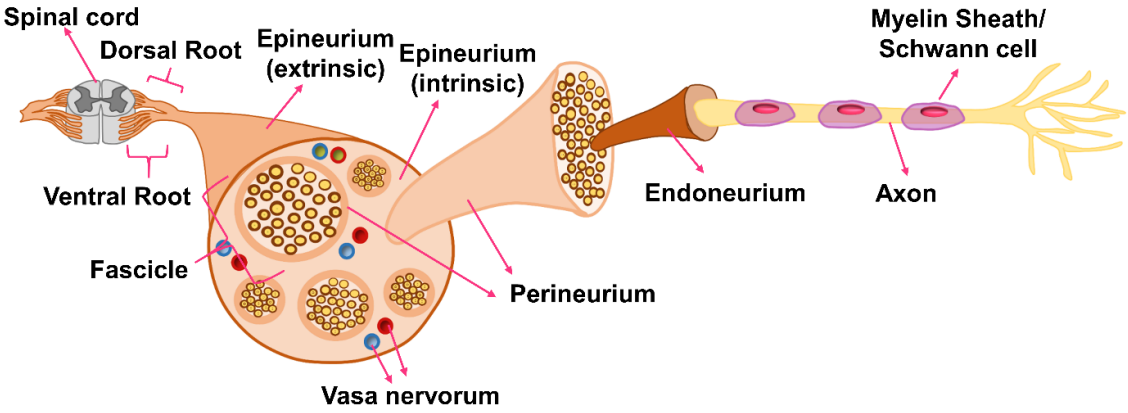

Figure 1: Anatomy of peripheral nerves

2.2. Peripheral Nerve Injuries (PNIs)

The brain and spinal cord of CNS are protected in bony structures such as the skull and vertebral column respectively. Whereas there are no bony coverings around the nerve fibers of PNS. This may expose the nerves of PNS to damages that may occur from trauma, surgery, diseases, etc. The damages may result in temporary or permanent impairments in some areas. Still, the solace is, that the neurons of PNS are capable of regeneration according to the severity of the damage (Chhabra et al., 2014).

When a nerve is severed completely, two parts occur, a proximal stump (proximal cut end) and a distal stump (distal cut end) (Figure 2; "1"). Since a nerve has bundles of axons, during a severe laceration, the majority of the axons will be damaged. Suddenly after an injury, the damaged neuron undergoes 'Wallerian degeneration, which is a series of events that occur before recovery of a nerve from injury (Figure 2; "3 and 4"). It is then followed by axonal regeneration from the proximal stump (Figure 2; "5") (Burnett and Zager, 2004; Terenghi, 1999).

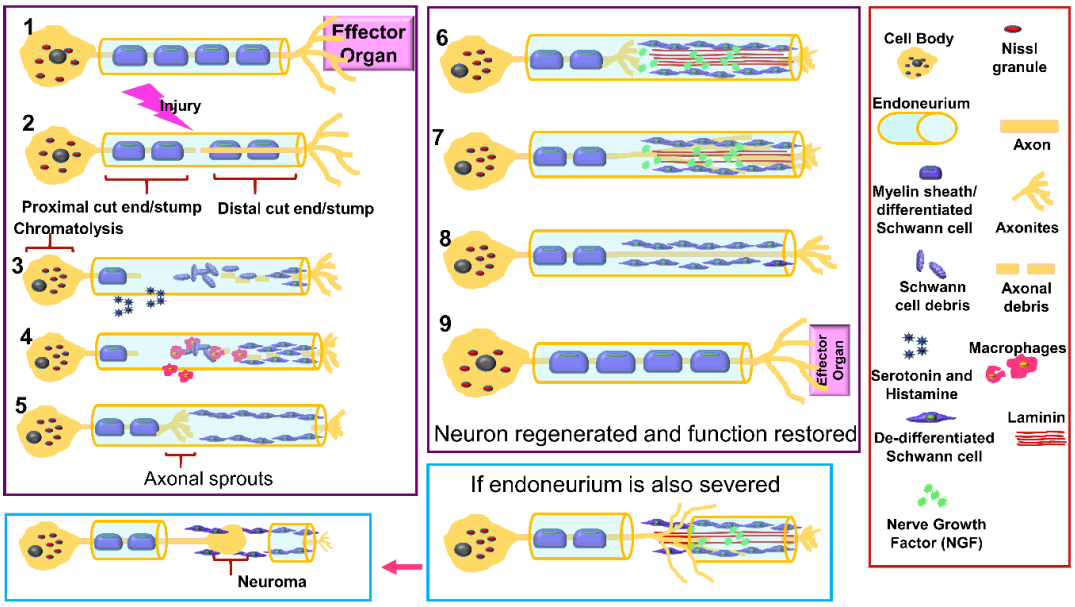

Figure 2: Diagrammatic representation showing nerve recovery after an injury.

The regeneration occurs only if the cell body and at least some portion of the axon continuing from the cell body with the myelin sheath in the proximal stump is intact (Figure 2; "2"). Just after the axonal injury, an intrinsic signaling pathway is activated at the proximal stump. The signaling leads to the activation of several transcription factors and finally promotes axon sprouts to emerge (Figure 2; "5"). Meanwhile, the distal stump axon undergoes axonal skeleton disintegration and membrane breakage resulting in axonal degradation (Figure 2; "3 and 4"). The Schwann cells of the myelin sheath at the degrading axon tend to dedifferentiate into non-myelinating, pro-regenerating phenotypes and then start to proliferate, migrate, secret neurotrophic factors, and deposit basal lamina proteins (Figure 2; "3, 4, and 5"). The Schwann cells then migrate to the injury site to attract the proximal stump axon sprouts by secreting growth factors and aligning on the basal lamina (Figure 2; "3"). Thereby the Schwann cells form 'bands of Bungner or Bungner's band' that guide the newly sprouting

proximal stump axons to reach the target (Figure 2; “6 and 7”) (Bunge, 1994; Burnett and Zager, 2004; Grinsell and Keating, 2014).

The recovery of nerves from injuries depends on the severity of damage that occurred to the nerve. Seddon (1943) and Sunderland (1951) classified nerve injuries into various grades based on the severity of the damages that occurred to the nerve (Figure 3). Seddon classified the injuries into 3 and Sunderland into 5 categories. The ‘Grade I or class I’ injury is known as neuropraxia in which the axon alone undergoes damages like a temporary interruption in impulse conduction and may lead to sensory-motor problems. Here there is no loss of axonal continuity and recovery of function can occur in days to weeks. ‘Grade II or class II’ injury is known as axonotmesis in which the connective tissues (endoneurium, perineurium, and epineurium) stay intact, and axonal continuity along with myelin sheath is lost. Wallerian degeneration occurs in the axon of the distal stump and may lead to sensory-motor impairments. Axonal regeneration is possible without surgery if there is no scar tissue formation. “Grade III, IV, and V or class III, IV, and V” are categorized as neurotmesis. Neurotmesis is the most severe form of nerve injury where along with, axon, and myelin sheath, the connective tissues also become injured. In grade III, endoneurium is damaged along with an axon. In grade IV, endoneurium and perineurium are damaged along with the axon. The endoneurium, perineurium, and epineurium are damaged along with the axon in grade V. So, neurotmesis (grade III to V) requires surgical methods to restore nerve function (Chhabra et al., 2014; Evans, 2001; Gaudin et al., 2016). MacKinnon and Dellon have

added one more injury type where a nerve has undergone a combination of previously mentioned injuries (Evans, 2001).

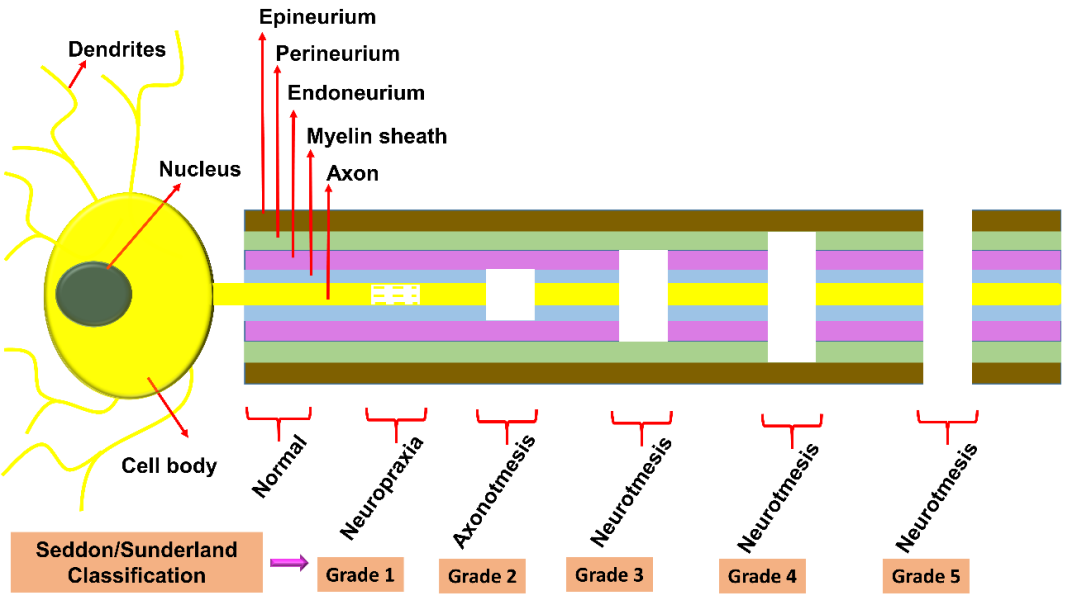

Figure 3: Diagrammatic representation of nerve injury classification by Seddon and Sunderland.

2.3. Treating Approaches

2.3.1. Surgical reconnection

Surgical reconnection is the method in which the injured or severed nerve is sutured in such a way that the end-to-end is connected (Figure 4). This is known as neurorrhaphy. This can restore the continuity of the injured nerve and eliminate the gap that occurred. For surgical reconnection, the gaps that occurred from injury must be <5 mm (Jiang et al., 2020; Kehoe et al., 2012). Sometimes a gap < 3 cm is also connected via surgical reconnection (Houshyar et al., 2019). Neurorrhaphy is done using several techniques, such as (1) conventional group fascicular repair: micro-sutures placed through the interfascicular and external epineural tissue, (2) perineural repair: suturing of the corresponding nerve fascicle and distal nerve stump for optimal

alignment, and (3) epineural repair: usually applied directly to the transected nerve injury and comprises sutures passes through the epineural sheath (Kehoe et al., 2012).

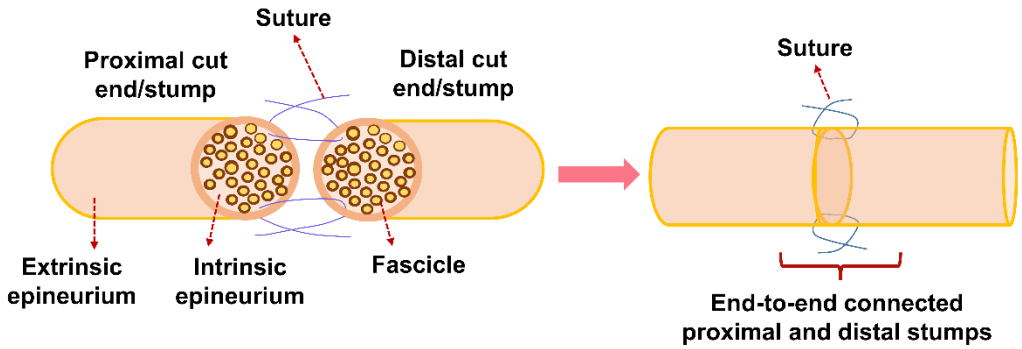

Figure 4: Diagrammatic representation of neurorrhaphy or surgical reconnection or (end-to-end reconnection).

2.3.2. Tissue graft

Tissue grafting is a gold standard option for treating the injured nerve. The injured nerves with > 3 cm gap are subjected to such treatments. The graft used can either be an autologous graft or an allograft. A graft bridges the severed nerve ends and provides physical guidance for the axonal sprouts that arise from the nerve end proximal to injury to reach the distal portion. Wallerian degeneration could occur in these grafts and result in increased secretion of neurotrophic factors which enhances axonal growth and nerve regeneration (Houshyar et al., 2019; Kehoe et al., 2012). Decalcified inside-out veins, blood vessels, arteries, xenografts, muscle fibers, bone conduit, and allogenic and autogenic nerve grafts are some of the biological grafts used. Limitations in availability, pain resulting from neuroma, and morbidity of the donor site are some of the issues faced after grafting (Grinsell and Keating, 2014; Muheremu and Ao, 2015).

Mostly nerve portions dissected elsewhere in a patient's body (eg; lower leg) are used as autologous nerve grafts. This harvest is done only when the diameter and average axon density match between donor-recipient nerves (Houshyar et al., 2019). Autologous grafts have both advantages and disadvantages. Less immune rejection, good biocompatibility, nontoxicity, and the presence of Schwann cells and other cells are the advantages. The disadvantage includes the multiple surgeries done to procure the nerve from a donor site elsewhere in the patient's body. This adds more to the patient morbidity (Chiono and Tonda-Turo, 2015; Sarker et al., 2018; Yi et al., 2019).

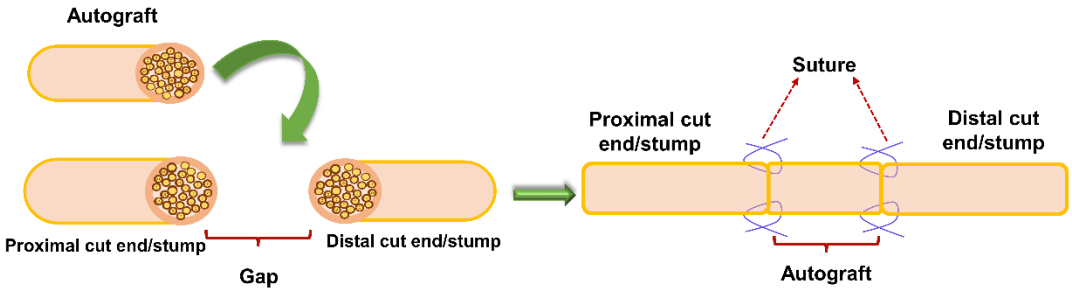

Figure 5: Diagrammatic representation of tissue grafting.

2.3.3. Scaffolds for Guidance

Substrates or scaffolds that could guide a severed nerve to regenerate, help to recover, and restore nerve function are considered artificial nerve guides or nerve repair scaffolds. Nowadays a wide range of research is occurring to construct such guidance conduits which could act as a substitute for autograft. Thereby solving the problems faced by the patient resulting from procuring and placing an autograft. Artificial nerve guides or nerve repair scaffolds are made of polymers and are known as nerve guidance conduits (NGC) or nerve wraps (NW). Together they can be abbreviated as NGC/NWs. (Daeschler et al., 2025; Jiang et al., 2020; Kehoe et al., 2012). The NGC/NWs could

act as a bridging support between proximal and distal stumps. Besides the support, they promote the extension of proximal axonal sprouts to reach the distal stump and enhance the recovery of the nerve (Gaudin et al., 2016; Houshyar et al., 2019).

According to the evolution of NGC/NWs, there are three generations. They are:

1. **First-generation NGC/NWs:**

First-generation NGC/NWs were developed according to the concept that, they must provide support and act as a barrier that prevents the excess infiltration of connective tissues. They would also guide the regrowth of the severed nerve. Polytetrafluoroethylene (ePTFE, Gore-Tex®; used as vascular graft), was an artificial conduit used to reconstruct the injured peripheral nerves. In humans, a nerve gap up to 4 cm was successfully treated using ePTFE tubes. Silicone in the form of polydimethylsiloxanes (PDMS), with flexibility and biocompatibility, was used as nerve guide tubes (Heath and Rutkowski, 1998; Houshyar et al., 2019). Since these nerve guides were non-biodegradable, compressions occur after complete nerve regeneration and are accompanied by fibrotic tissue formation. So, secondary surgery became necessary to remove the nerve guide (Gaudin et al., 2016).

2. **Second-generation NGC/NWs:**

The need for resorbable, biocompatible, and porous NGC/NWs started the second generation of nerve guides. They were mainly intended to avoid the second surgery conducted for the removal of the scaffold. The focus on the topography and biocompatibility enhanced the axonal remyelination and recovery of the transected nerve. There are several FDA-approved nerve guides in this generation. They include NGC/NWs made up of resorbable type I collagen, polyglycolic acid (PGA), and poly

DL-lactide-co-caprolactone (PLCL). A non-resorbable nerve guide made from polyvinyl alcohol (PVA), also comes under second-generation nerve guides.

U.S. Food and Drug Administration (FDA) approval has been received for several synthetic scaffolds that could act as NGC/NWs (Table 1). Scaffolds fabricated from collagen (NeuraGen®, NeuroFlex®, NeuroTube®), polyglycolic acid (PGA: NeuroTube®), polyvinyl alcohol (PVA: SaluTunnel®), etc. are some of the FDA-approved NGC/NWs. But they are limited in use because they can only be used for bridging gaps less than 3 cm (Kehoe et al., 2012).

Table 1: FDA-approved NGC/NWs

Product	**Material**	**Manufacturer**	**Degradation time**	**Type/maximum length (mm)**
Avance® nerve graft	Processed human peripheral nerve allograft	AxoGen Inc.	-	Conduit/25
AxoGuard® nerve connector	Extracellular matrix from porcine intestinal submucosa	Cook Biotech Inc.	-	Conduit/10
NeuraGen® nerve conduit (Hollow)	Type I Collagen (bovine)	Integra Life Sciences Corp.	3-4 years	Conduit/30
NeuroMatrix ™ nerve conduit (Hollow)	Type I Collagen	Stryker (Collagen Matrix Inc.)	4-8 months	Conduit/25
NeuroFlex™ nerve conduit (Hollow)	Type I Collagen	Stryker (Collagen Matrix Inc.)	4-8 months	Conduit/25
NeuraWrap™ nerve wrap	Type I Collagen (bovine)	Integra Life Sciences Corp.	36-48 months	Wrap/40
NeuroMend™ nerve wrap	Type I Collagen (bovine)	Stryker (Collagen Matrix Inc.)	4-8 months	Wrap/25

Salubridge nerve conduit	Polyvinyl alcohol (PVA)	Salumedica LLC	No degradation	-
SaluTunnel nerve wrap	Polyvinyl alcohol (PVA)	Salumedica LLC	No degradation	Wrap/40

3. Third-generation NGC/NWs:

The second-generation NGC/NWs (Figure 7) are just hollow tubes that lack autograft characteristics and have some limitations, even though they are FDA-approved. Here comes the need for third-generation nerve conduits which are still far from FDA approval but still under progressive research. These NGC/NWs are intended to be constructed with some special features that could be helpful in nerve regeneration. Scaffolds with micropatterned surfaces, intra-luminal channels, nerve growth factors, electrical conductivity, etc. could provide orientation or guidance to the regenerating nerve. The incorporation of neurotrophic factors, Schwann cells, and electroconductive agents that support nerve regeneration is under detailed research (Gaudin et al., 2016). Among these scaffolds with anisotropic surfaces are gaining more attention (Buskermolen et al., 2020; Cho et al., 2016; Hoffman-Kim et al., 2010; Sumam and Parameswaran, 2023; Zhang et al., 2020).

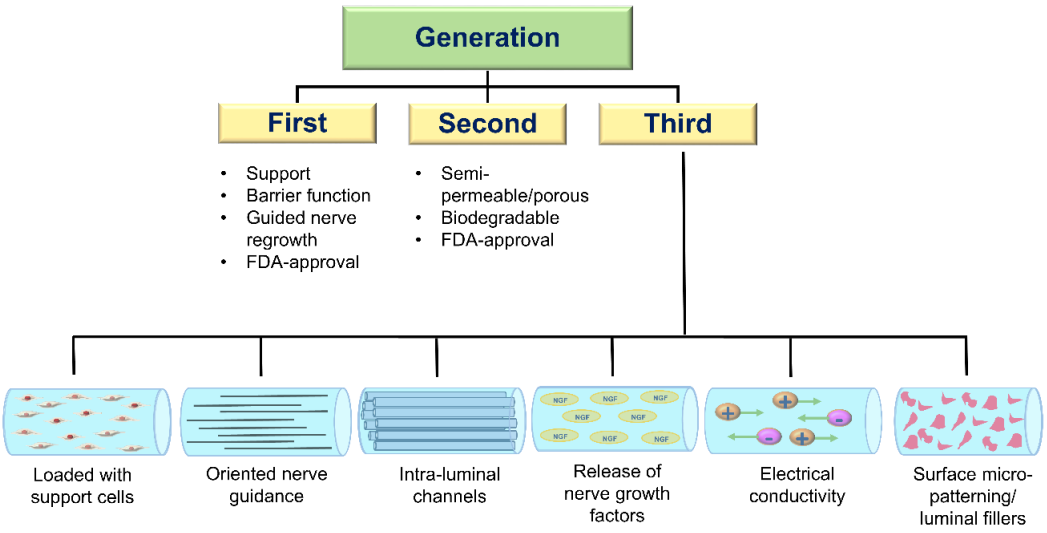

Figure 6: Types of third-generation nerve guidance conduits or nerve wraps (NGC/NWs).

2.4. Fabrication techniques for developing nerve repair scaffolds (NGC/NWs)

2.4.1. Solvent casting/particulate leaching

It is a simple technique used for producing films and porous scaffolds. A desired polymer is dissolved in a suitable solvent to prepare a homogeneous polymer solution. The solution is then poured onto a mold and the solvent in the solution is allowed to evaporate. The solvent evaporation depends on the volatility of the solvent used. The solvent evaporation results in a polymer film. This technique is useful in creating films with uniform thickness. To obtain a porous film, the polymer solution is mixed with some porogen, and the porogen-containing polymer film after solvent evaporation is submerged in a bath where the porogen is dissolved. This helps to obtain a porous film (Mi et al., 2015; Papadimitriou et al., 2020). The porogen's amount and size can determine the film's porosity and pore size, respectively. The disadvantage of the films

obtained through solvent casting is that the membranes obtained will have only a thickness of < 3mm (Papadimitriou et al., 2020).

Scaccini et al. fabricated a chitosan-based nerve engineering scaffold using the solvent casting method. These films were micro-structured substrates. The topography of the micro-structured substrates induced cell polarization, actin organization, and cell-cell contacts of Schwann cells (Scaccini et al., 2021). Polycaprolactone (PCL), poly (lactic-co-glycolic acid) (PLGA), and polypyrrole (PPy) fibers were used by Ferreira et al. to construct nerve repair scaffolds. The PPy fibers in the substrates made them thermally stable and electrically conductive material. So, these materials become suitable for constructing nerve repair scaffolds (Ferreira et al., 2019). Ghafaralahi et al. have constructed a nerve conduit made from poly(glycerol-sebacate) and poly(caprolactone). These constructs were found to be promising nerve conduits (Ghafaralahi et al., 2018; Kang et al., 2022).

2.4.2. Phase separation

Phase separation comprises two different fabrication methods. One is non-solvent-induced phase separation (NIPS) and the other is thermally-induced phase separation (TIPS). In NIPS a polymer is dissolved in its suitable solvent and poured onto a support structure. After exposing the poured solution to air for a short period, it is immersed in a non-solvent bath. This leads to polymer precipitation due to the formation of two phases, a polymer-rich, and a polymer-lean phase. A precipitated polymer obtained from NIPS will be porous and have applications such as scaffolds. In TIPS, a homogeneous solution is prepared at elevated temperatures, and polymer-lean and polymer-rich phases are created by cooling the solution. The polymer-rich portion can

act as a scaffold and the polymer-lean portion becomes pores. (Papadimitriou et al., 2020).

Yang et al. made Poly(L-lactic acid) (PLLA) scaffolds through the phase separation technique. These scaffolds were highly porous and also had fibers with diameter in nanoscales. These scaffolds mimicked the natural extracellular matrix (ECM) and promoted the differentiation of nerve stem cells (NSCs). They also provided positive cues for supporting the neurite outgrowth (Yang et al., 2004). Abzan et al. developed a nerve conduit through the phase separation method with polyvinylidene fluoride and graphene oxide (PVDF/GO). These scaffolds promoted PC12 cell proliferation due to the incorporation of GO (Abzan et al., 2019).

2.4.3. Freeze-drying

Freeze-drying is a scaffold fabrication technique that can create porous scaffolds even without a porogen. A polymer solution is cooled to lower temperatures like -70 to -80 ^{o}C where the solvent forms ice crystals. The polymer aggregates at the spaces around the ice crystals. A pressure lower than the frozen solvent's equilibrium vapor pressure is applied to remove the frozen solvent. This results in the solvent evaporation solid stage to the vapor stage directly. As the process completes, a porous polymer scaffold is obtained. These kinds of scaffolds have highly interconnected pores and these structures will promote cellular infiltration and tissue growth.

Collagen-based nerve guides with longitudinal guidance channels were fabricated by Bozkurt et al. through the freeze-drying technique with a 20-50 μm pore size. Dorsal root ganglion (DRG) was cultured on these scaffolds and after 21 days, the Schwann

cells (SCs) that migrated into the channels aligned to form “Bands of Bungner”(Bozkurt et al., 2007).

2.4.4. Hydrogel formation

The highly hydrophilic polymers that can hold high amounts of water in them are known as hydrogels. The polymer solution when cross-linked can produce porous hydrogels. The cross-linking can be achieved through UV photopolymerization, varying ionic concentrations, and changing the temperature or pH of the material. According to the polymer property, and crosslinking method, the hydrogel properties might vary. They can be soft, flexible, rigid, elastic, etc. Both natural and synthetic origin polymers are used in the preparation of hydrogels (Papadimitriou et al., 2020).

The gelatin methacrylyol (GelMA) hydrogels with photocrosslinkable properties were used by Wu et al. for culturing PC12 cells. The improvement in Young’s modulus of GelMA according to their concentration increased the stiffness of the gel and it promoted the cell spreading and neurite length (Wu et al., 2019). Wach et al. developed a nerve conduit made from poly(lactic acid) and poly(trimethylene carbonate) (PLLA-PTMC), intraluminally filled with carboxymethyl chitosan hydrogel. The construct was not only non-cytotoxic but also antimicrobial (Wach et al., 2020).

2.4.5. Compression/injection molding

These molding techniques require a polymer powder, porogen, and a mold. The polymer is melted down first, then the porogen is blended with the melt, and the polymer-porogen blend is inserted in a mold through compression or injection. The melt when cured the scaffold is obtained (Papadimitriou et al., 2020).

2.4.6. Soft lithography and photolithography

The lithography technique is used to fabricate substrates with complicated topographies very precisely. It also avoids contamination that can occur through contact. Photolithography, scanning beam lithography, electron beam lithography, nanoimprint lithography, dip-pen lithography, capillary lithography, and soft lithography are different forms of lithography. Among these, photolithography and soft lithography are mainly used in scaffold construction for neural tissue engineering. In photolithography, the desired pattern from a photomask is transferred to a photosensitive material called photoresist using ultraviolet or other lights. By etching or decomposing, the pattern is transferred to the underlying substrate. The high cost, difficulty in controlling surface properties, and suitability issues in using some materials limit this technique in biological applications. Soft lithography, which is cheap, fast, and precise overcomes the limitations of photolithography. The polymers are cast onto polydimethylsiloxane (PDMS) (Hu et al., 2022). Wang and Huang used the soft lithography technique to produce silicon-based structures which were filled with chitosan and developed the nerve conduits (Wang and Huang, 2008).

2.4.7. Laser texturing

A recently developed technique useful in surface texturing the substrates using ultrafast lasers. This technique is useful in precise tailoring morphologies using the laser with local excitations. Pointing the laser only at specific areas would prevent the surroundings from being damaged (Papadimitriou et al., 2020; Simitzi et al., 2017). The surface structuring and texturing can be done at the nanometer to micrometer range without contact with the substrate surfaces.

2.4.8. Electrospinning

Electrospinning is a fiber drawing technique that generates fibers from a polymer solution in the presence of electrostatic forces. A charged jet ejected from a blunt-ended needle-connected syringe is collected on a charged collector that is placed at a particular distance from the needle. The fibers collected on the collector finally resemble a mat/membrane/matrix. The fibers obtained are non-woven and can be used as scaffolds in several biological applications. The parameters considered during the spinning can determine the fiber morphology, orientation, and diameter. The fibers can be generated with diameters ranging from nanometers to micrometers. The scaffolds obtained will have a high surface area-to-volume ratio (Cho et al., 2016; Mamun et al., 2021; Mayuri et al., 2016; Meinel et al., 2012; Surendranath et al., 2022; Thampi et al., 2017). The electrospinning technique is detailed in section 2.6.

2.4.9. 3D bioprinting

3D bioprinting is an advanced version of traditional 3D printing in which a polymer solution with a particular consistency is used as the ink. This ink is known as bioink and the cells are mixed with this ink. With particular parameters, the printing is carried out to get cell-laden constructs. Laser-assisted printing, micro-extrusion, and inkjet printing are now available. Neural scaffolds that mimic neural tissue have been developed using the 3D bioprinting technique (Hu et al., 2022). Liu et al. constructed a neural scaffold from cell-laden hyaluronic acid derivative, chitosan bioink through one-step 3D bioprinting. The nerve regeneration and functional recovery were attained by using these constructs (Liu et al., 2021).

2.5. Role of Anisotropic substrates in neurite extension and nerve regeneration-Topography, contact guidance, and neuronal cell response

One of the main focuses of nerve repair research is to construct scaffolds that could provide topographical cues for the regenerating nerve. The neural cells and their processes (neurites: axons or dendrites) respond well to topographical cues of a substrate (Figure 7). These cues influence a neuron in polarization during the growth and branching of a neurite (Hoffman-Kim et al., 2010). In a spontaneous regeneration even in the absence of scaffolds, the axonal sprouts will follow the topographical cues provided by the basal lamina laid by Schwann cells (Figure 2; "6 and 7"). These cues will guide the axon to reach the distal stump. Such guidance provided by any substrate and perceived by the neurons is known as contact guidance (Figure 7). The term contact guidance was first introduced by Paul Weiss in 1945 (Weiss, 1945). So, nowadays extensive research is occurring to construct or fabricate the NGC/NWs with such topographical cues.

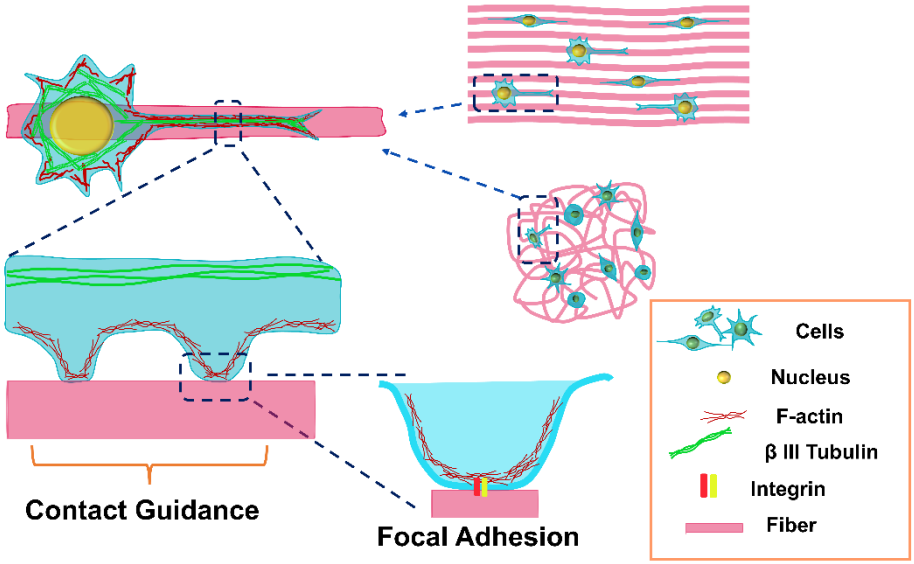

Figure 7: Diagrammatic representation showing cell/neurite response through contact guidance.

Contact guidance has an important role in the growth of nerves of PNS and CNS during the embryonic stage as well as regeneration after an injury (Hoffman-Kim et al., 2010). As described in nerve regeneration (section 2.2), after the Wallerian degeneration the Schwann cells secrete basal lamina proteins for the regenerating axon. The regenerating axons find topographical cues on these basal lamina tracks and respond via contact guidance to regenerate (Torigoe et al., 1996). The guidance cue of the surfaces influences the growth cones of the regenerating axons. Growth cones are highly motile structures found at the tip of the axons. These structures are responsible for retracting, advancing, branching, and turning of an axon and it occurs through the dynamics and reorganization of actin filaments and microtubules (Kalil and Dent, 2005). The actin filaments are found at the periphery and the microtubules are located at the central portion of an axon. The actin filaments in the lamellipodia and filopodia are mesh-like and bundled respectively. The actin filaments direct the leading edge of growth cones in response to the guidance cue provided by the surfaces. As the cells find the guidance cues on a surface, some cell receptors (eg; Integrin complexes) respond to the cues by activating some cell signaling pathways, and as a result, the actin-microtubule reorganization occurs. This enables the axons to advance, turn, branch, or retract (Huber et al., 2003; Kalil and Dent, 2005; Luo, 2002; Song and Poo, 2001).

Anisotropic substrates are the best constructs that can offer topographical cues for the neurons to extend their neurites unidirectionally/bidirectionally. A substrate is said to be anisotropic a physical property when measured, the value will be different for different directions. So, these surfaces have different roughness values along different axes. For example, a parallelly arranged grooved substrate, parallelly arranged ridges,

unidirectionally oriented fibers or filaments (Figure 8), and surfaces patterned with micropillars are considered anisotropic substrates. These substrates have continuous topographies. Anisotropic substrates can also be constructed from discontinuous topographies such as pillars and posts. These features will unidirectionally guide axon outgrowth and cellular orientation (Figure 8) (Hoffman-Kim et al., 2010; Leclech and Villard, 2020; Xue et al., 2021).

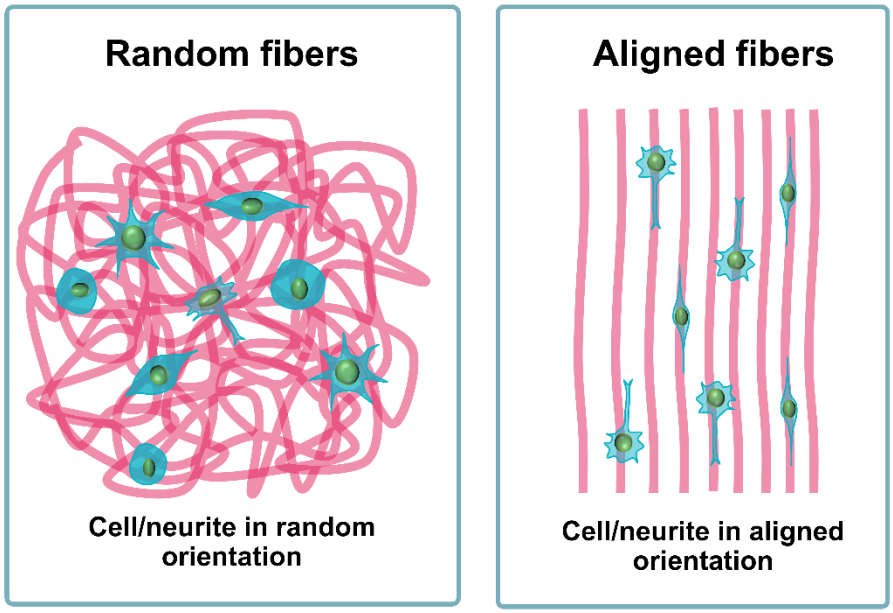

Figure 8: Diagrammatic representation showing cellular/neurite response according to fiber orientation.

2.6. Electrospinning for fabricating anisotropic substrates

The fibrous scaffolds are substrates with large surface area-to-volume ratios. A fibrous substrate is said to be anisotropic when the fibers are unidirectionally or parallelly aligned (aligned fibers). Several techniques are used to fabricate substrates with aligned fibers (eg; Self-assembly, Phase separation, Stretching, etc.). Electrospinning is a promising, versatile, and most commonly used technique for fabricating fibrous scaffolds from continuously produced fibers. The fibers are formed as a result of the play of some forces. These forces are gravitational force, electrostatic force (helps to

carry the charged jet to the collector), coulombic force (exerted by a charged carrier to push another charged carrier and cause stretching of the jet), viscoelastic force (helps to prevent the charged jet from stretching), surface tension (helps to prevent the stretching of the surface of the charged jet), and drag force (friction between the charged jet and surrounding air) (Mit-uppatham et al., 2004). Based on these forces electrospinning technique produces random and aligned fibers depending on some parameters (Robinson et al., 2021).

The working of the electrospinning technique is as follows. The polymer solution is first filled in a capillary or syringe which is fitted with a blunt-ended needle. The electrospinning system also has a conducting collector which is placed some distance far from the needle tip. The system is supplied with high voltage where the positive and negative potentials are supplied to the needle and collector respectively (Haider et al., 2018; Huang et al., 2003; Pham et al., 2006). The collectors used might be in various forms such as stationary flat surfaces and rotating structures (drums, mandrels, discs, etc.) (Teo and Ramakrishna, 2006). A required voltage is applied to the system and the solution in the syringe or capillary is ejected with a particular flow rate. With a voltage that is greater than the surface tension, the polymer solution ejected from the needle tip (positively charged) will turn into fibers and move forward to fall on the collector (negatively charged). The rate of solvent evaporation helps to obtain fibers. The scaffolds obtained from electrospinning are known as electrospun membranes, matrices, and mats. (Cho et al., 2016; Mamun et al., 2021; Mayuri et al., 2016; Meinel et al., 2012; Rashid et al., 2021; Sumam and Parameswaran, 2023; Surendranath et al., 2022). The fibers obtained are either random or aligned. After traveling a particular distance, the ejected fibers will show whipping motions due to the instability

developed within the solution due to charge densities (Burger et al., 2006; Pham et al., 2006). This whipping motion of fibers will result in the collection of random fibers on the collector (Rashid et al., 2021). Any method that helps to overcome the whipping motion of the fibers will give alignment to the fibers when collected on the collector (Cho et al., 2016; Robinson et al., 2021; Sumam and Parameswaran, 2023; Thampi et al., 2020).

Depending on the collector, one can fabricate a matrix that possesses aligned or random fibers. The fibers collected on a stationary flat surface are always random. Whereas, the fibers show alignment (parallelly aligned) when they are collected on rotating collectors such as drums and discs at high rotating speeds (Huang et al., 2003). Even when the fibers are collected on a rotating collector the velocity of the rotation and the flow rate of the ejecting polymer solution decide the alignment. When the rotation velocity is less and the flow rate is high, the fibers drawn by the collector will be random. The fiber alignment is achieved when the collector rotation velocity increases and the mechanical drawing force could reduce the whipping that occurred due to bending instability. As the velocity increases the degree of alignment also increases and indicates that a minimum velocity is required to fabricate anisotropic fibrous substrates. Rotating discs are more efficient in drawing aligned fibers than the drums. Since the fiber-collecting portion of the disc is too less and sharp, the fibrous substrate collected would resemble a limited-sized band. So, this would affect its utility. Whereas the collection on a rotating drum will give fibrous matrices. Under high rotational velocity, the stretching of the jet will result in fibers with fine diameters and more alignment. This would result in high tensile strength and modulus for the scaffold (Mayuri and Ramesh, 2016; Wong et al., 2008).

Gap electrospinning which was first introduced in 2003 by Li et al. can also be used to generate aligned fibers. Here for achieving a high degree of fiber alignment, two parallel electrodes which are either charged or grounded are employed. The fibers which fall on the electrodes stand perpendicular to the electrodes due to the electric field and this makes the fibers aligned.

In 2007 Yang et al. introduced a method for producing highly aligned fibers via magnetic field-assisted electrospinning. The polymer fibers in a solution can align in the presence of the magnetic field. In magnetic field-assisted electrospinning, permanent magnets are adhered to a grounded flat plate collector. The radial Lorenz force created due to the magnetic field will alter the whipping jet diameter and enhance jet stability. As a result of the magnetic field gradient, the jet reaching the collector will align and highly aligned fibers are collected on the jet (Yang et al., 2007).

Deitzel et al. found that the fiber deposition area could be reduced with the assistance of auxiliary electrodes during electrospinning (Deitzel et al., 2001). This later helped to generate aligned fiber matrices. The role of auxiliary electrodes is to stabilize and prevent the jet from bending which is a result of charge repulsions in the solution. The researchers have tried several auxiliary electrodes during electrospinning for aligning the fibers. Charged copper rings were used by Zhao et al. for stabilizing the jet for improving the fiber alignment. In one approach two plate-like electrodes were kept on either side of the jet path and were also parallel to the jet. Thus, the bending instability was reduced and aligned fibers were collected on a rotating collector (Robinson et al., 2021; Zhao et al., 2016). In another method, fibers were aligned on the rotating surface where the fibers collected on the rotating collector were perpendicular to the rotating

surface. In this method for getting such fibers the plate electrode was kept parallel to the rotating surface (Arras et al., 2012). In some methods placing an electrode behind the rotating collector also helps to get aligned fibers. This is usually done when the rotating collector is a mandrel with a small diameter which rotates with low linear velocity even at high rpm. A kind of knife-edged bars were kept behind the collectors to fabricate aligned matrices from mandrels (Teo et al., 2005).

With the association of both electrostatic and centrifugal forces fibers are assembled and aligned in centrifugal electrospinning. Liao et al. in 2010 tried the centrifugal electrospinning method. The charged or grounded spinneret rotates and supplies the polymer solution. A stationary circular (continuous or discontinuous) collector is placed around the spinneret setup and the fibers ejected from the rotating spinneret fall on the collector. Since the spinneret is rotating, the fibers falling on the collector undergo centrifugal forces and result in stretching and thinning. According to the speed of the spinneret rotation, the degree of alignment varies (Liao et al., 2011).

In 2003 Kameoka et al. reported a near-field electrospinning technique in which the aligned fibers are produced by keeping the working distance less than 10 mm. The name near-field electrospinning was given by Sun et al. in 2006 (Sun et al., 2006). The jet that is ejected from the needle tip (Taylor cone) is stable due to the longitudinal stress occurring from the electric field. This enables the jet to be in a straight path initially. So, the fibers fall on the collector before the jet shows bending instabilities and the fibers will be aligned (Kameoka et al., 2003).

Post-drawing setups are used to align fibers after the fiber drawing step. Here the fibers drawn randomly are stretched with a tensile stretching instrument to make the fibers

aligned. Poly(glycolide)-based fibers were aligned using post-drawing setups for creating anisotropic substrates for growing cardiomyocytes (Zong et al., 2003).

2.7. Salt-induced fiber alignment in electrospinning

It has a few reports that the salt incorporation in polymer solution induces fiber alignment during electrospinning (Cho et al., 2016; Mayuri and Ramesh, 2016; Song et al., 2011). Poly(vinylbutyral) (PVB) solution generated aligned fibers during electrospinning due to the incorporation of inorganic salts. The viscosity and conductivity were the main factors that influenced the alignment as a result of salt incorporation (Song et al., 2011). Ethylamine hydrochloride in the polycaprolactone (PCL) solutions also induced to generate aligned fibers during electrospinning (Cho et al., 2016).

Jet whipping is a phenomenon that occurs during electrospinning due to the instabilities developed in the jet as a result of surface charge repulsion under higher voltage. When salt is added in a higher amount, the surface charge repulsions increase drastically, and under higher voltage, the jet is stretched to overcome the repulsion. This reduces whipping motion and stretching leading to the generation of fibers that travel on a straight path and are collected as aligned fibers on a rotating drum collector (Cho et al., 2016; Song et al., 2011). The highly unstable jet takes the shortest path, which is usually a straight path to discharge and this could also lead to the generation of aligned fibers (Song et al., 2011).

2.8. Cellular and neurite response on aligned electrospun fibers

Electrospun scaffolds with aligned fibers mimic the topographically extracellular matrix secreted by the Schwann cells. The cell's response to these topographical features of fibers includes cell adhesion, spreading, proliferation, migration, etc. A substrate with aligned fibers that bridges the proximal and distal stumps provides topographical cues to the regenerating proximal stump axonal sprouts to reach the distal stump (Figure 9). The proximal axonal sprouts reach the distal stump through contact guidance.

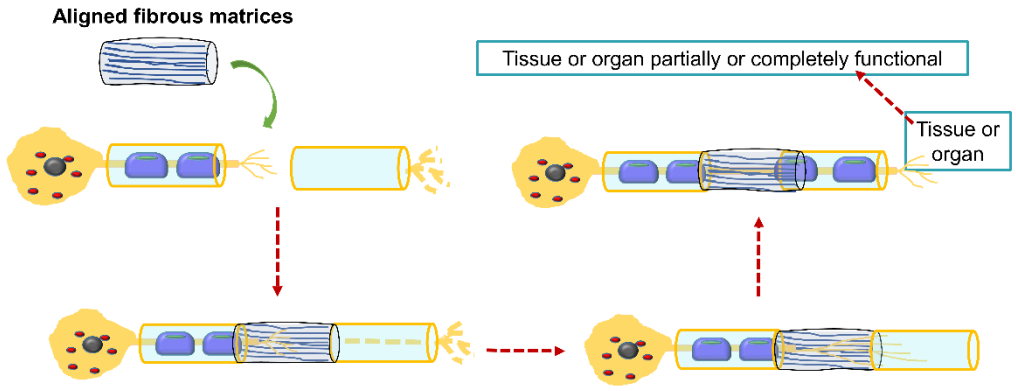

Figure 9: Diagrammatic representation of nerve regeneration with the support of aligned fibers.

Cho et al. fabricated three kinds of scaffolds from Poly (ε-caprolactone) (PCL) via the electrospinning technique. The scaffolds were: (1) PCL mats with randomly oriented fibers, (2) PCL mats with aligned fibers generated by collecting the fibers on high-speed rotating collectors, and (3) aligned PCL fiber bundles generated by incorporating salt in the polymer solution and known as salt-induced electrospun patterned bundles (SiEP bundles). The SiEP bundles promoted the elongation of PC12 cells. The SiEP bundles and aligned fibrous scaffolds oriented the neurites that emerged from the dorsal root ganglion (DRG) in an aligned manner. Here the SiEP bundles performed

better than the aligned fibers due to their soft nature which resembles the neural tissue (Cho et al., 2016). The studies of Xie et al. show that the PCL scaffolds when coated with laminin could provide more efficient guidance to the outgrowing neurites from DRG (Xie et al., 2014).

Zou et al. fabricated aligned poly(L-lactic acid) (PLLA) fibers from electrospinning. They also made the scaffold conductive by incorporating polypyrrole (PPy) on the scaffold. The fluorescent images of PC12 cells cultured on the random, aligned, and tissue culture plate (TCP) surface were evaluated for the spatial response of the neurites. They found that the neurites of PC12 cells cultured on TCP were short, numerous, and multi-directed. A similar cell response was observed in random fibers. However, the cells on the aligned fibers differentiated into a spindle shape with high polarization and largely stretched neurites along the fibers. 68% of the cells on the aligned fibers were oriented along the fiber axis (Zou et al., 2016). The study by Lü et al. has shown that the PC12 differentiation on PLLA-aligned fibers is predominantly through the integrin-mediated MAPK signaling pathway (Lü et al., 2017). Aligned PLLA nano/micro fibrous scaffolds fabricated by Yang et al. showed that the neural stem cells (NSCs) differentiated more on the PLLA nanofibrous substrates and the NSCs were elongated and extended their neurites along the fibers irrespective of fiber diameter (Yang et al., 2005). Along with the fiber alignment, Wang et al. proved the influence of fiber diameter in neurite and Schwann cell alignment. They found that the neurite outgrowth and Schwann cell migration were poor in small diameter fibers (293±65 nm). Whereas, the neurites extended very long in a directed manner on large-diameter (1325±383 nm) fibers. The large-diameter fibers also promoted Schwann cell migration (Wang et al., 2010).

When Corey et al. studied the effect of aligned fibers generated from poly-L-lactate on the spatial response of DRG also gave similar results. The staining images showed that the neurites emanating from the DRGs were highly oriented along the fibers in highly aligned fibers and poor neurite alignment was found in intermediate and random fibers. Using the Metamorph software analysis they found that the neurites on highly aligned fibers had significantly longer neurites than the ones on intermediate and random fibers. The ganglions on the highly aligned fibers were elliptical. The ganglions in the intermediate and random fibers were less elliptical and radial receptively. The Schwann cells in the DGR elongated narrowly along the fibers but spread well on glass. The SH-SY5Y neuroblastoma cell line also elongated narrowly on aligned fibers and spread with multi-directed neurites on glass (Corey et al., 2007).

The fabrication of aligned fibers from multi-walled carbon nanotube (MWCNTs)-coated poly(L-lactic acid-co-caprolactone) (PLCL) and culture of DRG showed that these scaffolds improved neuronal outgrowth *in vitro* and up-regulated Focal adhesion kinase (FAK) expression. FAK activation occurs in the integrin signaling pathway during neurite outgrowth (Jin et al., 2011). Gnavi et al. fabricated scaffolds with aligned gelatin fibers and suggested from their study that the gelatin nanofibers promote Schwann cell and neuronal viability. The gelatin fiber topography could modulate Schwann cell organization and proliferation. They could also induce axonal growth (Gnavi et al., 2015).

Fingolimod blended poly(lactic-co-glycolic) acid (PLGA) aligned electrospun fibers were made by Puhl et al. to assess the neurite extension and Schwann cell response. The extension of neurites emanated from the whole and dissociated DRG was

enhanced due to the fingolimod released from the aligned PLGA fibers. They also increased the Schwann cell migration. The neurite alignment was achieved due to the PLGA fiber alignment (Puhl et al., 2020).

A 3D fibrous scaffold was constructed with aligned fibers generated from the sodium salt of poly(γ-benzyl-L-glutamate)-r-poly(L-glutamic acid) (PBGA20-Na) by Lin et al. It was a peptide-based polyelectrolyte with a neuronal stimulant (glutamic acid). Electrical stimulation gave rise to longer neurites and the presence of glutamic acid enhanced cell adhesion, proliferation, and differentiation (Lin et al., 2019).

The nerve repair scaffolds fabricated from piezoelectric polymers are promising nerve regeneration substrates. Polyvinylidene fluoride-triflouroethylene (PVDF-TrEF) aligned electrospun fibers constructed by Orkwis et al. are one such material. The Schwann cells were viable on these constructs and also showed alignment (Orkwis et al., 2020).

2.9. Cells used for studying cellular or neurite response on nerve repair scaffolds

2.9.1. Pheochromocytoma cells (PC12)

PC12 cells originate from the rat adrenal medulla and exhibit characteristics similar to sympathetic neurons. These cells secrete catecholamines, dopamine, and norepinephrine. They also show the presence of ion channels and neurotransmitter receptors. These properties made them convenient for studies related to pharmacology, proliferation, differentiation, adhesion, etc. (Wiatrak et al., 2020). PC12 cells are small irregularly shaped and loosely adherent cells. These cells behave exactly as sympathetic neurons and sprout neurites only when they get nerve growth factor

(NGF). The neurite sprouting occurs due to the differentiation of PC12 cells (Cho et al., 2016; Guroff, 1985, 1985; Thampi et al., 2020).

In the world of neuro-regeneration research took advantage of the neurite sprouting in PC12 cells in response to NGF by studying the neurite extension, orientation, focal adhesion formation, etc. (Cho et al., 2016; Leach et al., 2007; Thampi et al., 2020; Wu et al., 2019).

2.9.2. Neuro 2a (N2a)

Neuro2a (N2a) is a cell line collected from neuroblastoma found in mouse (*Mus musculus*) brain. Since they have neuronal morphology, they are used in neurite extension studies. In GO-adsorbed poly(D,L-lactide-co-caprolactone) films made by Zhand et al. with micropatterned grooves and ridges, oriented the neurites of N2a cells along the micropatterns (Zhang et al., 2020). Sangsanoh et al. fabricated laminin immobilized Poly(3-hydroxybutyrate) (PHB) aligned electrospun fibers. These fibers supported the N2a cells to attach and proliferate more than the other PHB substrates in the study. The cells also aligned on laminin-PHB sustrates (Sangsanoh et al., 2017).

2.9.3. Schwann cells

Schwann cells (SCs) are glial cells of the peripheral nervous system found surrounding the peripheral neuronal axons as the myelin sheath. They have a significant role in nerve regeneration. SCs remove the axonal debris that occurred during the “Wallerian degeneration” after injury. The SCs arrange as a tube-like structure around the distal cut stump to produce the “Bands of Bungner” and secrete various growth factors. These interventions of SCs orient the proximal axonal sprouts to the distal stump. This enhances nerve regeneration and prevents delay and neuroma formation (Bunge, 1994;

Burnett and Zager, 2004; Grinsell and Keating, 2014). So, the SC orientation and migration studies on fibers are relevant to constructing NGC/NWs. Wang et al. have studied the effect of fiber diameter on the migration of Schwann cells on fibers. The Schwann cells migrated well on fibers with larger diameters (1325 ± 383 nm) (Wang et al., 2010). A fibrous scaffold fabricated with polyvinylidene fluoride-trifluoroethylene (PVDF-TrFE) copolymer by Orkwis et al. has shown that the variation in fiber thickness promoted SC adhesion and alignment (Orkwis et al., 2020). Wang et al. constructed a nerve repair scaffold from Antheraea pernyi silk fibroin (ApF)/(poly(L-(lactic acid-co-caprolactone)) (PLCL). The GO-coated ApF/PLCL scaffolds were used to study the SC biological behaviors on them. The *in vitro* and *in vivo* studies showed that the scaffold enhanced the proliferation, migration, and myelination behaviors of the SCs (Wang et al., 2019). Zhang et al made GO-adsorbed micropatterned poly(D,L-lactide-co-caprolactone) films with grooves and ridges. A directional migration and great adhesion of SCs were found on the film 3/3-GO (Zhang et al., 2020).

2.9.4. SH-SY5Y

SH-SY5Y is a human neuroblastoma cell line commonly used in *in vitro* neurobiological analysis. SK-N-SH is a primary neuroblast-like cell line obtained from a bone marrow biopsy with metastatic neuroblastoma tissue. Later the SH-SY was subcloned from SK-N-SH and again subcloned to obtain SH-SY5. Finally, SH-SY5Y was subcloned from SH-SY5. The SH-SY5Y cell line is usually used in studies related to neurodegenerative diseases. Upon manipulating the culture medium, these cells can be induced to differentiate into a neuron-like phenotype (Feles et al., 2022; Hoffmann et al., 2022). The SH-SY5Y cells can differentiate morphologically into two distinct

forms. One is N-type, neuron-like, and S-type, epithelial-like (Litowczenko et al., 2019). This advantage could save time and effort in isolating primary neurons and their culture. Litowczenko et al studied the differentiation and orientation of these cell lines according to the surface topography, surface stiffness, and chemistry when cultured on flat and groove-patterns made from Silicon (Si), gold (Au), and PCL. The techniques employed for constructing the substrates were photolithography and soft-lithography. The study revealed that even without differentiation factors, the SH-SY5Y neuroblastoma cells differentiated into N-type cells when grown on Au-Si groove patterns. The cells grown on flat Si, Au, and PCL and grooved Au-PCL resembled more like S-type (Litowczenko et al., 2019). Scaffolds fabricated from a hybrid system of graphene nanosheets and silk fibroin induced oriented growth and neuron-like differentiation in SH-SY5Y cells (Qing et al., 2018). The neuron-like appearance of these cells would be useful in studying neurite orientations on substrates. The human origin of these cells also provides more relevance in peripheral nerve repair studies.

2.10. Ethylene vinyl alcohol copolymer (EVAL)

Ethylene vinyl alcohol copolymer or poly(ethylene-co-vinyl alcohol) is abbreviated as EVAL or EVOH (Kenawy et al., 2003). The polymer is designated as EVAL in this entire thesis. The polymer comprises two units, one is ethylene and the other is vinyl alcohol. EVAL is a semicrystalline polymer developed by hydrolyzing poly(ethylene-co-vinyl acetate). The commercially developed EVAL is available in different compositions according to the vinyl alcohol content (55-70 mol %) (Aucejo et al., 1999; Kenawy et al., 2003). EVAL has a melting point (T_m) ranging from 170-190 ^oC, which is determined by the vinyl alcohol content. The glass transition temperature (T_g)

ranges from 45-50 ºC. The presence of -OH will help the polymer to absorb water via hydrogen bonding (Aucejo et al., 1999). The vinyl alcohol repeats provide hydrophilicity to the fibers generated from EVAL but the ethylene repeats make it water insoluble. The hydroxyl functionalities in the polymer provide opportunities for secondary functionalization before or after fabrication (Kenawy et al., 2003). The EVAL is considered biocompatible and the studies of Young et al claim that EVAL membranes (porous) are suitable for neuronal cultures (Young et al., 2001).

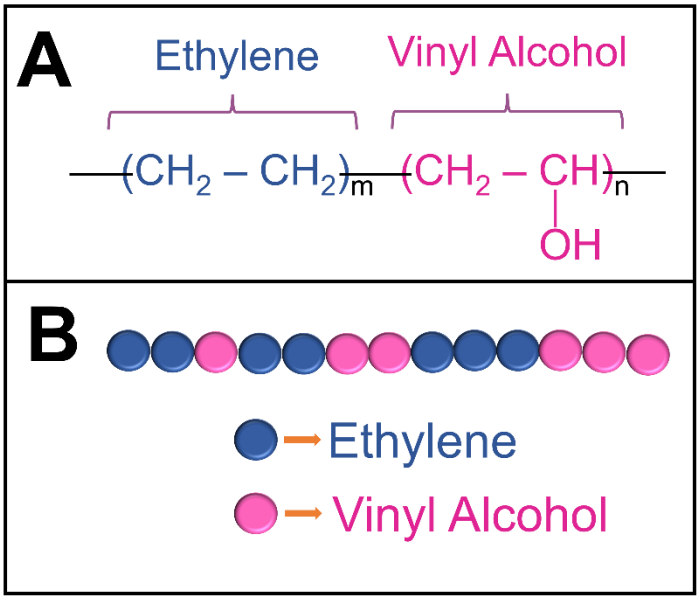

Figure 10: (A) Chemical structure of EVAL. **(B)** Random copolymer structure of EVAL.

Dimethyl sulfoxide and a mixture of isopropyl alcohol (isopropanol or 2-propanol; IPA) and water are the solvents commonly used for dissolving EVAL. It is claimed that using IPA:water mixture as the solvent to dissolve EVAL would help to generate a substrate or disinfected scaffold. So, studies propose that EVAL could be directly electrospun to the wounds (Kenawy et al., 2003). The attempt made by Mayuri et al. to generate unidirectionally aligned yarns from EVAL (Mayuri and Ramesh, 2016)

points out that it is possible to generate anisotropic substrates from EVAL which will be useful in constructing nerve guides. The easiness of EVAL solution preparation and electrospinning makes it more convenient to generate fibrous substrates for developing neural repair scaffolds.

2.11. Silver nitrate ($AgNO_3$)

$AgNO_3$ is an inorganic compound with silver ions (Ag^+) and nitrate (NO_3^-). In an approach, Mayuri et al have generated uniaxially aligned yarns from silver incorporated EVAL. The silver incorporation increased the solution conductivity and produced a highly stable jet, that followed a straight path (Mayuri and Ramesh, 2016). Alon et al. studied neuronal growth on substrates sputtered and coated with Ag, and AgNPs respectively. The study revealed that both substrates induced the cells to sprout a large number of neurites from the soma (Alon et al., 2014).

2.12. Graphene oxide (GO)

Among the graphene derivatives, GO is the nanomaterial that is used to increase the surface quality of the substrates and due to that, it induces neuronal cell proliferation (Chiacchiaretta et al., 2018; Zhang et al., 2016). GO has been widely used in tissue engineering and bioprinting (Kang et al., 2017). The presence of hydrophilic groups, large surface area, topographical features, and other physico-chemical properties have been given special attention by the research world to GO (Rahman et al., 2023). Thampi et al. in their study when they incorporated the GO in polyurethane electrospun fibrous matrices found the mechanical properties were improved (Thampi et al., 2020). Several studies showed that cell adhesion, growth, proliferation, migration, etc increased for neuronal and non-neuronal cells (Thampi et al., 2020; Wang et al., 2019;

Zhang et al., 2020). Qian et al. constructed nerve guidance conduits from integration molding by incorporating GO in polycaprolactone scaffolds. After the in vitro and in vivo studies, they found the GO/PCL scaffolds performed similarly to autografts. The morphological and functional restoration of a long nerve defect was achieved (Qian et al., 2018). Fang et al. developed neural repair scaffolds with gelatin methacrylyol/polycaprolactone hybrid nanofibers including reduced GO which performed well as a nerve repair scaffold (Fang et al., 2020).

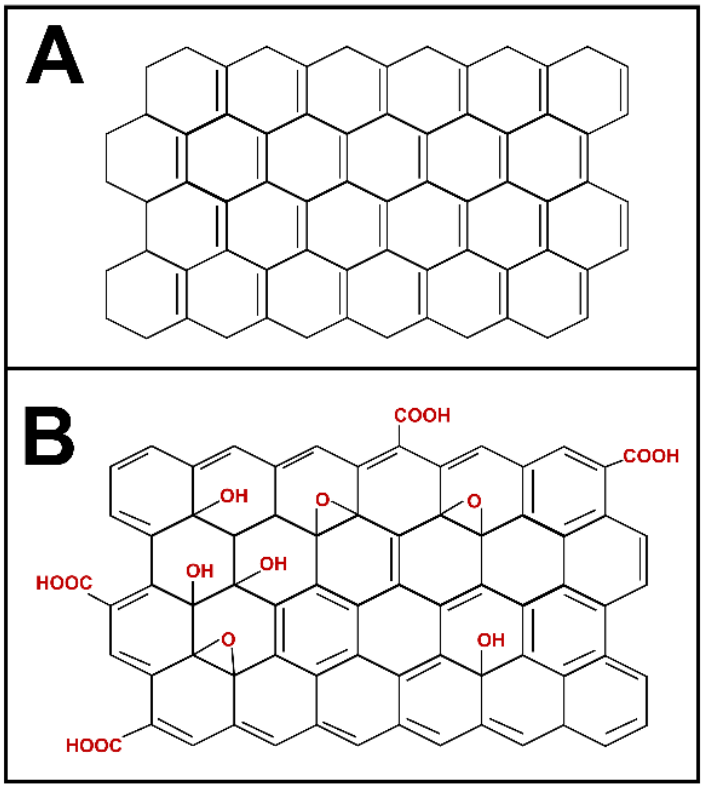

Figure 11: (A) Graphene and **(B)** Graphene oxide.

2.13. Scope and Objective of the Present Work

Researchers have done several studies to develop nerve repair scaffolds (NGC/NWs) to support nerve regeneration post-injury. The researchers have focused on different aspects of fabricating the scaffolds based on features such as topographical cues,

porosity, degradability, suturing properties, flexibility, cell or growth factor incorporation, etc. A second generation of NGC/NWs that are FDA-approved are just tubular constructs. The third-generation NGC/NWs with the previously mentioned features are still far from FDA approval. In such a scenario, here we have attempted to fabricate a scaffold from EVAL that could orient the cells and neurites in an aligned manner with the influence of its topographical cues. EVAL is a biocompatible polymer that supports neuronal cell growth (Young et al., 2001). It is also possible to generate aligned yarns from EVAL (Mayuri and Ramesh, 2016). This scaffold fabrication is the first step to constructing a substrate that has the potential to act as an NGC/NWs. The scaffold will be subjected to further studies in the future to develop it as an NGC/NWs.

- So, the above-mentioned knowledge led to a hypothesis,

  "Would electrospun matrices with aligned fibers fabricated from Ethylene vinyl alcohol copolymer be a suitable substrate for neuronal alignment?"

- The objectives to test the hypothesis are as follows:
  1. To fabricate electrospun matrices incorporated with silver ions and/or graphene oxide.
  2. To evaluate the physico-chemical properties of the matrices.
  3. To evaluate the cell-material interactions *in vitro*.
     - Evaluation of cytotoxic effects of the matrices *in vitro.*
     - Evaluation of guided neurite extension based on cell and neurite response on fibers of the matrices.

The first objective was formulated based on the pieces of literature. $AgNO_3$, an inorganic salt increases the conductivity of the solution and induces the production of

aligned yarns (Mayuri and Ramesh, 2016). Ag-sputtered and AgNP-coated substrates increase neurite outgrowth from the soma (Alon et al., 2014). GO was incorporated into the study by considering its biocompatible properties. GO enhances the Schwann cell functions during peripheral nerve regeneration (Wang et al., 2019). Morphological and functional restoration of the nerve after regeneration is possible through neural scaffolds prepared by incorporating GO (Qian et al., 2018). GO also improves the mechanical properties of a polymer (Thampi et al., 2020). Three different systems were fabricated. The systems are (1) EVAL matrices with only GO, (2) EVAL matrices with only $AgNO_3$, and (3) EVAL matrices with $AgNO_3$ and GO.

The second objective was formulated to evaluate the physico-chemical properties of the matrices. The second objective evaluates the presence and chemical changes that occur due to the incorporation of $AgNO_3$ and GO in the EVAL. The morphological differences that might occur due to the incorporation of $AgNO_3$ and GO in the electrospun fibers. The mechanical properties of the matrices fabricated with $AgNO_3$ and GO are evaluated.

The third objective was formulated to assess the cell viability after the interaction with the EVAL systems. It also evaluates the cell-material interaction based on the cellular and neurite response to the fibers.

CHAPTER 3: MATERIALS AND METHODS

3.1. Materials

The materials and solvents used for the study are given in Table 2.

Table 2: Materials and solvents used in the study

Sl. No.	Name of the material/chemical/reagent	Grade/Specifications	Source
1.	Antibiotic-antimycotic solution (100x)	Contains 10,000 units of Penicillin, 10,000 µg of Streptomycin, and 25 µg of Amphotericin B in a 0.85 % saline solution. Effective against bacteria, fungi, and yeast.	Genetix, Cell Clone, India
2.	DAPI	Solution	Santa Cruz Biotechnology, USA
3.	Disodium hydrogen phosphate (Na_2HPO_4)	Anhydrous for analysis EMSURE®, ACS reagent Ph Eur	Merck, India
4.	Dulbecco's Modified Eagle Medium (DMEM)	With high glucose L-glutamine and sodium pyruvate	Himedia, India
5.	Ethylene Vinyl Alcohol copolymer (EVAL)	38 mol% ethylene content	Sigma Aldrich, USA
6.	Fetal Bovine Serum (FBS)	South American Origin	Genetix, Cell Clone, India
7.	Fluorescein diacetate (FDA)	Powder	Merk-Sigma, Germany
8.	Goat anti-mouse IgG antibody	Goat pAb to Ms IgG-Alexa Fluor® 488	Abcam, USA
9.	Graphite	Powder (< 20 µm)	Sigma Aldrich, Switzerland
10.	Hydrogen peroxide (H_2O_2)	For analysis EMSURE® ISO	Merk, India
11.	Isopropanol (Isopropyl alcohol or 2-propanol)	ACS reagent; ≥ 99.0 %	Merck, India
12.	Live/Dead Assay Kit	Double stain apoptosis detection kit, (Acridine orange/Ethidium bromide)	Origin Lab, India
13.	Mouse anti β III Tubulin antibody	Ms mAb to Beta III Tubulin	Abcam, USA

14.	MTT reagent	Study of cell and mitochondrial health	Himedia, India
15.	Nerve growth factor (NGF)	β-NGF, murine recombinant, lyophilised solid (20 µg)	Sigma Aldrich, USA
15.	Paraformaldehyde (PFA)	Reagent grade, crystalline	Sigma Aldrich, USA
16.	Potassium chloride (KCl)	For analysis EMSURE® ISO	Merck, India
17.	Potassium dihydrogen phosphate (KH_2PO_4)	For analysis EMSURE® ISO	Merck, India
18.	Potassium permanganate ($KMnO_4$)	For analysis EMSURE® ISO	Merk, India
19.	Propidium iodide (PI)	Powder	Himedia, India
20.	Rhodamine Labelled Phalloidin	Invitrogen	Thermo Fisher Scientific
21.	Sodium chloride	EMSURE®	Merck, India
22.	Sodium nitrate ($NaNO_3$)	Reagent plus® ≥ 99.0 %	Sigma Aldrich, India
23.	Silver nitrate ($AgNO_3$)	ACS reagent; ≥ 99.0 %	Sigma Aldrich, USA
24.	Sulphuric acid (H_2SO_4) conc.	ACS reagent; 95.0 – 98.0 %	Merck, India
25.	Triton X 100		
26.	Trypsin-EDTA 0.25 % solution	Contains 0.05 % Trypsin and 1 mM EDTA in Hank's Balanced Salt Solution without calcium and magnesium sterile filtered Porcine parvovirus and mycoplasma tested.	Himedia, India

3.2. Methods

3.2.1. Graphene oxide (GO) synthesis and its dispersion

Graphite powder was subjected to reactions based on a modified Hummer's method to obtain graphene oxide. A glass vessel was kept in an ice bath and concentrated H_2SO_4 (18 M) was added to it. Under vigorous stirring, graphite powder (5g) and $NaNO_3$ (2.5 g) were added into the flask to react with H_2SO_4. The reaction setup was maintained in an ice bath to prevent the reaction temperature from exceeding 20 ºC. Next, the

reaction was added with $KMnO_4$ (15 g) with extreme care due to the exothermic nature of the reaction. After adding $KMnO_4$, the ice bath was removed and the reaction setup was transferred to an oil bath. The reaction was then continued at 35 ºC for 30 minutes. After 30 minutes, the reaction mixture was mixed with distilled water (230 mL) and continued the reaction at 35 ºC for another 30 minutes. The temperature was then slightly raised to 85 ºC and the reaction was continued for 45 minutes. Under vigorous stirring distilled water and 30 % H_2O_2 were added to terminate the reaction at 50 ºC. After completing the reaction, a brown colour suspension was obtained. This suspension settles as a slurry when kept undisturbed. This suspension was washed continuously until the slurry reaches a neutral pH (6 or above). Upon attaining the neutral pH, the slurry was filtered and vacuum-dried.

The dried GO obtained was then powdered using a motor and pestle and sieved through a sieve of mesh size 75 microns. The fine powder obtained was stored for further use. The required concentration of GO suspension was prepared by dispersing the GO powder in distilled water using ultrasonication.

3.2.2. Physico-chemical characterization GO

3.2.2.1. Raman spectral analysis of graphite and GO

Raman spectral analysis is a commonly preferred characterization method for carbon compounds. The conversion of graphite to graphene oxide was evaluated from Raman spectroscopy (Confocal Raman Microscope, alpha 300A, Witec Inc. Germany). The instrument was calibrated with the silicon calibration standard before the experiment. The samples were kept on the microscope table and observed using a 20 x objective.

The sample was excited with a 523 nm laser and the spectra were recorded. The integration time was 2s and the grating was 600 lines/mm.

3.2.2.2. Fourier Transform Infrared spectral analysis of graphite and GO

Fourier Transform Infrared spectra were obtained from FTIR; Thermo Fisher Scientific FTIR Spectrometer, Nicolet 5700 Model (USA) to evaluate the chemical groups appearing in graphite and GO. The analysis was done using the Attenuated Total Reflectance (ATR) method. Samples were in the form of powder. The spectra were recorded in the range of 4000 – 400 cm^{-1}.

3.2.2.3. X-ray diffraction (XRD) spectral analysis of GO

XRD analysis was done for GO with Bruker D8 Advance diffractometer (Germany) to confirm the formation of GO from graphite.

3.2.3. Solution preparation

3.2.3.1. Solution preparation of EVAL-neat

EVAL pellets were dissolved in IPA and water mixture (7:3) at 70 ºC to get 9 % EVAL solution (w/v) and were designated as EVAL-neat. For example, 0.9 g of EVAL pellets were dissolved in 10 mL IPA:water (7 mL:3mL respectively) mixture at 70 ºC under gentle stirring.

3.2.3.2. Solution preparation of EVAL-GO

EVAL pellets were dissolved in IPA:water mixture. Meanwhile, the required amount of GO was dispersed in distilled water and added to the EVAL solution. This solution is designated as EVAL-GO. The concentration of EVAL in the whole solution was 9 % (w/v). According to the concentration of GO, three different solutions were

prepared. (1) EVAL-GO-0.01 [EVAL was 9 % (w/v) and GO was 0.01 % (w/v)], EVAL-GO-0.05 [EVAL was 9 % (w/v) and GO was 0.05 % (w/v)], and EVAL-GO-0.1 [EVAL was 9 % (w/v) and GO was 0.1 % (w/v)].

Example; To prepare a 20 mL EVAL-GO-0.01 solution, 1.8 g of EVAL pellets are dissolved in 14 mL IPA and 3 mL water mixture at 70 ºC. Meanwhile, 0.002 g of GO was dispersed in 3 mL water by sonication. This 3 mL dispersed GO is then added to the EVAL solution and stirred for 1 h. Thus, 20 mL of 9 % (w/v) EVAL with 0.01 % (w/v) GO was obtained.

3.2.3.3. Solution preparation of EVAL-Ag

EVAL pellets were dissolved at 70 ºC in IPA: water mixture. After the complete dissolution of EVAL pellets, the required quantity of $AgNO_3$ was added to the solution. According to the concentrations of $AgNO_3$, five different solutions were prepared. EVAL-Ag-0.01 [0.01 % (w/v) $AgNO_3$], EVAL-Ag-0.05 [0.05 % (w/v) $AgNO_3$], EVAL-Ag-0.1 [0.1 % (w/v) $AgNO_3$], EVAL-Ag-0.2 [0.2 % (w/v) $AgNO_3$], and EVAL-Ag-0.3 [0.3 % (w/v) $AgNO_3$].

Example; To prepare a 20 mL EVAL-Ag-0.01 solution, 1.8 g of EVAL pellets are dissolved in 14 mL IPA and 3 mL water mixture at 70 ºC. After the complete dissolution of EVAL pellets, 0.002 g of $AgNO_3$ was dissolved in 3 mL of water. The $AgNO_3$ solution was added to the EVAL solution and stirred for 1 h. Thus, the 20 mL solution will have 9 % (w/v) EVAL with 0.01 % (w/v) $AgNO_3$ in the whole solution.

3.2.3.4. Solution preparation of EVAL-Ag-GO

EVAL pellets were dissolved in an IPA and water mixture. First $AgNO_3$ was introduced into the EVAL solution, then the GO dispersion was added to get the EVAL-Ag-GO solution. Three different compositions of EVAL-Ag-GO solutions were prepared. In all the EVAL-Ag-GO compositions, EVAL was 9 % (w/v), and $AgNO_3$ was 0.01 % (w/v). The GO content in this system was 0.01 % (w/v), 0.05 % (w/v), and 0.1 % (w/v) in EVAL-Ag-GO-0.01, EVAL-Ag-GO-0.05, and EVAL-Ag-GO-0.1 respectively.

Example; To prepare a 20 mL EVAL-Ag-GO-0.01 solution, 1.8 g of EVAL pellets are dissolved in 14 mL IPA and 3 mL water mixture at 70 ºC. After the complete dissolution of EVAL pellets, 0.002 g of $AgNO_3$ was added to the EVAL solution and stirred for 1 h. This solution is EVAL-Ag solution. Meanwhile, 0.002 g of GO was dispersed in 3 mL of water by sonication. This dispersed GO was then added to the EVAL-Ag solution and stirred for another 1 h. Thus, the 20 mL solution will have 9 % (w/v) EVAL, 0.01 % (w/v) $AgNO_3$, and 0.01% GO in the whole solution. Table 3 shows all the solution compositions and designations.

3.2.4. Viscosity analysis of EVAL-Ag system

The solution viscosity of EVAL solutions with different concentrations of $AgNO_3$ was analyzed with a rolling ball micro viscometer (Lovis 2000 M/ME, Anton Par, USA), at 28 ºC. The instrument was set with an auto-angle measurement. The 2.5 capillary was used to measure the viscosity of the samples. The sample solution (1 mL) was weighed to calculate the sample density. The following equation was used to calculate the density:

$$\textbf{Density} = \textbf{Mass/Volume}$$

Table 3: Composition of EVAL with either silver nitrate or graphene oxide and both solutions.

Sl. No.	Solution designation	Solution composition		
		EVAL (%) (w/v)	$AgNO_3$ (%) (w/v)	GO (%) (w/v)
1	EVAL-neat	9	-	-
2	EVAL-GO-0.01	9	-	0.01
3	EVAL-GO-0.05	9	-	0.05
4	EVAL-GO-0.1	9	-	0.1
5	EVAL-Ag-0.01	9	0.01	-
6	EVAL-Ag-0.05	9	0.05	-
7	EVAL-Ag-0.1	9	0.1	-
8	EVAL-Ag-0.2	9	0.2	-
9	EVAL-Ag-0.3	9	0.3	-
10	EVAL-Ag-GO-0.01	9	0.01	0.01
11	EVAL-Ag-GO-0.05	9	0.01	0.05
12	EVAL-Ag-GO-0.1	9	0.01	0.01

3.2.5. UV-Visible spectral analysis of EVAL-Ag and EVAL-Ag-GO systems

Spectral analysis was performed in a UV spectrophotometer (UV-1800 240 Shimadzu, Japan). $AgNO_3$ solution, EVAL-Ag-0.01, and EVAL-Ag-GO-0.01 solutions were considered for the spectral analysis. A small portion of EVAL-Ag-0.01 and EVAL-Ag-GO-0.01 matrices were re-dissolved in an IPA:water mixture to prepare their corresponding solutions. 3 mL IPA: water mixture was used as the blank.

3.2.6. Conductivity analysis of EVAL solutions

The solution conductivity of EVAL-neat, EVAL-Ag, and EVAL-Ag-GO systems was measured with a conductivity meter (Thermo Scientific, Orion Star A215, USA).

3.2.7. Electrospinning of EVAL matrices

An electrospinning unit that had a syringe pump (KD Scientific pump), a high-voltage power (Zeonics Systech, India) supply, and a collector (rotating metal drum) was arranged. A 20 mL syringe fitted with a blunt-ended needle (18 gauge) was filled with the polymer solution. The polymer-fed syringes were placed on the syringe pump in such a way that the distance between the needle tip and the collector was 10-15 cm. The needle and collector were given the positive and negative potential of the high-voltage power supply, respectively. The collector rotated at 500 rpm, the flow rate of solution was 5 mL/h, and the voltage supplied was 20 kV. The fibers collected on the drum collector were later peeled off. Electrospinning parameters are mentioned in Table 4.

Table 4: Electrospinning parameters

Sl. No.	**Parameters**	
1	Flow rate	5 mL/h
2	Applied voltage	20 kV
3	Drum rotation speed	500 rpm
4	Distance between the needle and collector	10-15 cm
5	Syringe Needle	18 Gauge

3.2.8. Fourier Transform Infrared Spectroscopy (FTIR)

The chemical nature of the matrices was evaluated from the spectral images obtained from Fourier Transform Infrared Spectroscopy (FTIR: Thermo Fisher Scientific FTIR Spectrometer, Nicolet 5700 Model, USA). The analysis was done using the attenuated

Total Reflectance (ATR) method. Samples were in the form of electrospun sheets. The spectra were recorded in the range of 4000 – 400 cm^{-1}.

3.2.9. Raman spectral and imaging analysis of EVAL-GO and EVAL-Ag-GO systems

Raman spectroscopy (Confocal Raman Microscope, alpha 300A, Witec Inc. Germany) was employed to analyze the presence of GO in EVAL-GO and EVAL-Ag-GO matrices.

After recording single spectra, a required area of EVAL-GO samples was selected for chemical mapping. Chemical mapping was done in an area of 100 x 100 sq. microns with a resolution of 80 points and 80 lines. The integration time used was 0.5 s. The scan data was subjected to cluster analysis using Witec Project Plus software to identify the different chemical clusters available in the scan area of interest. Individual clusters identified were assigned false colours and the scan data was mapped.

3.2.10. Energy Dispersive X-ray (EDX) Spectroscopy analysis of EVAL-Ag matrix

The presence of silver in the fibers of the EVAL-Ag matrix was detected by Energy Dispersive X-ray (EDX) Spectroscopy, performed by Quanta 200 Environmental SEM (FEI Company, Netherlands). Since EVAL-Ag-0.3 had the highest amount of $AgNO_3$, it was considered for the analysis.

3.2.11. X-ray Photon Spectroscopy (XPS) of EVAL-Ag and EVAL-Ag-GO matrices

A piece of the EVAL-Ag-0.01 and EVAL-Ag-GO-0.01 matrices were subjected to XPS analysis performed by Thermo Scientific™ ESCALAB™ Xi+ to investigate the presence of silver and its oxidation state.

3.2.12. Scanning Electron Microscopy (SEM) EVAL matrices

The fiber morphology and its orientation in the matrices were evaluated from SEM images captured from Quanta 200 Environmental SEM (FEI Company, Netherlands), with an accelerating voltage of 15 kV. The images were also used to analyze the diameter and orientation of the fibers with the assistance of ImageJ software.

3.2.13. Mechanical Properties of EVAL matrices

The mechanical performances of the matrices were evaluated with a Universal Testing Machine (UTM; Instron, model 3345, single column, UK) with a 100 N load cell. The tests were done with a crosshead speed of 10 mm min^{-1} at an ambient temperature. A die cutter (ISO-527-2 type-5B) was used to punch out the micro dumbbells (15 mm length and 2 mm width). A minimum of six specimens from each matrix were considered for the test.

3.2.14. Optical Emission Spectroscopy with Inductive Coupled Plasma (ICP-OES) analysis of EVAL-Ag and EVAL-Ag-GO matrices

The amount of silver in the matrices and the extracts prepared in PBS were analyzed with Optical Emission Spectroscopy with Inductive Coupled Plasma (ICP-OES: Perkin Elmer OES-ICP, Model: 5300DV). The EVAL-Ag-0.01 matrix, EVAL-Ag-

GO-0.01 matrix, and extracts collected after 24 h and one week from both the matrices were analyzed in ICP-OES.

The EVAL-Ag-0.01 matrix used as such for ICP weighed about 0.025 g, and the matrices kept for 24 and 1-week extraction weighed about 0.023 g and 0.023 g respectively. The EVAL-Ag-GO-0.01 matrix used as such for ICP weighed 0.016 g and the matrices considered for 24 h and 1-week extraction weighed 0.014 g and 0.013 g respectively. The intention of considering both the matrices and extracts for the analysis was to evaluate whether the silver in the matrices was released completely into the medium after a particular period.

3.2.15. Cell culture

In vitro evaluations of the EVAL-Ag matrices were done with L-929, N2a, C6, and PC12 cell lines. The L-929, N2a, and C6 cell lines were cultured in DMEM complete media [DMEM media, 10 % FBS, and 1 % antibiotic (penicillin and streptomycin)] at 37 ^{o}C, with 5 % CO_2 and 95 % relative humidity in a CO_2 incubator. Upon 75 % confluency, the cell monolayers were sub-cultured. 0.25 % Trypsin-0.02 % EDTA solution was used to harvest the cell monolayers. The culture of PC12 cells is described in section 3.2.23.

3.2.16. IC 50 analysis

An IC 50 evaluation of the $AgNO_3$ solution was carried out in L-929 cells. Cells were seeded in a 96-well culture plate where the seeding density was 5000 cells/well. After a 24 h incubation, a stock concentration of $AgNO_3$ solution was made in distilled water, and serial dilutions were prepared in DMEM complete media just before the addition

to the wells. The cells were then exposed to the serially diluted $AgNO_3$ solution for 24 h in a CO_2 incubator. 20 µL MTT (5 mg/mL in PBS) was added to all the wells and 4 h incubation was given. After 4 h, the existing media was removed and 100 µL DMSO was added to each well to dissolve formazan. Absorbance was measured at 570 nm and the percentage cell viability was calculated as per the following equation.

$$\%\ \boldsymbol{Cell\ activity} = \frac{\boldsymbol{OD\ of\ Test}}{\boldsymbol{OD\ of\ Control}} \times \mathbf{100}$$

3.2.17. Direct contact test

Based on ISO 10993-5 guidelines, a direct contact test was conducted to evaluate the cytotoxic effects of the EVAL matrices. The test was conducted on a 48-well culture plate. The L-929 cells were seeded in each well with a cell density of 5000 cells. The cell seeding was followed by incubation with DMEM complete media in a CO_2 incubator. The cells upon reaching the sub-confluent population, the materials were placed in the wells. 4 mm discs of each material in triplicates were tested. The discs of Tin compound-incorporated polyvinyl chloride (Tin-PVC) and Ultra-high molecular-weight polyethylene (UHMWPE) were the positive and negative controls respectively. A 24 h incubation was provided in a CO_2 incubator and the cytotoxicity assessment was done by observing the cells and capturing their images with a phase-contrast microscope (Leica DMI 3000; Germany).

3.2.18. MTT assay

The effect of EVAL-GO, EVAL-Ag, and EVAL-Ag-GO matrix extracts on the metabolic activity of L-929 cells was studied by conducting an MTT assay. The extracts were prepared by placing the matrices (dimension: 15 mm x 20 mm) in

DMEM complete media for 72 h. Meanwhile, the cells were seeded in a 96-well culture plate where each well had 5000 cells and incubated in a CO_2 incubator. When the wells became sub-confluent, existing media was removed and extracts were added. Two different concentrations of extracts were used, (1) undiluted (100 % extract), and (2) 50 % diluted (50 % extract and 50 % fresh media). The designations of undiluted and diluted extracts are given in Table 5.

Table 5: Designations given to extracts of electrospun matrices for conducting MTT assay.

Sl. No.	Matrix	Designation	
		Undiluted	50 % diluted
1	EVAL-GO-0.01	EVAL-GO-0.01 100	EVAL-GO-0.01 50
2	EVAL-GO-0.05	EVAL-GO-0.05 100	EVAL-GO-0.05 50
3	EVAL-GO-0.1	EVAL-GO-0.1 100	EVAL-GO-0.1 50
4	EVAL-Ag-0.01	EVAL-Ag-0.01 100	EVAL-Ag-0.01 50
5	EVAL-Ag-GO-0.01	EVAL-Ag-GO-0.01 100	EVAL-Ag-GO-0.01 50

Wells provided only with DMEM complete media were considered to be the negative control. The wells added with phenol (13 mg/mL) to the culture medium were positive control. The cells under treatment were incubated for 24 h in a CO_2 incubator. Following the 24 h incubation, 20 µL MTT (5 mg/mL in PBS) was added to all the wells and 4 h incubation was given. After 4 h, the existing media was removed and 100 µL DMSO was added to each well to dissolve formazan. Absorbance was measured at 570 nm and the percentage cell viability was calculated as per the following equation.

$$\% \, Cell \, activity = \frac{OD \, of \, Test}{OD \, of \, Control} \times 100$$

3.2.19. Viability assessment of N2a and C6 cells with EVAL systems

The extracts of EVAL matrices (mentioned in section 3.2.18) were collected and were used for live/dead assay. The cells cultured in a 48-well culture plate with a seeding density of 1 x 10^4 cells/well were exposed to the 72 h extracts for 24 hours in a CO_2 incubator. A control well was considered in which the cells were left untreated. Then the viability of the cells was qualitatively evaluated by adding Acridine orange/Ethidium bromide (AO/EtBr) live/dead stain (prepared according to the manufacturer's protocol). A fluorescence microscope (Leica DMI 3000; Germany) was used to observe and capture the images.

A quantitative assessment regarding the viability of C6 glioma cells was carried out using flow cytometry (Flow Cytometer, Beckman Coulter, Cytoflex). The C6 cells were cultured in a 6-well plate with a cell density of 1 x 10^5 cells/well for 24 h. The test wells were treated with EVAL-GO, EVAL-Ag, and EVAL-Ag-GO extracts (72 h extracts prepared as per section 3.2.18) for 24 h. Three wells were considered as controls. Among them, two wells were kept untreated and considered as negative controls. One well was treated with a toxic chemical (0.1 % Triton X-100) to induce cell death and was considered a positive control. After the treatment period, the cells were trypsinized and transferred to 1 or 2 mL centrifuge vials. The vials with cell suspension were centrifuged and the supernatant was decanted. One negative control was kept unstained and was used to count the total number of cells. The other negative control was stained with the Fluorescein diacetate (FDA) alone. The positive control was stained with Propidium iodide (PI) alone. The cell pellets of the tests were stained

with FDA/PI. The staining was done for 2 minutes and all the vials (controls and tests) were subjected to flow cytometry.

3.2.20. N2a and C6 cell response on EVAL matrices

The cells (N2a and C6) were cultured on the EVAL matrices to investigate the cell and neurite orientation. The cells were also cultured on an EVAL-neat matrix and tissue culture plate (TCP; control). The matrices and the TCP surfaces were seeded with cells with a seeding density of 7 x 10^3 cells/cm^2. A 30 min incubation in a CO_2 incubator was given for the cells to settle and adhere properly to the surfaces. The DMEM complete media was added to the wells after 30 min and incubation was continued for 72 h.

Followed by 72 h of incubation, the cells on the surfaces (matrices and TCP) were fixed with 4 % PFA for 15 min. The PFA was removed and PBS wash (3 times) was given. A 2-3 min treatment with 0.1 % Triton X-100 was given to cells to permeabilize them. Then a PBS wash (3 times) was given to remove the Triton X-100. The F-actin of cells was stained overnight with Rhodamine-labelled Phalloidin (1 µL stock) diluted in PBS (40 µL stock). The unreacted stain was washed away with PBS (3 times). The nucleus of the cells was counter-stained with DAPI (4', 6-diamidino-2-phenylindole) with a concentration of 0.5 µg/mL in PBS. The cellular and neurite arrangements were visualized and images were captured using a fluorescence microscope (Leica DMI 3000; Germany).

The N2a cells cultured on the matrix surfaces were also subjected to immunostaining to evaluate the neurite arrangement. The neuronal marker β III tubulin was targeted for staining with antibodies to evaluate the neurite orientation. Following the cell fixation

and permeabilization (described previously), the cells were blocked with freshly prepared blocking solution [1 % BSA; prepared in PBS with Tween (PBST; 0.1%) and glycine (22.52.mg/mL)] for 10 min and PBS wash (3 times) was given. The cells were incubated overnight with mouse anti-β III tubulin (primary antibody) with a dilution of 1:100. After incubation a PBS wash (3 times) was given to wash away the unbound antibody. A secondary antibody, a Goat anti-mouse antibody tagged with Alexa Fluor 488 with a dilution of 1:100 was allowed to react with the cells for 1 h. The cells were then washed with PBS (3 times) and the nucleus was counter-stained with DAPI (0.5 µg/mL in PBS). A fluorescence microscope (Leica DMI 3000; Germany) was used to capture the images.

3.2.21. N2a and C6 cell adhesion on EVAL-Ag-GO matrix

The cell adhesion (N2a and C6 cells) on the fibers of the EVAL-Ag-GO matrix was evaluated from SEM analysis. The cell-seeded EVAL-Ag-GO matrix after 72 h incubation was fixed with 4 % PFA (overnight), and washed with PBS (3 times). The dehydration of the wet matrices was done with ethanol of concentrations 30 %, 50 %, 70 %, 90 %, and 100%. Each concentration was considered twice. The matrices were immersed in 30 %, 50 %, and 70 % for 15 minutes each and 90 and 100 % for 30 min each. The dehydrated samples were used for SEM analysis.

3.2.22. Spatial response of PC12 cells on EVAL-Ag and EVAL-Ag-GO matrices in response to NGF

PC12 cells are model cell lines used very often in neurite extension studies. These cells are small, irregularly shaped (~ 8-10 µm size), and loosely attached cells which are usually found as floating clusters. These cells were cultured in a complete media which

consists of RPMI 1640 media, 10 % horse serum, 5 % Fetal bovine serum, and 1 % antibiotic-antimycotic solution. These cells manifest neurite extension like a peripheral neuron only in the presence of NGF. So, the spatial response of PC12 cells to the fibers of EVAL-Ag and EVAL-Ag-GO matrices was evaluated in the presence of NGF-supplemented media.

The PC12 cells harvested from the culture flask were seeded on TCP surface (control), EVAL-Ag, and EVAL-Ag-GO matrices. The cells were seeded with a density of 7 x 10^3 cells/cm^2 and incubated for 30 min. The RPMI 1640 complete media was added to the wells and incubated in a CO_2 incubator at 37 ºC and 5 % CO_2 for 24 h. The cell-seeded day was considered as day 0. On days 1, 3, 5, and 7 the media was replaced with RPMI1640 media having 100 ng/mL NGF. On the 8^{th} day, the cells were fixed with 4 % PFA for 15 min, permeabilized with 0.1 % Triton X-100 for 2-3 min, and blocked [1 % BSA; prepared in PBS with Tween (PBST; 0.1%) and glycine (22.52.mg/mL)] for 10 min. PBS wash (3 times) was given after each step. Incubated with mouse anti-β III tubulin antibody (primary antibody; 1:100 dilution) overnight and then with goat anti-mouse Alexa Fluor 488 (secondary antibody; 1:100 dilution) for 1 h. The nucleus was counterstained with DAPI with a working concentration of 0.5 µg/mL in PBS. The fluorescence images were captured from Leica DMI 3000 (Germany).

CHAPTER 4: RESULT AND DISCUSSION

4.1. Graphene Oxide: Physico-chemical characterization

Graphene oxide (GO) is a graphene derivative (Rodrigues et al., 2018; Zhang et al., 2020) that is obtained by oxidation of graphene. Graphene layers are held together by van der Waals force in graphite. So, graphite is one of the naturally occurring allotropes of carbon (Sharma et al., 2021). The oxidation reactions introduce hydroxyl, carboxy, and epoxide groups into the graphene layers and produce GO (Kim and Choi, 2015; Rodrigues et al., 2018; Wang et al., 2019). Graphene is exclusively made up of sp^2 hybridized carbon atoms and is conductive (Hansora et al., 2015; Rodrigues et al., 2018; Sharma et al., 2021; Wahab et al., 2015; Wang et al., 2018). The GO that has sp^2 and sp^3 hybridized carbon atoms covalently linked to hydrophilic groups is non-conductive (Kim et al., 2012; Sharma et al., 2021). The hydrophilic nature, large surface area, and topographical features enable the GO in cellular interactions like adhesion, proliferation, migration, and differentiation (Kanjwal and Ghaferi, 2022; Zhang et al., 2020).

4.1.1. Raman spectral analysis

Raman spectroscopy is an important technique for characterizing carbon allotropes (carbon nanotubes; CNT, graphite, fullerenes, etc.) (Sharma et al., 2021). It is also employed in characterizing graphite and its derivatives. Raman spectroscopy helps to evaluate the nature of the carbon allotropes and their derivatives by analyzing the D (defective) and G (graphitic) bands. The G band occurs due to the sp^2 hybridized carbon forms and it represents a graphitic nature (Ranjan et al., 2018; Sharma et al., 2021). So, graphite which is exclusively made up of carbon always expresses a sharp

G band (graphitic band). Whereas, the D band appears due to the defects (imperfection, and impurities) that occurred in the graphitic nature and represents the sp^3 hybridization of carbon atoms (Ranjan et al., 2018). The imperfections and impurities in GO (oxidized graphite derivative) are functional groups like -OH, -COOH, and C-O-C (Marcano et al., 2010; Ranjan et al., 2018; Rodrigues et al., 2018; Sharma et al., 2021; Zhang et al., 2020).

The Raman spectra of graphite and GO are depicted in Figure 12A. The graphite showed a D band at 1344 cm^{-1} and a G band at 1566 cm^{-1}. The D and G bands of GO appeared at 1358 cm^{-1} and 1590 cm^{-1} respectively. The increase in the intensity of the D band of GO occurred due to the appearance of sp^3 hybridization of C atoms. The reduction in intensity of the G band indicates the decrease in sp^2 hybridized carbon atoms. Some sp^2 hybridized C atoms bond to functional groups (-OH, -COOH, and C-O-C) as a result of oxidation and become sp^3 hybridized C atoms (Marcano et al., 2010; Ranjan et al., 2018; Rodrigues et al., 2018; Sharma et al., 2021). The change occurred in D and G band intensities was reflected in the ID/IG ratio of graphite and GO. The ID/IG ratio of graphite and GO was 0.04 and 0.8 respectively. An increase in the ID/IG ratio of GO compared to graphite substantiates the formation of GO (Sharma et al., 2021; Wang et al., 2018).

4.1.2. FTIR spectral analysis

FTIR spectroscopy is an important characterization technique for analyzing graphitic derivatives. The graphite made up of carbon atoms, shows few peaks in FTIR spectra. GO, a product of graphitic oxidation contains hydroxyl, carboxyl, and epoxy groups in the graphene sheets (Marcano et al., 2010; Ming et al., 2020; Ranjan et al., 2018;

Rodrigues et al., 2018). The presence of functional groups will be reflected in the FTIR spectra of GO.

In the FTIR spectra (Figure 12B), a peak appeared at 3345 cm^{-1} due to the O-H stretching vibrations occurring in the hydroxyl and carboxyl groups (Çiplak et al., 2014; Kim and Choi, 2015; Ming et al., 2020; Ranjan et al., 2018; Rodrigues et al., 2018). The carbonyl and carboxyl (C=O) stretching vibrations were reflected from the peak at 1727 cm^{-1} (Çiplak et al., 2014; Ranjan et al., 2018; Rodrigues et al., 2018). A peak at 1635 cm^{-1} also represented C=O of carboxyl groups (Ming et al., 2020). The O-H bending vibration in C-O-H was shown by the peak at 1388 cm^{-1} (Çiplak et al., 2014). The epoxy group presence was found in the peak at 1085 cm^{-1} (Çiplak et al., 2014; Ranjan et al., 2018). The bending vibrations of alkenes were found at 917 cm^{-1}.

4.1.3. XRD analysis

XRD is a technique performed either on powder or thin films. For GO the XRD peak is usually obtained between 7 º to 12 º (2θ degree) in a plane of '001' (Ikram et al., 2020; Ranjan et al., 2018; Rattana et al., 2012; Sharma et al., 2021; Wahab et al., 2015). The XRD analysis of GO synthesized for the present work is shown in Figure 12C. In the present work, the 2θ degree of GO in XRD was 11.4 º. A 2θ corresponding to 11.4 indicates that the layer-to-layer spacing (inter-layer distance; d) between graphene oxide sheets is ~ 0.78 nm (7.8 Aº). Le et al. mentioned that the spacing in natural graphite is 0.33 nm. They also observed a similar peak at 11.4 º for GO in XRD (Le et al., 2023). The d ~ 0.78 nm also substantiates that the graphene layers are intercalated with hydroxyl. carboxyl, and epoxy functional groups (Hsiao et al., 2010; Le et al., 2023).

The oxidation of graphite to GO was thus confirmed by Raman spectroscopy, FTIR spectroscopy, and XRD analysis.

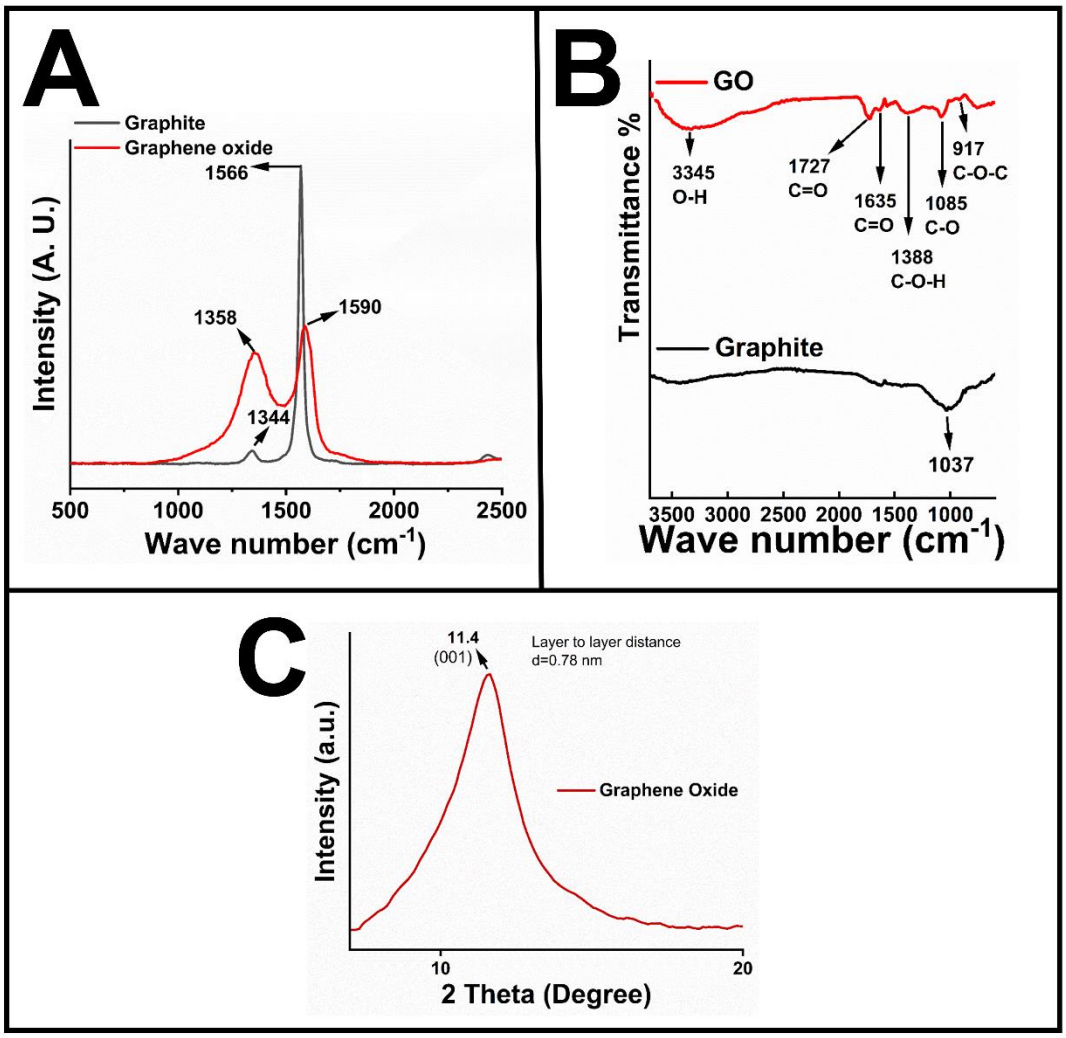

Figure 12: (A) Raman spectra of graphite and GO, **(B)** FTIR spectra of graphite and GO, and **(C)** XRD analysis of GO.

4.2. GO incorporated EVAL electrospun matrices

GO was incorporated into the EVAL solution to get EVAL-GO matrices. The incorporation of GO in polymer substrates would enhance cellular activities like cell adhesion, growth, proliferation, migration, differentiation, etc (Thampi et al., 2017, 2020; Wang et al., 2019; Zhang et al., 2020). GO incorporation also improves the mechanical properties of fibrous polymer membranes (Thampi et al., 2015).

4.2.1. FTIR spectral analysis of EVAL-GO system

Figure 13A depicts the FTIR spectra of EVAL-neat and EVAL-GO matrices. The peaks found in EVAL-neat and EVAL-GO matrices were similar with slight shifts indicating the influence of incorporated GO. The -OH stretching peak of EVAL-neat was observed in 3307 cm^{-1}. The -CH stretching vibrations of EVAL-neat were found in 2921 and 2849 cm^{-1}. A peak at 1436 cm^{-1} represented C-H bending vibrations and 1327 cm^{-1} represented C-H deformation (Mayuri et al., 2016). A C-OH stretching was observed at 1083 cm^{-1}.

All the peaks in EVAL-neat FTIR spectra also appeared in EVAL-GO but with a slight red shift (Figure 13A). The -OH peaks red-shifted to 3280 cm^{-1} in EVAL-GO matrices. The -CH stretching peaks (2921 cm^{-1} and 2849 in EVAL-neat) were red-shifted to 2894 cm^{-1} and 2828 cm^{-1} in EVAL-GO system. The C-H bending and deformation peaks were also shifted to 1409 and 1300 cm^{-1} respectively. The C-OH stretching also showed a noticeable red shift to 1056 cm^{-1}. The incorporation of GO in EVAL shifted the -OH stretching peaks (~3400 cm^{-1}) to a lower wave number. This is due to the breakage of intramolecular hydrogen bonding and the formation of intermolecular hydrogen bonding between the -OH of EVAL and oxygen-containing functional groups of GO (Yang et al., 2023).

Polyvinyl alcohol (PVA) is a polymer very similar to EVAL. The similarity is the vinyl alcohol monomer and the difference is the absence of an ethylene monomer. The GO nanosheets incorporated PVA films (GONS/PVA films) fabricated by Huang et al. also showed a similar redshift in the hydroxyl (-OH) peaks around 3600 cm^{-1} indicating the hydrogen bonding between the hydroxyl groups of PVA and oxygen-containing

functional groups of GO (Huang et al., 2012). A similar redshift was found in GO-PVA nanocomposites made by Ma et al, and Wang et al. in separate studies which strengthens the fact of disrupting intramolecular hydrogen bonding and formation of intermolecular hydrogen bonding (Ma et al., 2016; Wang et al., 2018).

4.2.2. Raman spectral analysis of EVAL-GO system

Raman spectral analysis helps to identify the presence of GO in a polymer matrix by locating two characteristic bands (D and G bands) in the polymer which occur due to the GO. The D band represents the defects in the graphite and the G band is the characteristic band of C compounds (graphite, fullerenes, carbon nanotubes). It is visible from Figure 13B (Raman spectra) that the D and G band intensities were increasing in the EVAL-GO matrices according to the rising GO content. These bands become more evident in EVAL-GO-0.1 since it is the matrix with a higher amount of GO. A peak at 1432 cm^{-1} appeared due to the CH_2 bending vibrations (similar peaks are also observed in FTIR spectra; Figure 13A) (Cooney et al., 1994). The intensity of the peaks around 2900 and 3400 cm^{-1} was diminishing. GO might have caused changes in the -CH and -OH stretching vibrations.

Similar results were obtained in the study done by Wang et al. where the GO-incorporated PVA films (PVA/GO) were fabricated. They reported that hydrogen bonding was formed between -OH and COOH of GO with -OH of the PVA. This hydrogen bonding affects the vibration movement of C-C bonds in the carbon plane. So, peak shifts were obtained for PVA/GO composites to lower wave numbers when compared to PVA films (Wang et al., 2018). The intensity reduction found in the peak around 2900 cm^{-1} (stretching vibration of -CH) in EVAL-GO matrices compared to

EVAL-neat was similar to the PVA/GO composites compared to its bare material (PVA). This reduction might be due to the CH-π interactions (Wang et al., 2018).

4.2.3. Raman imaging analysis of EVAL-GO system

The Raman images (Figure 13C) clearly show the presence and increase in GO content in the EVAL matrices as the GO in the matrices increases. The blue colour represents the EVAL fibers and the red spots indicate the GO. As the GO increased the red spots on the fibers also increased.

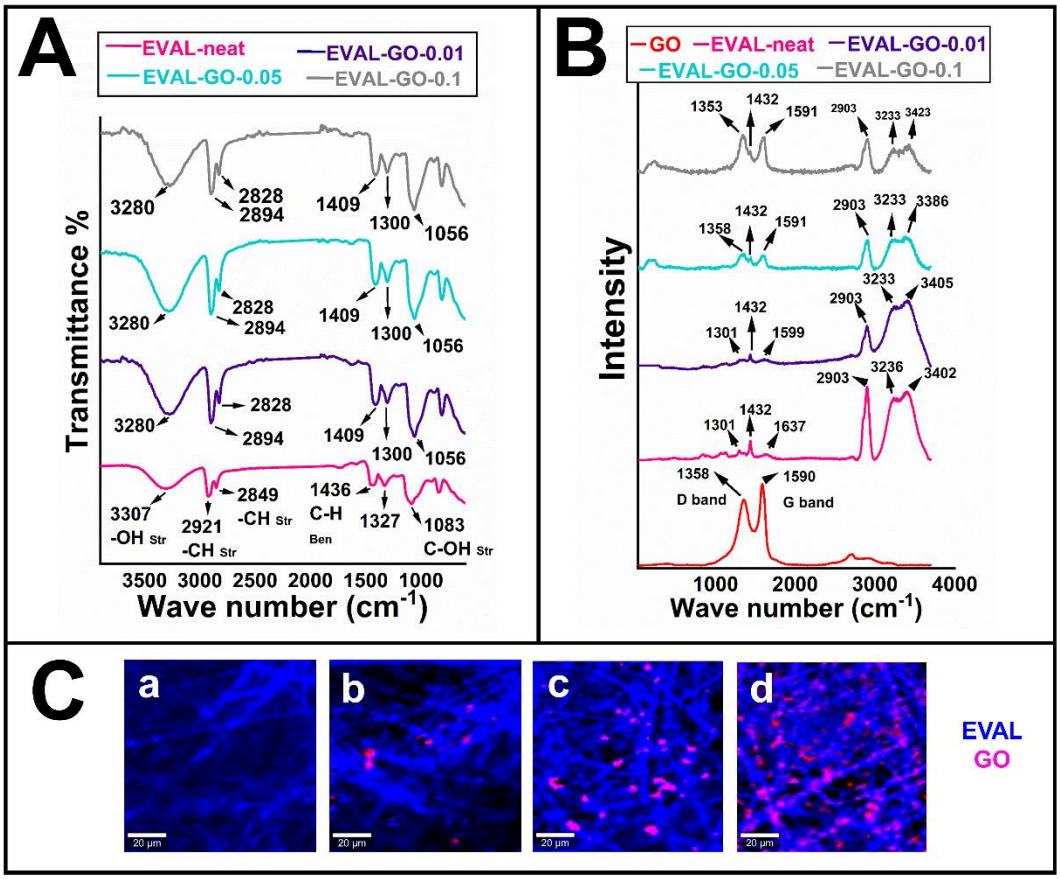

Figure 13: (A) FTIR spectra, **(B)** Raman spectra, and **(C)** Raman imaging of EVAL-GO system. **(a)** EVAL-neat, **(b)** EVAL-GO-0.01, **(c)** EVAL-GO-0.05, and **(d)** EVAL-GO-0.1. Scale bar = 20 µm

4.2.4. Fiber morphology, orientation, and diameter evaluation from SEM analysis of EVAL-GO system

The effect of an increase in GO in the EVAL matrix was evident from the appearance of the matrices (Figure 14A). As the GO content increased, the matrix became greyer. Whereas, the appearance of EVAL-neat was white. The SEM images (Figure 14B) of EVAL-neat and EVAL-GO matrices show that all had random fibers (unaligned fibers). Besides the random orientation, the fibers were beadles (EVAL-neat and EVAL-GO) and thinner (EVAL-GO). The fiber orientation analyzed using ImageJ software also confirmed the random orientation of the fibers (Figure 14C). In all the cases, the peaks representing various angles were widely distributed. So, the wide distribution of angles is due to the random fiber orientation.

The fiber diameter of the EVAL-GO system analyzed using ImageJ software is shown in Figure 15A. The fiber diameter of EVAL-neat was 1.3 ± 0.4 μm (Figure 15A). The GO incorporation into the EVAL significantly reduced the fiber diameter to < 1 μm (submicron) in EVAL-GO matrices. Mit-uppatham et al. have mentioned that any polymer solution with a decreased viscosity could generate fibers with decreased fiber diameter. In a low viscous solution, the coulombic forces overrule the viscoelastic force and the solution undergoes stretching and finally leads to the generation of thin fibers during electrospinning (Mit-uppatham et al., 2004). Here the GO intercalated within the polymer chains of the solution might be reducing the viscosity and leading to over-stretching of the jet. Ma et al. have also found that the PLLA electrospun mats with GO (PLLA/GO) had thinner fiber diameters compared to neat PLLA fibers (Ma et al., 2020).

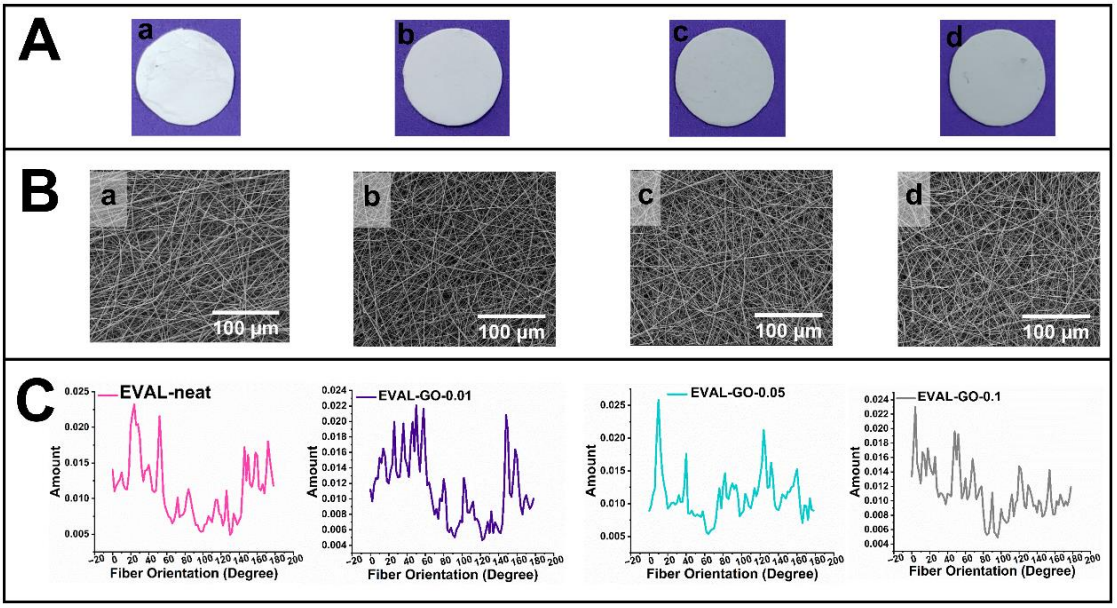

Figure 14: (A) Images of EVAL-GO matrices: **(a)** EVAL-neat**, (b)** EVAL-GO-0.01**,** EVAL-GO-0.05, **(c)** EVAL-GO-0.1. **(B)** SEM analysis of EVAL-Ag-GO system: **(a)** EVAL-neat**, (b)** EVAL-GO-0.01**,** EVAL-GO-0.05, **(c)** EVAL-GO-0.1. **(C)** Fiber orientation analysis of EVAL-GO system. Scale bar = 100 µm.

4.2.5. Mechanical property analysis of EVAL-GO system

A significant decrease occurred in the fiber diameter as a result of GO incorporation and it was reflected in the tensile properties of the EVAL-GO matrices. A decrease in fiber diameter significantly improved the tensile strength and Young's modulus (Figure 15B and C) of the EVAL-GO matrices. The tensile strength of EVAL-neat (1.5 ± 0.1 MPa) significantly increased beyond 3 MPa in EVAL-GO matrices (Figure 15B). Similarly, Young's modulus of EVAL-neat (3.2 ± 0.2 MPa) was also significantly improved to more than 5 MPa (Figure 15C). Wong et al. had a similar finding that the decrease in fiber diameter of PCL fibers increased the tensile properties (Wong et al., 2008). The finer fibers form when the jet stretching is increased. As a result, the macromolecular chains show higher orientation. This leads to enhanced tensile properties (Wong et al., 2008). Studies have shown that the incorporation of GO would

improve the tensile properties. At the polymer-GO interface, the applied load will be transmitted to the GO platelets and thus improve the tensile property (Thampi et al., 2015). Ma et al. found that in the PLLA/GO fibers, the GO nanosheets were oriented along the fiber axis and achieved better mechanical properties than the neat PLLA fibers. They also observed the thinning of fibers in the PLLA mats incorporated with GO (PLLA/GO) (Ma et al., 2020). Some studies say that the GO/PVA nanocomposite films also have better tensile properties than the bare material due to excellent delamination, uniform dispersion, aligned distribution, and strong intermolecular hydrogen bonding of GO (Ma et al., 2016). The GO nanosheets have a high surface area and many surface functionality. So, the GO strongly interacts with the polymer chains. Additionally, the high tensile strength and stiffness of GO contribute to the mechanical properties (Mohammadi et al., 2017).

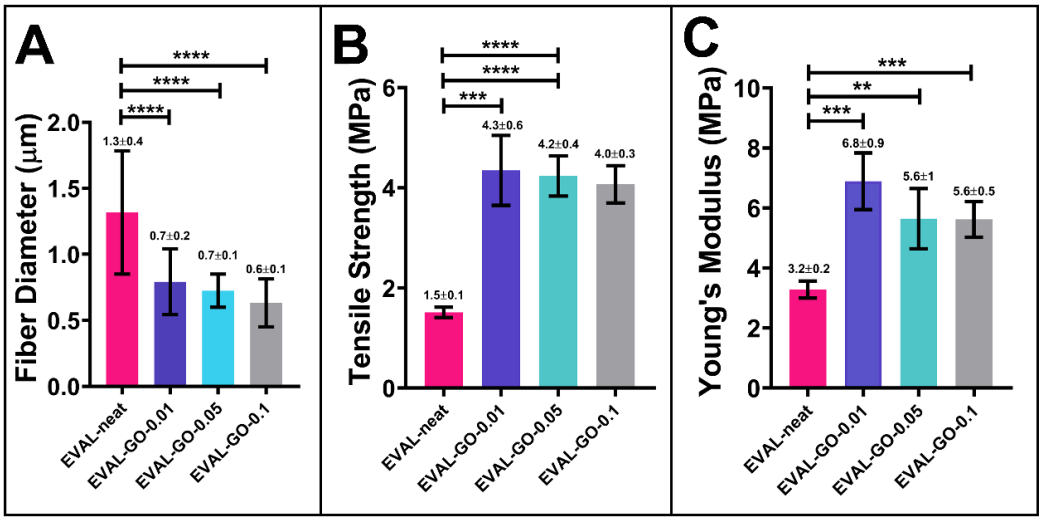

Figure 15: (A) Fiber diameter analysis of EVAL-GO system. **(B)** Tensile strength and **(C)** Young's modulus of EVAL-GO system. Statistical significance: **, ***, and **** indicates 'p-value' < 0.01, 0.001, and 0.0001 respectively.

4.2.6. Direct contact test with EVAL-GO system

The matrices were evaluated for their cytotoxic effects via Direct contact test. For the viability assessment of the EVAL-GO matrices, they were subjected to a Direct contact test. Here the matrices were kept on a monolayer of L-929 cells for 24 h to observe the cell response. The phase contrast images (Figure 16A a, c, d, e, and f) show that the cells seen around the negative control (Ultra high molecular weight polyethylene; UHMWPE), EVAL-neat, EVAL-GO-0.01, EVAL-GO-0.05, and EVAL-GO-0.1 materials were alive. No cell death or morphological abnormalities were observed. The cells maintained their original morphology. All these observations indicate that the cells were viable with these materials after 24 h interaction. The cells that interacted with the positive control (Tin compound incorporated polyvinyl chloride; Tin-PVC) were mostly dead and had shrunken morphologically (Figure 16A b). The toxicity of the Tin compound affected the cell health in positive control wells and caused cell death. So, qualitatively the EVAL-GO matrices can be considered as noncytotoxic.

4.2.7. MTT assay with EVAL-GO system

It is necessary to quantify the cytotoxic effects of a material, though the Direct contact test images convey their nontoxic nature. So, to assess the cytotoxic nature of the material quantitatively, MTT assay was carried out with the extracts of the EVAL-GO matrices collected after 72 h. After interacting with the extracts, 90 % of the cells were viable (Figure 16B). It indicates that the cell activities were not affected by the extracts. It was also found that the cell viability was above 100 % for the undiluted extracts of EVAL-GO matrices. Some studies have reported that the GO promotes cell

proliferation (Magaz et al., 2021; Mohammadi et al., 2017; Rosa et al., 2016; Thampi et al., 2017).

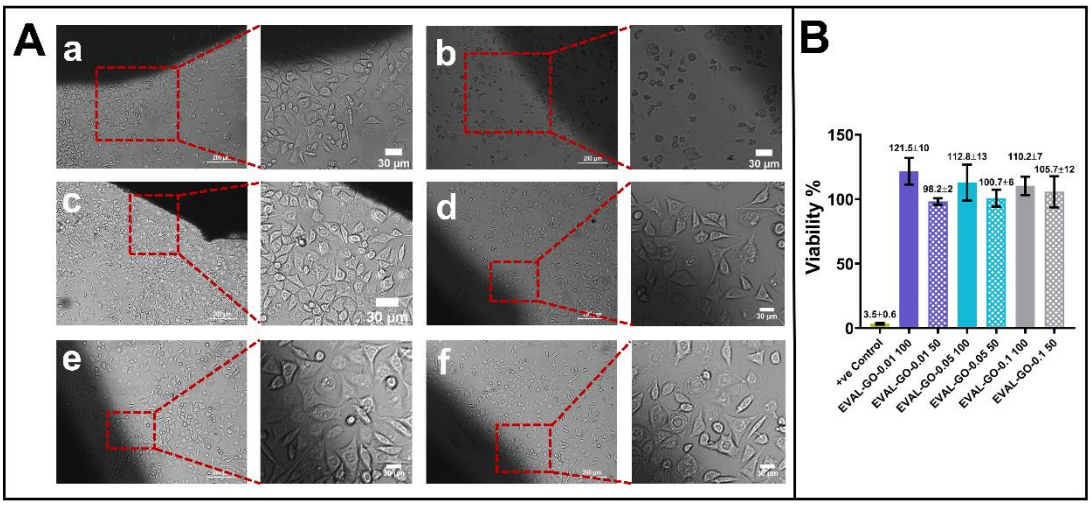

Figure 16: (A) Phase contrast images of Direct contact test **(a)** negative control (Ultra High Molecular Weight Poly Ethylene; UHMWPE), **(b)** positive control (Tin compound incorporated Polyvinyl chloride; Tin-PVC) **(c)** EVAL-neat, and **(d)** EVAL-GO-0.01, **(e)** EVAL-GO-0.05. and **(f)** EVAL-GO-0.1 **(B)** MTT assay. Scale bar: main images are 200 µm and cropped images are 30 µm.

4.2.8. Cell viability assessment of N2a and C6 cell lines with EVAL-GO system

The study was mainly focused on the neuronal cell response with the matrices. It was necessary to assess the viability of the neuronal and glial cells with the material. So, the extracts of the matrices were used to find the cell viability. Since the study was based on neuronal and glial cell response with the material, N2a (represents neuronal cell), and C6 cells (considered instead of Schwann cells) were considered for the experiments. The N2a cells treated with the extracts of EVAL-GO matrices were viable, healthy, and maintained the morphology (Figure 17A c, d, and e). The viability was visible in Figure 17A (c, d, and e), where the majority of cells were in green fluorescence. Similarly, the C6 cells also appeared mostly with green fluorescence indicating the cell viability. Red fluorescence occurs only when the EtBr enters the

cells that have lost the cell membrane integrity. The negligible amounts of red fluoresced cells in Figure 17A and B indicate that only a few cells died. Viability quantification done with C6 cells using Flow cytometry also showed that more than 80 % of the cells were viable after the EVAL-GO extract treatment (Figure 17C). So, it was confirmed from the live/dead assay and flow cytometry that the matrices act as a favorable substrate for the neuronal and glial cells.

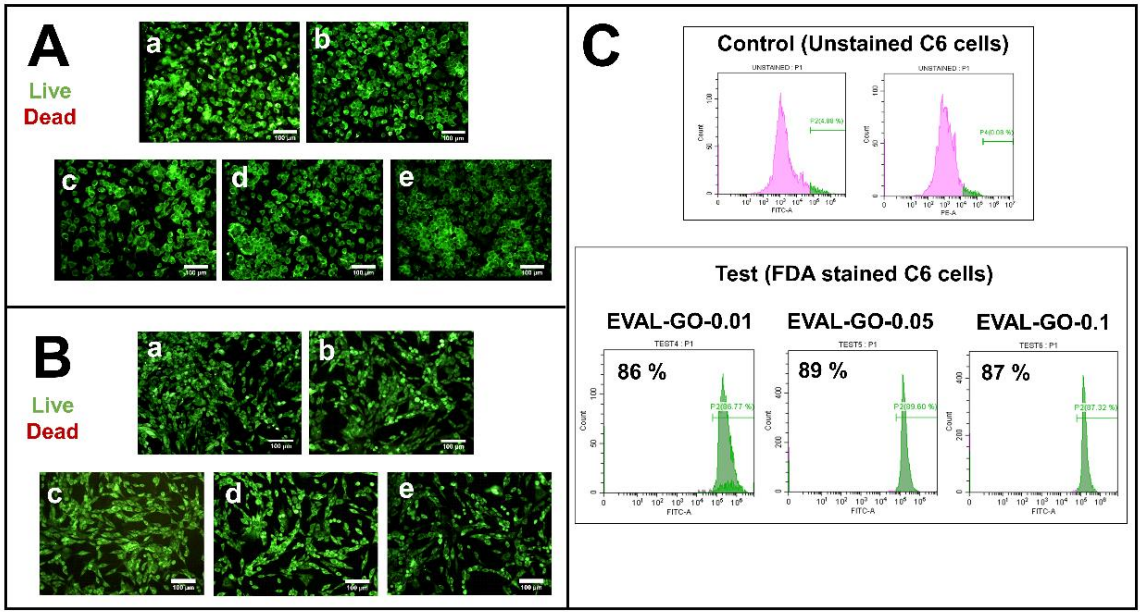

Figure 17: Fluorescence images of Live/dead assay (viability assessment) done on **(A)** N2a cell line and **(B)** C6 cell line after treatment with extracts of EVAL-neat and EVAL-GO. **(a)** Control (TCP), **(b)** EVAL-neat, **(c)** EVAL-GO-0.01, **(d)** EVAL-GO-0.05, and **(e)** EVAL-GO-0.1. **(C)** Viability assessment of C6 cell line using flow cytometry. Scale bar = 100 µm.

4.2.9. Cellular/neurite response of N2a and C6 cell lines on EVAL-GO system

Cell adhesion, focal adhesion formation, and cellular or neurite orientation on the matrices were evaluated from the cell response studies with cell-seeded matrices. The spatial response of neurites on the EVAL-GO matrices was assessed from the F-actin staining and β III tubulin staining images. When a neuronal cell approaches a fiber, the

cell adheres to the fiber by forming focal adhesions. Figure 18A and B show the cell response on control (TCP) and EVAL-neat fibers respectively. The cells on the control extended their neurites in multiple orientations. The random orientation of the neurites on the TCP surface was due to its homogeneous surface. The TCP surface is a continuous isotropic surface. A cell adhered to the isotropic surface anchors its FAs in multiple locations. So, the neurites extended also show random orientations. The F-actin plays a critical role in FAs and helps the cellular processes to orient. Visualizing the F-actin via staining determines the FA directions and neurite orientations. The cells adhered to EVAL-neat and EVAL-GO matrices extended their neurites in multiple directions (Figure 18B-E). The surface of these matrices was not as similar to TCP due to their fibrous nature. The cells on the matrices make their FAs only on the fibers, and their neurite extension is restricted to the fiber surface. The cells avoided the voids between the fibers. So, the neurite extension also had a random fashion. The random neurite orientation on random fibers is evident in Figure 18 (B-E).

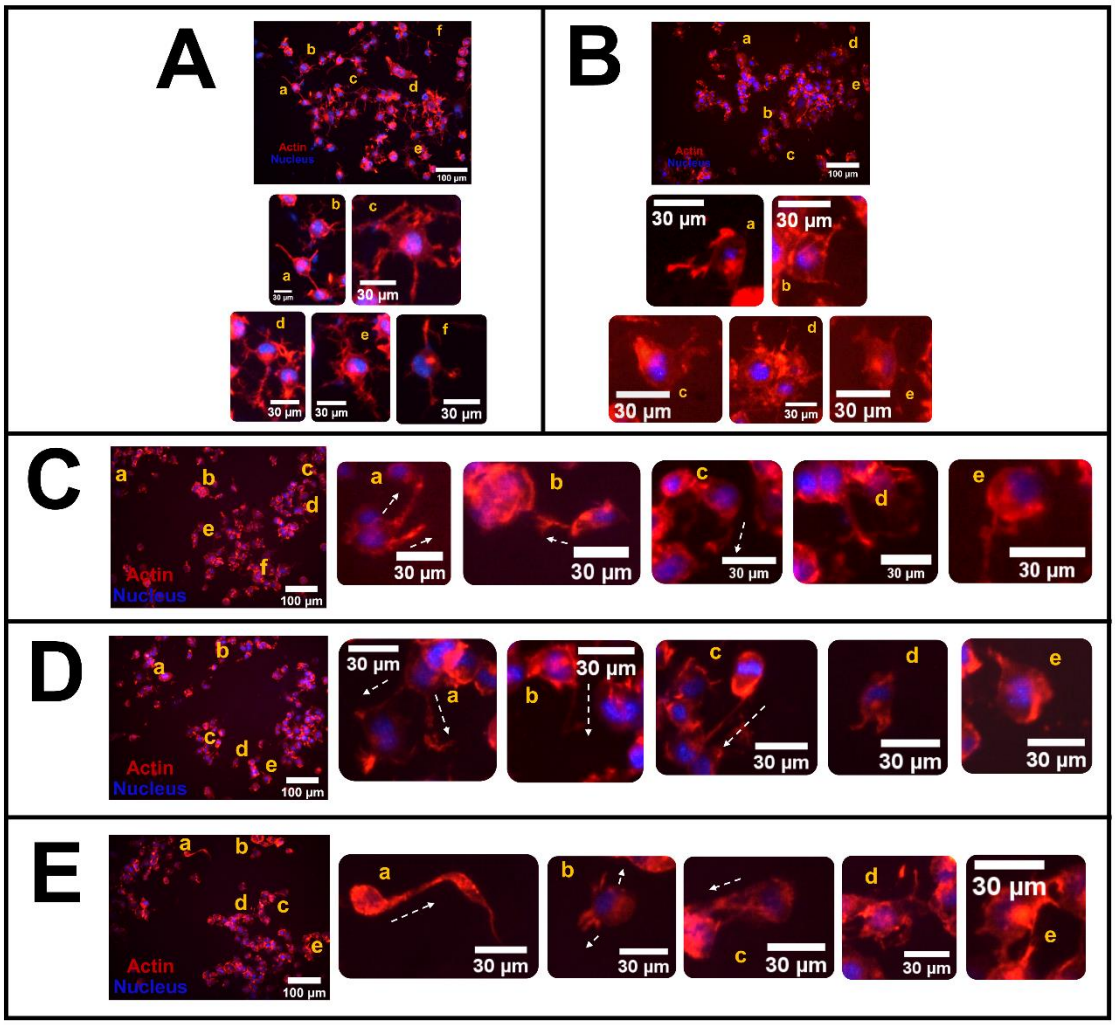

Figure 18: Fluorescence images of F-actin staining of N2a cells cultured on **(A)** control; Tissue culture plate (TCP), **(B)** EVAL-neat and **(C)** EVAL-GO-0.01, **(D)** EVAL-GO-0.05, and **(E)** EVAL-GO-0.1. Scale bar: main images are 100 µm and cropped images are 30 µm.

The cellular orientation of C6 cells was also evaluated using F-actin staining. The C6 cells were considered instead of Schwann cells. The C6 cells in the TCP (control) had an elliptical morphology and were oriented in multiple directions (Figure 19A). The isotropic flat surface of the TCP allows the cells to form randomly oriented FAs. These FAs lead to the random orientation of the cells. Similarly, the C6 cells showed random orientation on the EVAL-neat matrix. Figure 19B shows the filopodia extension of C6 cells in multiple directions on the EVAL-neat fibers. Interestingly, the C6 cells on the

EVAL-GO fibers had a spherical morphology. No cells showed an elliptical morphology (Figure 19 C-E). The NIH3T3 fibroblast cells in the study of Bashur et al. also responded similarly to randomly oriented submicron-sized fibers. They reported that the cell area, aspect ratio, and long axis length were decreased in NIH3T3 fibroblast cells that were adhered to submicron diameter fibers (Bashur et al., 2006). The limited cell spreading on submicron-sized fibers might be due to two reasons. The FAs are formed from integrin clusters that bind to the ECM proteins (fibronectin, collagen, etc.,) that are adhered to the fibers from the biological fluid. The size of an FA is usually > 1 μm (Badami et al., 2006; Liu et al., 2009). So, it would be difficult for a fiber with submicron diameters to support the FAs. Another reason is that the submicron size of the fibers would also limit the adherence of ECM proteins on the fibers and that will limit the integrin-fibronectin binding (Bashur et al., 2006). The fiber diameter of EVAL-GO matrices is less than 1 μm (Figure 15 A). So, it would be difficult for a cell to make its FAs on the fibers as discussed above.

β III tubulin, the neuronal marker that is exclusively found in neuronal cells is also targeted for staining to evaluate the neurite orientation on matrices. Figure 20 (A-D) shows the fluorescence image of neurites with stained (immunostaining) β III tubulin in N2a cells cultured on EVAL-neat and EVAL-GO matrices. It is evident from the figures that the cells extended their neurites in multiple directions in all the matrices. The random orientation of the fibers randomly guided the neurites via contact guidance.

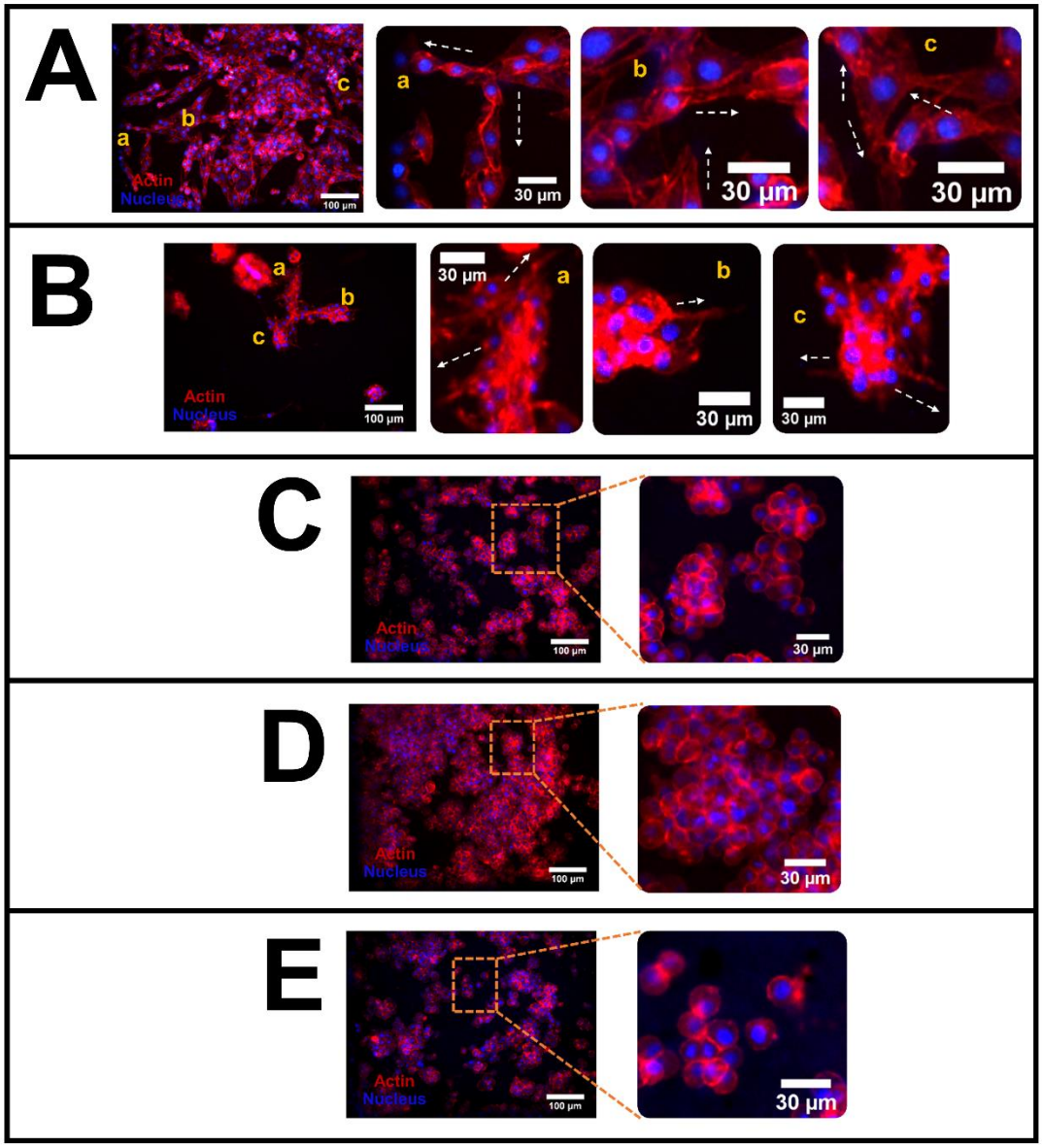

Figure 19: Fluorescence images of F-actin staining of C6 cells cultured on **(A)** control; Tissue culture plate (TCP), **(B)** EVAL-neat and **(C)** EVAL-GO-0.01, **(D)** EVAL-GO-0.05, and **(E)** EVAL-GO-0.1. Scale bar: main images are 100 µm and cropped images are 30 µm.

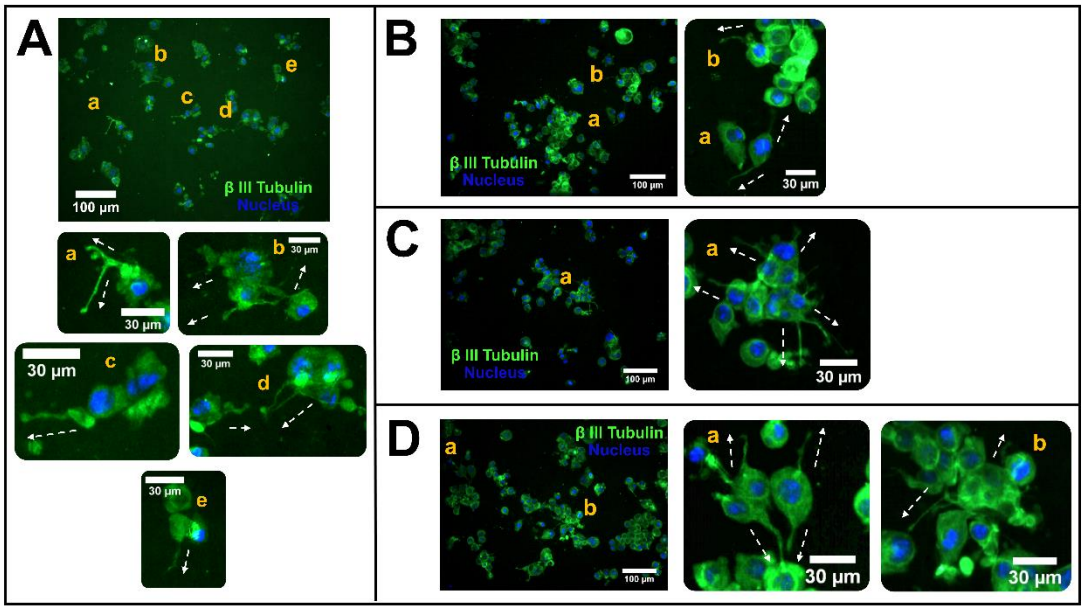

Figure 20: Fluorescence images of immunostained β III tubulin of N2a cells cultured on **(A)** EVAL-neat and **(B)** EVAL-GO-0.01, **(C)** EVAL-GO-0.05, and **(D)** EVAL-GO-0.1 matrices. Scale bar: main images are 100 µm and cropped images are 30 µm.

4.3. Ag^+ incorporated EVAL electrospun matrices

4.3.1. Viscosity analysis of EVAL-Ag system

Viscosity is one of the factors that could determine the fiber morphology, diameter, and beading in electrospinning. The viscoelastic force of the polymer solution prevents the charged jet from stretching (Mit-uppatham et al., 2004). The viscosity (Lovis density viscosity) of the EVAL-Ag solutions with different $AgNO_3$ concentrations is shown in Figure 21A. It was observed that the viscosity increased significantly as the $AgNO_3$ concentration increased in the solution. The EVAL-neat had a viscosity of 129 ± 2 mPa and increased significantly to 135 ± 1 mPa when 0.01 % $AgNO_3$ was added to the solution. The viscosity rose beyond 130 mPa as the concentration of $AgNO_3$ became 0.3 %. Such an increase indicates that the polymer chains of EVAL might be engaged in some interactions with the $AgNO_3$. This interaction must be a complex formation between Ag^+ and -OH of the polymer. An interaction between Ag^+ and -OH of EVAL would restrict the polymer chain movement and increase the viscosity.

4.3.2. Solution conductivity analysis of EVAL-Ag system

The solution conductivity could influence the jet whipping of the electrospinning solution. It is reported that the increase in solution conductivity would lead to less jet whipping and result in the collection of aligned fibers on a rotating collector. The solution conductivity of the EVAL-Ag system is shown in Figure 21B. The EVAL-neat (EVAL alone) solution had a solution conductivity of 27 ± 0.5 µS/cm. The EVAL-Ag-0.01, considered for the analysis had a solution conductivity of 50.3 ± 1.2 µS/cm. Several studies have reported that the incorporation of ionic salts will increase the solution conductivity (Cho et al., 2016; Mayuri and Ramesh, 2016; Song et al., 2011).

The addition of even a small amount of salt to the polymer solution increases the solution charge density and determines the fiber alignment (Mayuri and Ramesh, 2016). The addition of salt to the polymer solution also influences the fiber diameter of the electrospun matrices (Mit-uppatham et al., 2004).

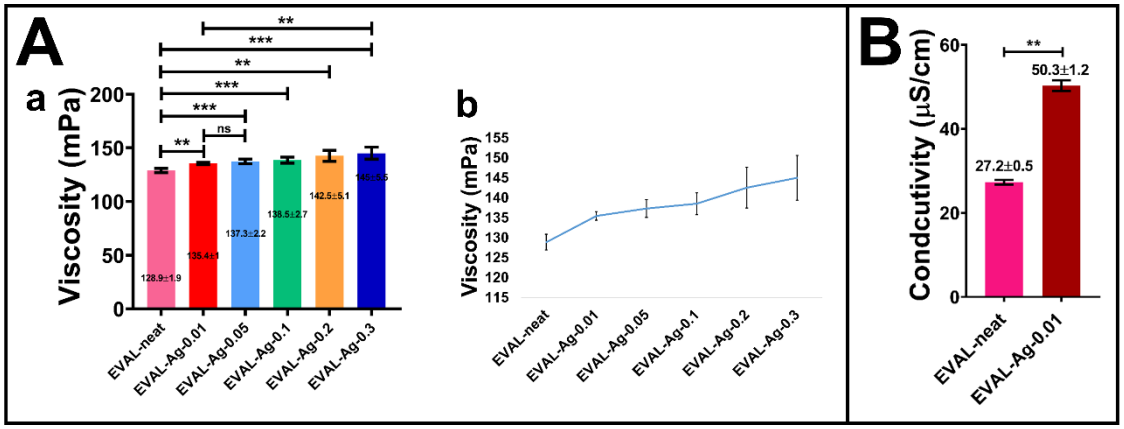

Figure 21: (A) (a) and **(b)** Viscosity analysis. **(B)** Conductivity analysis of EVAL-Ag system. Statistical significance: **, ***, and ns indicates 'p-value' < 0.01, 0.001, and non-significance respectively.

4.3.3. UV-Visible spectral analysis of EVAL-Ag system

Since the EVAL-Ag system contains silver, it was necessary to investigate the presence of AgNPs in the system. The intention was to incorporate Ag^+ in the system and increase the solution conductivity, which would enhance the fiber alignment. UV-Visible spectroscopy is a commonly used technique to confirm the presence of AgNPs. The presence of AgNPs usually gives a sharp peak around 400 nm (Gan et al., 2016; Huang et al., 2014; Resmi et al., 2021; Yen et al., 1990).

EVAL-Ag-0.01 solution was considered for the UV-Visible spectral analysis (Figure 22B). A small portion of the matrix was redissolved in an IPA:water (7:3) mixture and subjected to UV-Visible spectral analysis. The peak of $AgNO_3$ was obtained at 312 nm. The Ag^+ in $AgNO_3$ interacts with the water molecules to form the H_2O-Ag^+ complex. This interaction gives the peak for $AgNO_3$ solution around 300 nm (Gan et al., 2016;

Resmi et al., 2021). The Ag^+ in the polymer solution also complex with the -OH of the polymer. So, the peak of EVAL-Ag-0.01 was obtained as a shoulder peak at 268 nm. Similarly, Gan et al. obtained a shoulder peak for PVA/$AgNO_3$ films around 300 (Gan et al., 2016). Chau et al. also obtained a shoulder peak for PVA/Ag^+ complex formation at 305 nm (Chou et al., 2014).

4.3.4. EDX spectral analysis of EVAL-Ag system

EDX analysis was done to find the presence of silver in the matrix. EVAL-Ag-0.3 (matrix with the highest concentration of $AgNO_3$) was considered for the analysis. The presence of silver in the EVAL-Ag system was confirmed from a peak that appeared at 3 keV in the spectrum, which was absent in EVAL-neat (Figure 22A). Mayuri et al. also obtained a small peak around 3 k eV for the AgNP-impregnated EVAL yarns indicating the presence of silver (Mayuri and Ramesh, 2016).

4.3.5. XPS spectral analysis of EVAL-Ag system

The oxidation state of silver in EVAL-Ag-0.01 was evaluated using the XPS spectral analysis. According to some studies the binding energy of $Ag3d_{5/2}$ is around 368 eV (Ferraria et al., 2012; Gan et al., 2016). The binding energy for $Ag3d_{3/2}$ and $Ag3d_{5/2}$ of EVAL-Ag-0.01 was obtained at 373.5 and 367.5 eV respectively (Figure 22C). Studies show that the binding energies obtained for $Ag3d_{5/2}$ at a range of 366-368 eV indicate the presence of Ag^+ and over 368 eV indicate Ag^0 (He et al., 2010; Kumar et al., 2015; Li et al., 2019). This downshift in the binding energies in EVAL-Ag-0.01 indicates an interaction between Ag^+ and -OH of the polymer. A similar finding was made by Gan et al., where the binding energy of $Ag3d_{5/2}$ of $AgNO_3$ (368.6 eV) was downshifted in PVA/$AgNO_3$ hybrid films (367.9 eV) due to the interaction of the silver ion with

hydroxyl groups of PVA (Gan et al., 2016). When Resmi et al. synthesized AgNPs using alginate dialdehyde, the binding energies for $Ag3d_{5/2}$ was 368.3 eV (Resmi et al., 2021). As mentioned earlier the $Ag3d_{5/2}$ for Ag^0 is obtained above 368 eV (He et al., 2010; Kumar et al., 2015).

4.3.6. FTIR spectral analysis of EVAL-Ag system

The interaction of Ag^+ with the EVAL was analyzed by comparing the FTIR spectra of EVAL-neat and EVAL-Ag-0.1 matrices (Figure 22D). The functional group vibrations in EVAL-neat are as follows. An -OH stretching peak was observed at 3307 cm^{-1}. C-H stretching vibrations were found at 2921 and 2849 cm^{-1}. A C-H bending vibration was observed at 1436 cm^{-1} and deformation at 1327 cm^{-1} (Mayuri et al., 2016). A peak at 1083 represented the C-OH stretching vibrations (Gan et al., 2016).

The FTIR spectra of the EVAL-Ag system are shown in Figure 22D. The -OH stretching vibrations slightly red-shifted to 3292 cm^{-1}. The -CH stretching peak at 2921 cm^{-1} (EVAL-neat) was also red-shifted to 2914 cm^{-1}. The -CH stretching peak at 2849 cm^{-1} showed a negligible shift in the EVAL-Ag-0.1 matrix. The C-H bending and deformation vibrations also showed a negligible shift in EVAL-Ag-0.1. However, the C-OH stretching vibration at 1083 cm^{-1} (EVAL-neat) was red-shifted to 1076 cm^{-1} in EVAL-Ag-0.1. The redshift occurring in -OH and C-OH stretching vibrations is due to the coordination interactions of Ag^+ with the -OH groups of the EVAL (Gan et al., 2016). The Ag^+ complexation with -OH disrupts the intramolecular hydrogen bonding in EVAL. The Ag^+ holds the polymer chains closer and might lead to the restricted movements of the polymer chains. This restriction increases the solution viscosity. It

is evident from the viscosity analysis (Figure 21 A) that the increase in Ag^+ content also increased the solution viscosity.

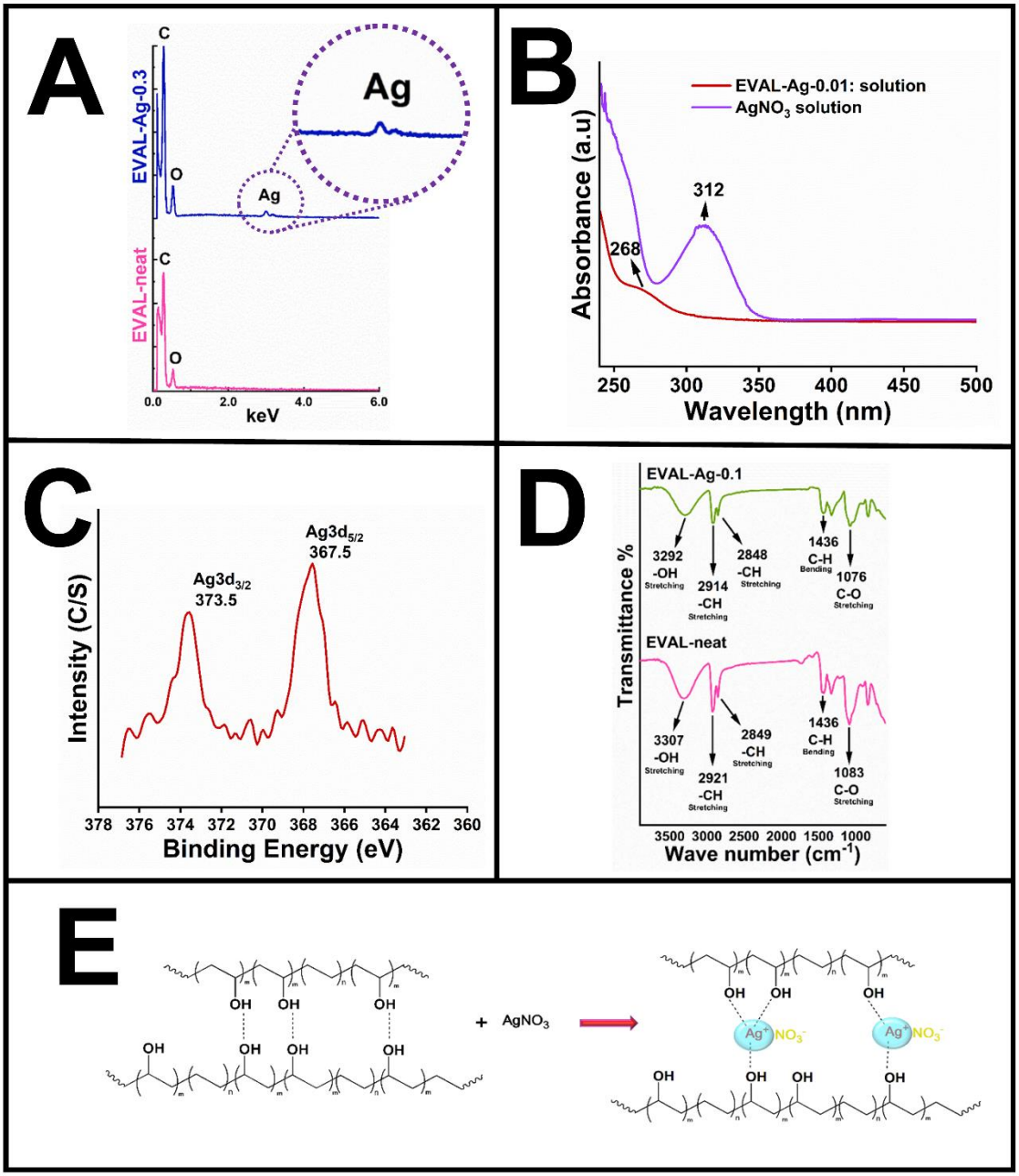

Figure 22: (A) EDX analysis **(B)** UV-Visible spectra **(C)** XPS spectra, **(D)** FTIR spectra of EVAL-Ag system, and **(E)** Schematic representation of Ag^+ complexed EVAL.

Considering the information from viscosity, EDX, UV-Visible, XPS, FTIR, and EDX analysis, the complexation of Ag^+ with the -OH of the polymer was schematically represented in Figure 22E (Sumam and Parameswaran, 2023).

4.3.7. Fiber morphology, orientation, and diameter evaluation from SEM analysis EVAL-Ag system

The appearance of the EVAL-Ag matrices according to the $AgNO_3$ concentration in the system is shown in Figure 23A. It is evident from the image that as the $AgNO_3$ content in the matrices increases, the colour of the matrices becomes darker. It indicates the complexation of silver with -OH of the polymer (Yen et al., 1990).

It was understood from the SEM images that the fibers of all matrices were beadles (Figure 23B). It is very well clear from the images that the EVAL-Ag fibers were aligned compared to the randomly oriented EVAL-neat fibers. The fiber orientation analysis done with ImageJ software also substantiates the findings (Figure 23C). In Figure 23C, a wide range of peak distribution was found in EVAL-neat, but for the EVAL-Ag matrices, the peaks were concentrated to a short range of angles. This narrowing of peaks represents fiber alignment. The EDX, UV-Visible, and XPS analysis (Figure 22A, B, and C respectively) had already indicated the presence of silver in the EVAL-Ag system. From the UV-visible, XPS, and FTIR analysis, the Ag^+ form was also confirmed (Figure 23B-D). It is known that the presence of ionic salts (eg; $AgNO_3$) in the polymer solution will reduce the jet whipping and induce fiber alignment (Cho et al., 2016; Mayuri and Ramesh, 2016; Song et al., 2011). The fiber alignment occurs due to increased conductivity which is evident from the conductivity analysis (Figure 21B). The net charge density increases as conductivity increases, and

stronger whipping occurs. However, under high applied voltage (20 kV in this case) the stretching force is so large and this leads to a highly stretched jet traveling in a straight path. This leads to the collection of aligned fibers on the rotating collector (Song et al., 2011). Here the repulsive forces are insignificant when compared to the large stretching force.

The fiber alignment was reduced as the $AgNO_3$ concentration increased beyond 0.2 % (w/v). The $AgNO_3$ content increased, and the viscosity of the polymer solution (EVAL-Ag-0.3) also increased (Figure 21A). As the solution becomes more viscous, the needle tip is blocked and the electrospinning faces discontinuity (Song et al., 2011). Since $AgNO_3$ is a non-volatile solute (Mayuri and Ramesh, 2016) and its complexation with -OH (Sumam and Parameswaran, 2023) of the polymer and water molecules, will reduce the solvent evaporation. Such a solution sometimes forms large viscous bubbles at the needle tip. However, the high applied voltage attracted the Tylor cone and resulted in the bursting of the bubble. The solution thus ejected from the bubble, fell randomly on the rotating collector. So, the matrix (EVAL-Ag-0.3) had a mixture of aligned and random fibers (Figure 23B f). It is visible in Figure 23C, which represents the fiber orientation analysis of EVAL-Ag-0.3 using ImageJ software. The peaks were not concentrated to a short range of angles and instead had a slightly wide range of distribution.

Fiber bundling was observed in EVAL-Ag matrices (Figure 23B b-f). Wang et al. had very well described in their work about this phenomenon. They induced the self-bundling of fibers via (1) a grounded metallic needle (kept near the collector facing the spinneret) and (2) using a highly conductive solution. The grounded metallic

needle (negatively charged) will converge the splay (positively charged) that emerged from the spinneret. This occurs due to the change in the electrostatic field due to the negative charge of the grounded needle. When the splay unites, the self-bundling of fibers occurs. In the second case, when a highly conductive solution was used, the splay stretched fast and fell on the collector to discharge. The following parts of the fiber also discharge fast, the negative charge is induced in that part of the fiber, and the positively charged spinneret attracts the fiber, and the fiber continuity breaks. Now the broken part of the fiber on the collector acts like the needle tip. This broken fiber tip induces the self-bundling of the fibers (Wang et al., 2008). A conductivity of 50.3 ± 1.2 µS/cm (EVAL-Ag-0.01) was sufficient to show the self-bundling effect in the EVAL-Ag system. The EVAL-neat solution with a 27 ± 0.5 µS/cm conductivity generated random fibers indicating that this conductivity is insufficient for fiber self-bundling.

The fiber diameter of the EVAL-Ag system is shown in Figure 23D. The fiber diameter significantly increased in EVAL-Ag matrices when compared with EVAL-neat. The fiber diameter of EVAL-neat was 1.3 ± 0.4 µm, whereas the EVAL-Ag-0.01 was 3.1 ± 0.6 µm. The slow evaporation of the solvent might also contribute to the increase in fiber diameter (Mayuri and Ramesh, 2016). The viscosity analysis has shown that the rise in $AgNO_3$ in the solution increased the viscosity due to the complex formation of Ag^+ with -OH of EVAL. An increase in viscoelastic force occurs due to an increase in polymer chain entanglement and thereby the jet resists stretching which results in increased fiber diameter (Mit-uppatham et al., 2004). The slow solvent evaporation also led to the flattening of the fibers in the EVAL-Ag system as the concentration of $AgNO_3$ increased in the polymer solution. As the $AgNO_3$ increases, the solvent on the

fiber surface evaporates fast, but the bulk remains and evaporates slowly. So, the fibers will have polymer-rich skin while the inner portions undergo evaporation (Mayuri and Ramesh, 2016). After the complete evaporation, the fiber collapses and flattens (Mit-uppatham et al., 2004). Such flattened fibers were mostly found in EVAL-Ag-0.05, EVAL-Ag-0.1, and EVAL-Ag-0.2 (Figure 23B).

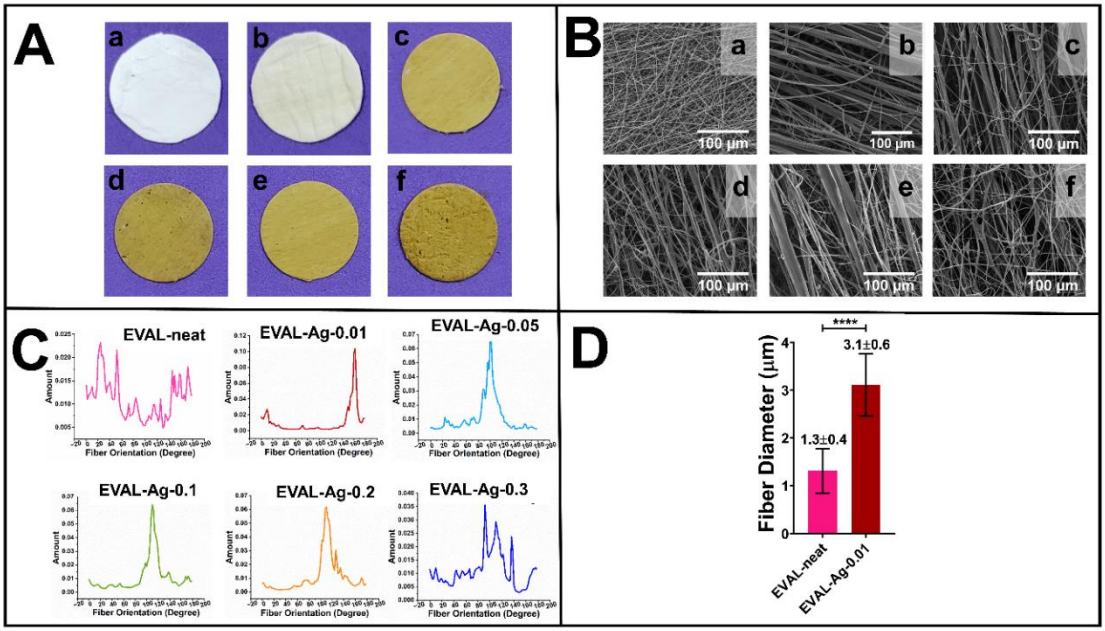

Figure 23: (A) Images of EVAL-Ag matrices: **(a)** EVAL-neat**, (b)** EVAL-Ag-0.01**,** EVAL-Ag-0.05, **(c)** EVAL-Ag-0.1, **(d)** EVAL-Ag-0.2, and **(e)** EVAL-Ag-0.3. **(B)** SEM analysis of EVAL-Ag-GO system: **(a)** EVAL-neat**, (b)** EVAL-Ag-0.01**,** EVAL-Ag-0.05, **(c)** EVAL-Ag-0.1, **(d)** EVAL-Ag-0.2, and **(e)** EVAL-Ag-0.3. **(C)** Fiber orientation analysis of EVAL-Ag system, **(D)** Fiber diameter analysis of EVAL-Ag system. Scale bar: 100 µm. Statistical significance: **** indicates 'p-value' < 0.0001.

4.3.8. Mechanical property analysis of EVAL-Ag system

The nerve repair scaffolds should have similar or better tensile properties than the original nerve to perform daily activities (Borschel et al., 2003). The fiber fusion, flattening, and discontinuity in electrospinning of EVAL-Ag matrices with $AgNO_3$ concentration of more than 0.01 % (w/v) led to the selection of EVAL-Ag-0.01 for further study. Since the EVAL-Ag system had aligned fibers, the tensile properties were carried out with dumbbells punched in two directions. These dumbbells were

designated with “L” (representing longitudinal) and “T” (representing transverse) based on the arrangement of the fibers in the dumbbells concerning the collector drum rotation direction. The longitudinal dumbbells have fibers parallel to the collector drum rotation direction. The transverse dumbbells have fibers perpendicular to the collector drum rotation direction. So, the dumbbells of EVAL-Ag-0.01 were designated as EVAL-Ag-0.01 L and EVAL-Ag-0.01 T according to the fiber direction in the dumbbells. Punching the dumbbells in either direction (L and T) from EVAL-neat was irrelevant because of the random fiber orientation.

The tensile strength of EVAL-neat was 1.5 ± 0.1 MPa. EVAL-Ag-0.01 L and EVAL-Ag-0.01 T had a tensile strength of 8 ± 0.1 and 1 ± 0.05 MPa respectively. A significant increase in tensile strength was observed in EVAL-Ag-0.01 L dumbbells compared to EVAL-neat. The fiber orientation in the longitudinal dumbbells were in the direction of tensile loading. Whereas, the fibers in the transverse dumbbells were perpendicular to the tensile loading. A significant increase in tensile strength was observed in longitudinal dumbbells (EVAL-Ag-0.01 L) than EVAL-neat. EVAL-Ag-0.01 T dumbbells had a significantly lesser tensile strength than EVAL-Ag-0.01 L and EVAL-neat dumbbells. A similar result was obtained for Young’s modulus also. A significant increase occurred in EVAL-Ag-0.01 L (159 ± 35 MPa) and EVAL-Ag-0.01 T (8 ± 1 MPa) than EVAL-neat (3.2 ± 0.2 MPa).

The tensile properties of longitudinal dumbbells rather than the transverse dumbbells must be better because when the proximal and distal stumps are bridged using a nerve repair scaffold, the aligned fibers must run parallel to the nerve long axis. Only in such a scaffold could the regenerating nerve elongate in an aligned manner and reach the

destination. The longitudinal samples could resist the breakage compared to the transverse samples and withstand the daily *in vivo* mechanical forces. The tensile properties of EVAL-Ag-0.01 are adequate for withstanding the mechanical forces according to some studies that have mentioned the tensile properties of animal peripheral nerves (Borschel et al., 2003; Menzies et al., 2013; Rydevik et al., 1990).

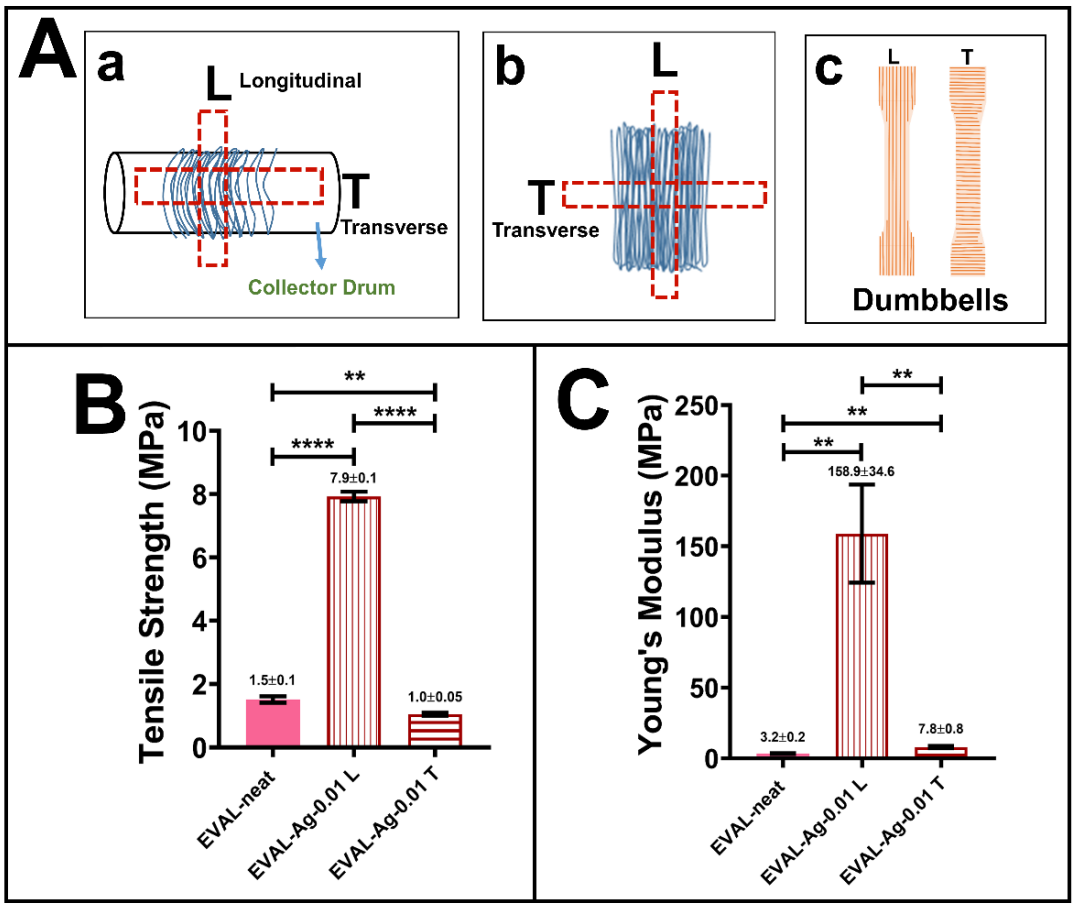

Figure 24: (A) Diagrammatic representation of **(a)** Punching orientation of dumbbells according to the collector drum rotation, **(b)** punching orientation of dumbbells from the matrix, and **(c)** fiber orientation in dumbbells. "L" represents longitudinal and "T" represents transverse. **(B)** Tensile strength of EVAL-Ag-0.01 matrix. **(C)** Young's modulus of EVAL-Ag-0.01 matrix. Statistical significance: ** and **** indicate 'p-value' < 0.01 and 0.0001 respectively.

4.3.9. ICP-OES analysis of EVAL-Ag system

The amount of silver in the matrix and released from the matrix was evaluated using ICP-OES analysis. Whenever a substrate incorporated with Ag^{+} comes in contact with a water-based medium (biological or non-biological), the Ag^{+} can be released into the

medium. If it occurs in the biological medium, the released Ag^+ ions could interfere with cellular functions and cause cytotoxicity leading to cell death. Here, PBS (7.4 pH) was used as the extraction medium and the extract was subjected to ICP-OES analysis. EVAL-Ag-0.01 was considered in the analysis since it was used in further studies.

The EVAL-Ag-0.01 matrix weighed 0.025 g and had a total content of 963.33 ppm. The EVAL-Ag-0.01 matrix that weighed 0.023 g was subjected to extraction for 24 h in PBS and had 0.124 ppm silver content in the extract. Whereas, the EVAL-Ag-0.01 matrix weighed 0.0233 g and was kept for 1-week extraction (cumulative) in PBS, and the silver content in the extract was 0.262 ppm. The results show that only a negligible amount of silver was released from the matrices after 24 h and 1 week. The silver incorporated in the polymer might be complexed within the fibers and prevented from migrating into the medium. Such a response could contribute to less cytotoxicity when the substrate comes in contact with the cells.

4.3.10. IC50 analysis of $AgNO_3$ solution

IC50 (Half-maximal inhibitory concentration) of $AgNO_3$ solution prepared in water was analyzed using the MTT assay. The study was done in L-929 fibroblast cells. The cells were treated with $AgNO_3$ solution ranging from 0.001 – 0.0001 % (w/v) to find the IC50 value. Approximately 50 % cell viability was observed at the concentration of 0.0004 % $AgNO_3$ (w/v) (Figure 25). So, it is evident that a concentration below 0.0004 % would be favorable to prevent cell death. The $AgNO_3$ in the EVAL-Ag-0.01 solution is 0.01 % (w/v). The ICP-OES analysis indicated that a small portion of the matrix releases negligible silver in the medium even after 24 h or 1 week. Therefore it

can be inferred that the leached silver will not adversely affect the performance of the membrane in biological medium.

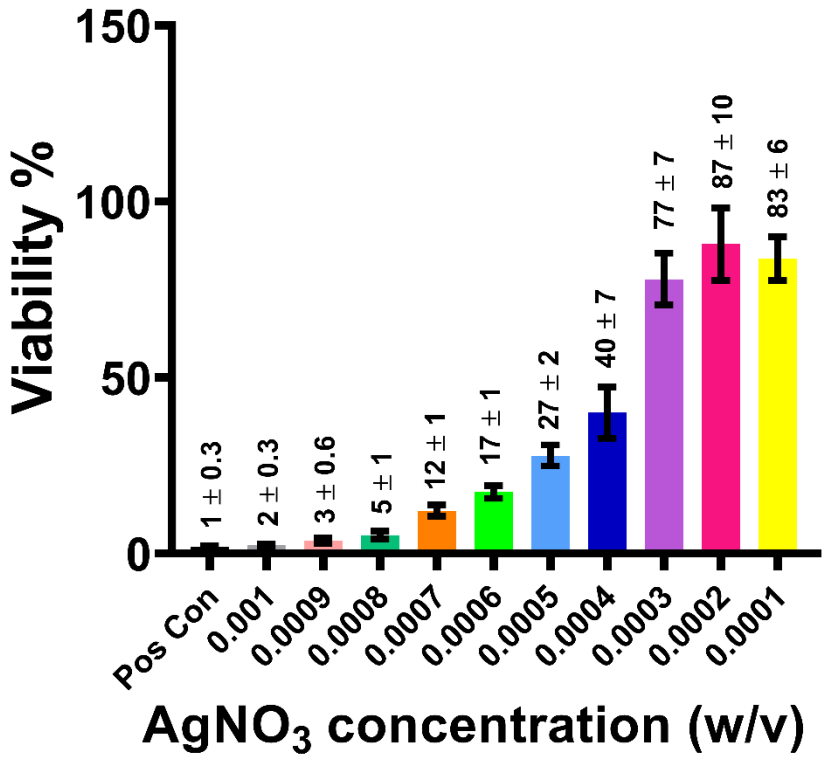

Figure 25: Graphical representation of IC50 (Half-maximal inhibitory concentration) of $AgNO_3$ solution prepared in water.

4.3.11. Direct contact test with EVAL-Ag system

The material toxicity was assessed with a Direct contact test. The cell death and cellular morphological changes were observed using phase contrast microscope imaging. The positive control (Tin-PVC) caused severe cell death after 24 h interaction (Figure 26A b). The Tin released from the PVC became cytotoxic and induced cell death. The negative control (UHMWPE) caused no damage to the cells and cell death was not observed. Similarly, the cells that interacted with EVAL-neat and EVAL-Ag-0.01 also showed more alive cells after interacting for 24 h. It is visible from the enlarged images of EVAL-neat (Figure 26A c) and EVAL-Ag-0.01 (Figure 26 d) that

the cell has maintained its morphology. It is evident from the IC50 results (Figure 25) that the cell viability is above 70 % at a concentration above 0.0002 %. So, the Ag^+ released from the matrices might be less than 0.0002 %. The cells are safe at a concentration of Ag^+ released from the matrices.

4.3.12. MTT assay with EVAL-Ag system

The viability of L929 cells upon interacting with EVAL-Ag-0.01 extracts was quantified from MTT assay. The yellow-coloured permeable MTT picked up by the viable cells was converted to purple-coloured non-permeable formazan. It was observed that the purple colour intensity was high in the wells treated with EVAL-Ag-0.01 72 h-extracts when compared to the positive control (phenol). The viability calculations showed that more than 90 % of the cells were viable after interacting with undiluted (100 % extract) and diluted (50 % extract with 50 % medium) extracts of EVAL-Ag-0.01 (Figure 26B). The cell viability of positive control was < 5 %.

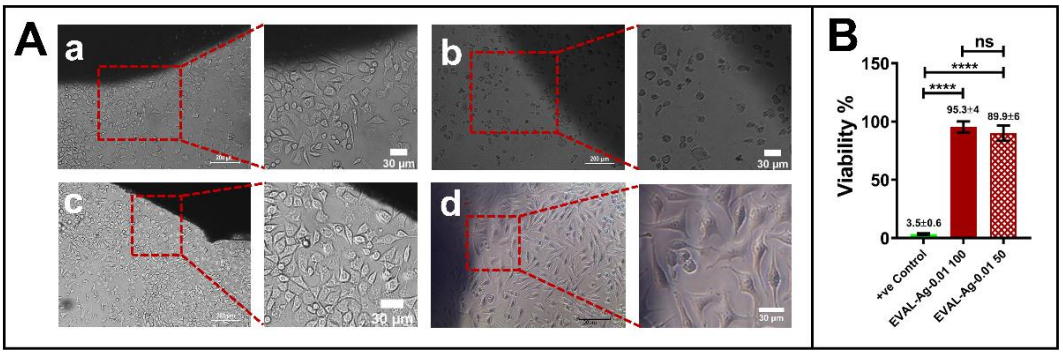

Figure 26: (A) Phase contrast images of Direct contact test **(a)** negative control (Ultra High Molecular Weight Poly Ethylene; UHMWPE), **(b)** positive control (Tin compound incorporated Polyvinyl chloride; Tin-PVC) **(c)** EVAL-neat, and (d) EVAL-Ag-0.01. **(B)** MTT assay. Scale bar: main images are 200 µm and cropped images are 30 µm. Statistical significance: **** and ns indicate 'p-value' < 0.0001 and non-significance respectively.

Both the Direct contact test and MTT assay showed that the Ag^{+} released from the EVAL-Ag-0.01 matrix does not cause damage to the cells.

4.3.13. Cell viability assessment of N2a and C6 cell lines with EVAL-Ag system

A live/dead staining assay was done to assess the viability of the N2a and C6 cells after treatment with EVAL-Ag-0.01 extracts. Acridine orange (AO) was used to identify the live cells and ethidium bromide (EtBr) was used to identify the dead cells. The AO was picked up by the live cells and emitted green fluorescence. The dead cell lost its membrane integrity was permeable to EtBr and permitted the stain to bind DNA. So, the dead cells emitted red fluorescence.

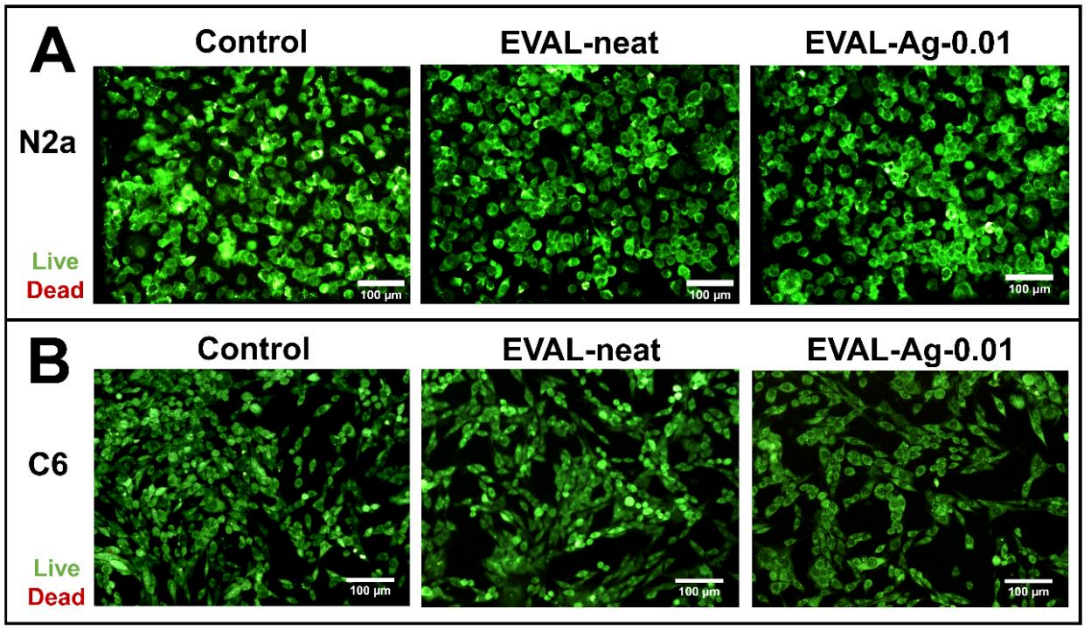

Figure 27: Fluorescence images of Live/dead assay (viability assessment) done on **(A)** N2a cell line and **(B)** C6 cell line after treatment with extracts of EVAL-neat and EVAL-Ag-0.01. Control are untreated cells cultured on TCP surface. Scale bar: 100 µm.

The live/dead assay (Figure 27A and B) carried out with the extract of EVAL-Ag-0.01 kept the majority of the cells viable. The extracts of EVAL-Ag-0.01 did not cause cell death in N2a and C6 cells (Figure 27A and B respectively). So, the number of dead cells was negligible.

Quantification of the cell viability was done in C6 cells using flow cytometry. The cells treated with the 72 h extracts of EVAL-Ag-0.01 for 24 h were stained with FDA and subjected to Flow cytometry. The results showed that more than 80 % of the cells were viable after extract treatment (Figure 28B). This indicates that the cell membrane integrity was fine and the viable cells metabolized the FDA. So, the live/dead assay and Flow cytometry confirmed the noncytotoxic nature of the EVAL-Ag-0.01 matrix.

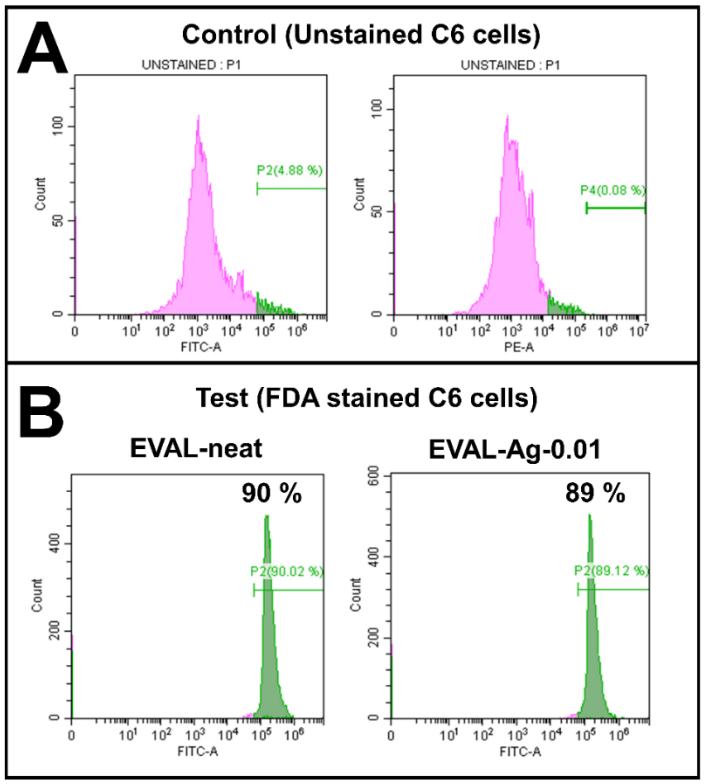

Figure 28: Viability assessment of C6 cell line using flow cytometry: **(A)** Control C6 cells (unstained) and **(B)** Cells stained after treatment with EVAL-neat and EVAL-Ag-0.01 extracts.

4.3.14. Cellular/neurite response of N2a and C6 cell lines on EVAL-Ag system

A successful nerve regeneration needs neuronal alignment during the regeneration process. In the natural scenario, to achieve neuronal alignment the Schwann cells play a critical role by proliferation and forming “Bands of Bungner” (Wang et al., 2019). The basal lamina secreted by these “Bands of Bungner” is the physical cue for the axonal sprouts to regenerate. Despite the basal lamina secretion, the Schwann cells also secrete growth factors that attract the growing neurites (axonal sprouts). These events successfully occur only if the endoneurium is intact. In neurotmesis, it is difficult for the Schwann cells to arrange as “Bands of Bungner”, secrete basal lamina, and provide guidance cues for the regenerating axonal sprouts. All these events lead to neuroma formation and loss of organ function. It is beneficial if anisotropic substrates are fabricated to bridge proximal and distal stumps in neurotmesis. An anisotropic substrate provides guidance cues for the Schwann cells and axonal sprouts to orient in an aligned manner. These properties of a nerve repair scaffold could enhance nerve regeneration (Hoffman-Kim et al., 2010; Leclech and Villard, 2020). Aligned fibers are the substrates that mostly resemble the extracellular matrix (Cho et al., 2016; Lin et al., 2019; Orkwis et al., 2020; Thampi et al., 2020; Zou et al., 2016).

The N2a cell line was considered to assess the neurite orientation on the aligned fibers. The cells cultured on the matrices were subjected to F-actin staining. F-actin is a cytoskeletal filament associated with focal adhesions (FAs) and neurite extensions. The substrate topography influences the FA formation and that determines the F-actin orientation. So, the F-actin staining could give an idea about the FA arrangement and neurite orientation (Leclech and Villard, 2020). Figure 29A shows that the cells on the

control (TCP) were oriented randomly. The TCP's homogeneous surface (isotropic surface) allows the cells to form FAs randomly. In response to this, the cells extend their neurites in random directions. The cells cultured on the EVAL-neat (Figure 29B) also randomly extend their neurites. However, the number of neurites will be lesser than the cells grown in control. This is because the cells on the EVAL-neat adhere to the fibers and the availability and diameter of the fibers determines the number of neurites (Figure 31D). The N2a cells adhered to EVAL-Ag-0.01 extended their neurites in an aligned fashion in response to the aligned nature of the fibers (Figure 29C). The aligned neurite arrangement indicates that the FAs of cells grown on EVAL-Ag-0.01 were also aligned on the fibers.

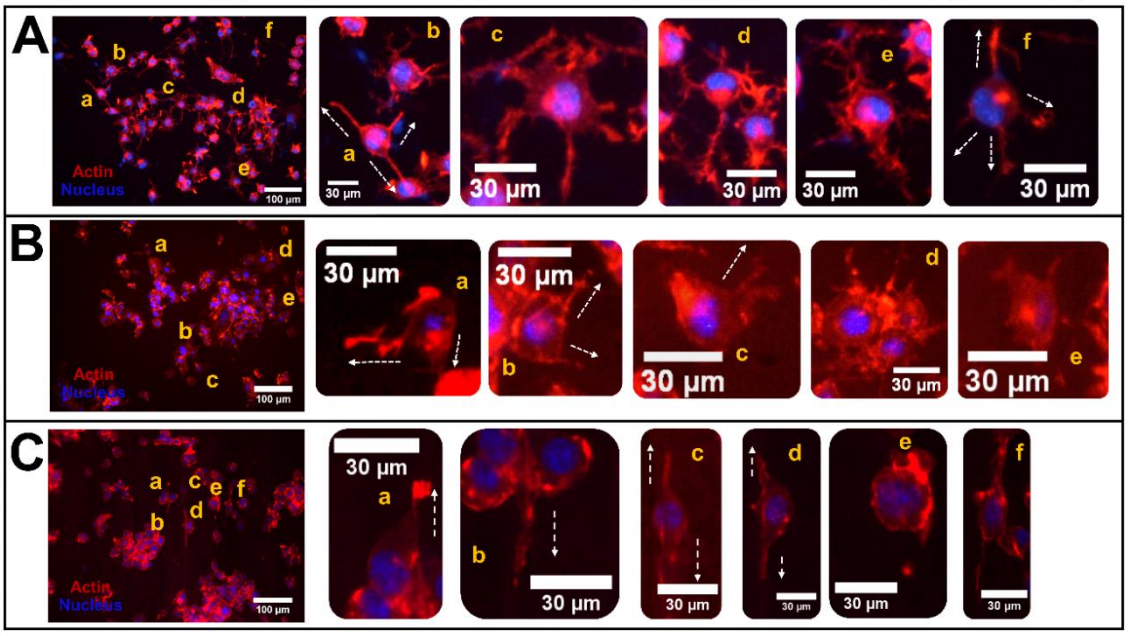

Figure 29: Fluorescence images of F-actin staining of N2a cells cultured on **(A)** control; Tissue culture plate (TCP), **(B)** EVAL-neat and **(C)** EVAL-Ag-0.01. Scale bar: main images is 100 µm and cropped images are 30 µm.

The C6 cell lines were considered instead of Schwann cells. The C6 cell lines were cultured on TCP surface, EVAL-neat, and EVAL-Ag-0.01 matrices to study the cell response according to fiber orientation. Since the Schwann cell arrangement is

important in neurite extension, F-actin staining was done on the cells cultured on TCP, EVAL-neat, and EVAL-Ag-0.01. The F-actin staining image of C6 cultured on TCP, EVAL-neat, and EVAL-Ag-0.01 matrices is shown in Figure 30. The staining indicated that the C6 cells cultured on TCP and EVAL-neat were oriented in various directions (Figure 30A and B). Whereas, the cells adhered to EVAL-Ag-0.01 fibers were aligned on the matrices (Figure 30C). The fiber diameter of EVAL-Ag-0.01 (3.1 ± 0.6 µm) could promote proper adhesion of cells. Several studies have reported that a fiber diameter greater than 1 µm promotes the cells to anchor on the fiber perfectly and spread well (Badami et al., 2006; Liu et al., 2009).

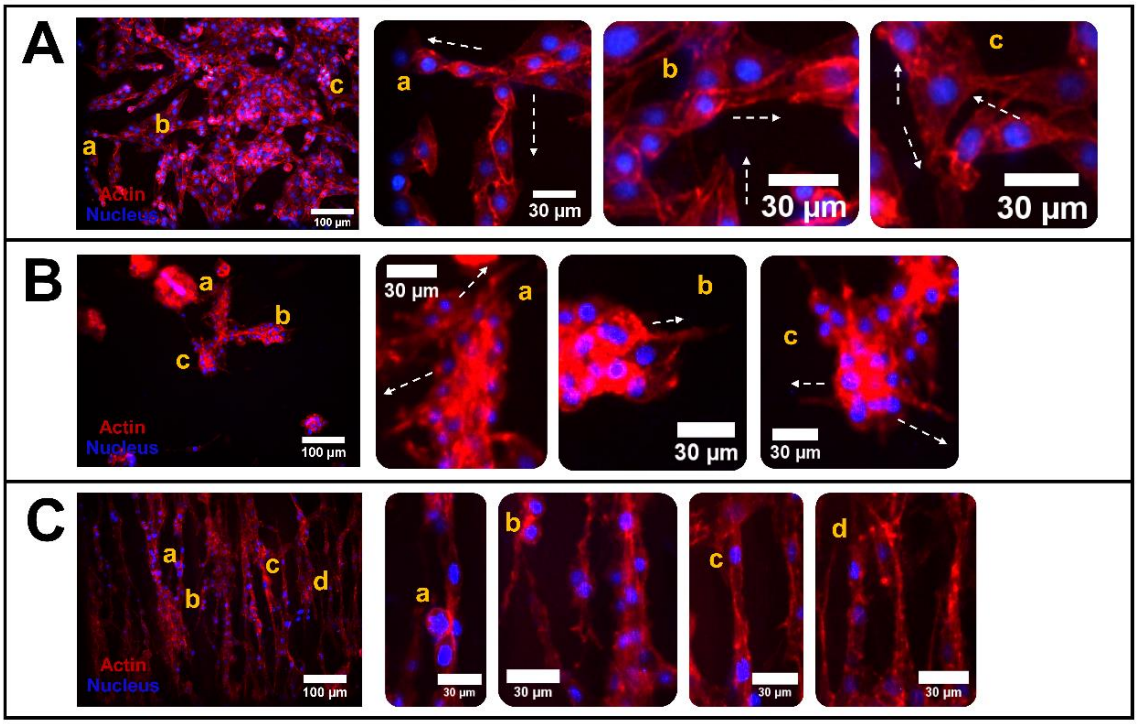

Figure 30: Fluorescence images of F-actin staining of C6 cells cultured on **(A)** control; Tissue culture plate (TCP), **(B)** EVAL-neat and **(C)** EVAL-Ag-0.01. Scale bar: main images is 100 µm and cropped images are 30 µm.

The neurite alignment was also evaluated with β III tubulin staining in N2a neurites. β III tubulin is a neuronal marker since it is exclusively found in neurons. So, β III tubulin staining could help to confirm the cellular or neurite response on fiber orientation. From Figure 31A and B, it is evident that the neurites of EVAL-neat are oriented in random directions and EVAL-Ag-0.01 in an aligned fashion. These results were similar to the F-actin staining results of N2a cells.

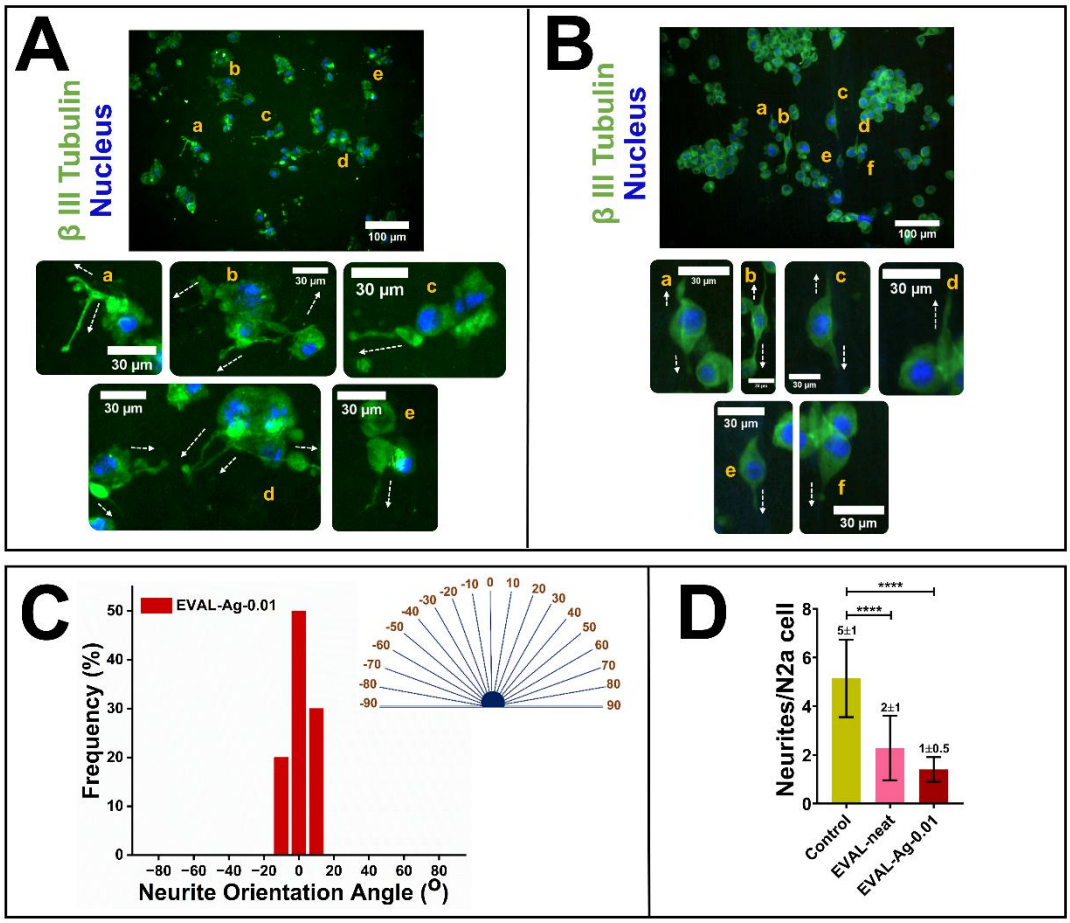

Figure 31: Fluorescence images of immunostained β III tubulin of N2a cells cultured on **(A)** EVAL-neat and **(B)** EVAL-Ag-0.01. **(C)** Quantification of neurite orientation on EVAL-Ag-0.01. **(D)** Neurites per N2a cell on control, EVAL-neat, and EVAL-Ag-0.01. Scale bar: main images are 100 µm and cropped images are 30 µm. Statistical significance: **** indicate 'p-value' < 0.0001.

The neurite alignment was quantified from the immunostaining images. It was observed that the orientation of more than 70 % of cells was between -20^{o} and +20^{o} angles (Figure 31C). These results substantiate the cells or neurites responding concerning the fiber alignment.

4.4. Ag^+ and GO incorporated EVAL electrospun matrices

4.4.1. Solution conductivity analysis of EVAL-Ag-GO system

The solution conductivity is a relevant parameter that could decide the polymer jet whipping. The solution conductivity of EVAL-neat was 27 ± 0.5 µS/cm. The Ag^+ incorporation increased the solution conductivity in EVAL-Ag-GO-0.01 to 49 ± 2 µS/cm (Figure 32A). Since the GO is insulating, its effect on conductivity is negligible. Mayuri et al. have reported that the $AgNO_3$ incorporation in EVAL solution would increase the conductivity 10-fold (Mayuri and Ramesh, 2016). The ionic salts in a polymer solution would influence the polymer jet's journey. Increasing ionic salts usually creates fiber stretching and less jet-whipping (Cho et al., 2016; Mayuri and Ramesh, 2016; Song et al., 2011).

4.4.2. UV-Visible spectral analysis of EVAL-Ag-GO system

UV-Visible spectroscopy was done to evaluate the presence of silver nanoparticles (AgNP) in the system. Since the reaction is carried out in higher temperatures (70 ºC), the chance of AgNP formation exists. The EVAL-Ag-GO system contains Ag^+, any reduction to Ag^+ can convert into Ag^0 and the aggregation of Ag^0 can lead to AgNP formation. Many studies show that the presence of AgNP would express sharp peaks at around 400 nm in UV-Visible spectra (Gan et al., 2016; Huang et al., 2014; Resmi et al., 2021; Yen et al., 1990). The EVAL-Ag-GO system needs an Ag^+ form in the solution, therefore, UV-Visible spectroscopy could confirm it.

In the EVAL-Ag-GO system, the EVAL-Ag-GO-0.01 solution was considered for the UV-Visible analysis (Figure 32B). A portion from the EVAL-Ag-GO-0.01 matrix was dissolved in an IPA:water (7:3) mixture and used for spectral analysis. The spectra did

not show any peak around 400 nm. This confirmed the absence of AgNPs in the system. $AgNO_3$ solution (control) showed a peak at 312 nm and a shoulder peak appeared for EVAL-Ag-GO-0.01 around 264 nm. The disappearance of the main peak around 312 nm and the appearance of a shoulder peak (264 nm) indicates that the Ag^+ is interacting with the polymer.

Gan et al. doped $AgNO_3$ in poly(vinyl alcohol) (PVA) for fabricating novel functional material. They created $AgNO_3$-doped PVA films (PVA/$AgNO_3$) provided with and without thermal treatment. A peak for $AgNO_3$ solution was obtained at 300 nm due to the H_2O-Ag^+ complex. The PVA/$AgNO_3$ films not subjected to thermal treatment showed only a shoulder peak around 300 nm (Gan et al., 2016). The similar results obtained in the present work show that the Ag^+ has complexed with the -OH of the EVAL. The UV-Visible spectrum of PVA/Ag nanofibers fabricated by Chou et al. also showed a peak at 305 representing the PVA/Ag^+ complex (Chou et al., 2014).

4.4.3. XPS spectral analysis of EVAL-Ag-GO system

XPS analysis was performed to confirm the oxidation state of silver in the EVAL-Ag-GO system. The EVAL-Ag-GO-0.01 was considered for XPS analysis. $Ag3d_{3/2}$ and $Ag3d_{5/2}$ peaks of EVAL-Ag-GO-0.01 appeared at 371.7 and 365.6 eV respectively (Figure 32C). According to reports of Gan et al., the $Ag3d_{3/2}$ and $Ag3d_{5/2}$ for $AgNO_3$ are 374.6 and 368.6 eV respectively. They also prepared PVA/$AgNO_3$ hybrid films that expressed $Ag3d_{3/2}$ and $Ag3d_{5/2}$ peaks at 373.9 eV and 367.9 eV. This downshift in the peaks was due to the coordination interaction of Ag^+ with the hydroxyl groups of PVA (Gan et al., 2016).

Ferraria et al. also states that the $Ag3d_{5/2}$ of $AgNO_3$ is around 368 eV (Ferraria et al., 2012). It is reported that the binding energy for $Ag3d_{5/2}$ of Ag^+ is usually obtained between 366-368 eV and Ag^0 over 368 eV (He et al., 2010; Kumar et al., 2015). Similarly, Li et al. reported that the $Ag3d_{5/2}$ of Ag^0 was at 369.5 eV (Li et al., 2019). The AgNPs synthesized by Resmi et al. using alginate dialdehyde also show an $Ag3d_{5/2}$ peak at 368.3 eV, confirming the silver is in Ag^0 form (Resmi et al., 2021). In support of the information mentioned above, it was confirmed that the silver incorporated in EVAL-Ag-GO-0.01 was in Ag^+ form and not reduced to Ag^0. So, the formation of AgNP was ruled out.

A downshift was observed for the $Ag3d_{3/2}$ and $Ag3d_{5/2}$ in EVAL-Ag-GO-0.01 when compared to EVAL-Ag-0.01. The $Ag3d_{3/2}$ and $Ag3d_{5/2}$ of EVAL-Ag-0.01 were 373.5 and 367.5 eV. The downshift observed for these peaks in EVAL-Ag-GO-0.01 might be due to the presence of GO. The Ag^+ might make complexes with the -OH groups of both EVAL and GO. The downshifts in $Ag3d_{3/2}$ and $Ag3d_{5/2}$ peaks are attributed to the complex formation (coordination interactions) of Ag^+ with hydroxyl and carbonyl

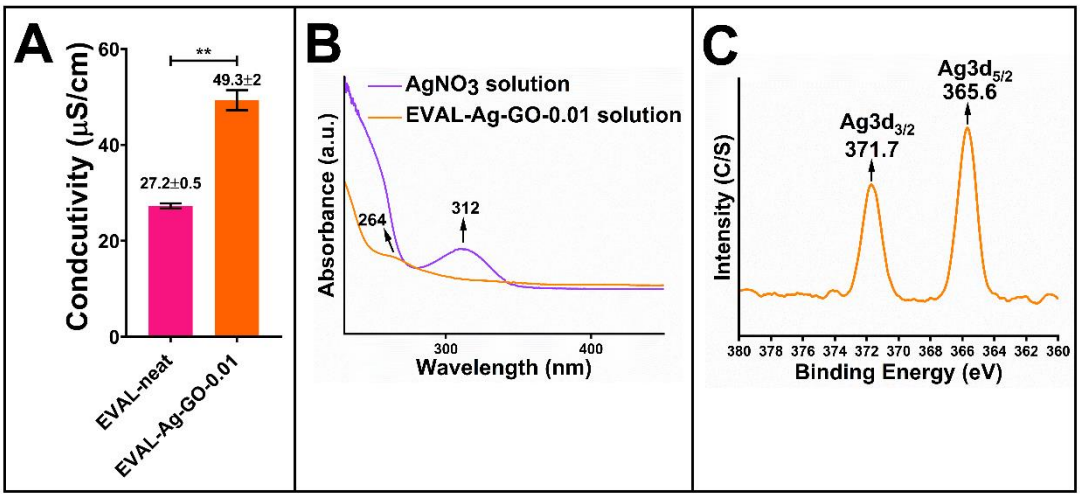

Figure 32: (A) Solution conductivity analysis, **(B)** UV-Visible spectral analysis, and **(C)** XPS spectral analysis of EVAL-Ag-GO system. Statistical significance: ** indicate 'p-value' < 0.01.

oxygens (Gan et al., 2016). Here the Ag^+ could be complex with the carbonyl groups present in GO also.

4.4.4. FTIR spectral analysis of EVAL-Ag-GO system

The EVAL-Ag-GO system was subjected to FTIR spectroscopy analysis to evaluate the influence of Ag^+ and GO on the EVAL. The peaks that appeared in EVAL-neat are as follows (Figure 33A). A peak appeared at 3307 cm^{-1} representing the -OH stretching vibrations. Two peaks at 2921 and 2849 cm^{-1} represented -CH stretching vibrations. A peak representing C-H bending appeared at 1436 cm^{-1} (Mayuri et al., 2016). A C-H deformation peak was also found at 1327 cm^{-1} (Mayuri et al., 2016). The peak at 1083 cm^{-1} was attributed to C-OH stretching (Gan et al., 2016).

The EVAL-Ag-GO-0.01 also had these same peaks, but slightly shifted (Figure 33B). The -OH stretching was red-shifted to 3293 cm^{-1}. The -CH stretching peaks appeared without much change at 2926 and 2849 cm^{-1}. The C-H bending did not differ much and appeared at 1432 cm^{-1} (Mayuri et al., 2016). The C-H deformation peak remained at 1327 cm^{-1} (Mayuri et al., 2016). However, the C-OH stretching peak was slightly red-shifted to 1072 cm^{-1}. The red shift of -OH and C-OH stretching peaks observed in EVAL-Ag-GO-0.01 also shows that Ag^+ is complexing with the -OH of the polymer. A similar observation was made by Gan et al. in PVA/$AgNO_3$ hybrid films where a peak at 1090 red-shifted to 1084 cm^{-1} indicating the Ag^+ complex formation (Gan et al., 2016).

4.4.5. Raman spectral analysis of EVAL-Ag-GO system

The D and G bands are two characteristic peaks that appear for GO at 1358 and 1590 cm^{-1} respectively. The presence and intensity of D and G band peaks were increased

in EVAL-Ag-GO matrices according to the increase in GO content (Figure 33C). The D and G band intensity for EVAL-Ag-GO-0.01 was less since the GO is only 0.01 % (w/v) in EVAL-Ag-GO-0.01. The band intensity increased more in EVAL-Ag-GO-0.05 [GO is 0.05 % (w/v)] and was highest in EVAL-Ag-GO-0.1 matrix with highest GO (0.1 % w/v).

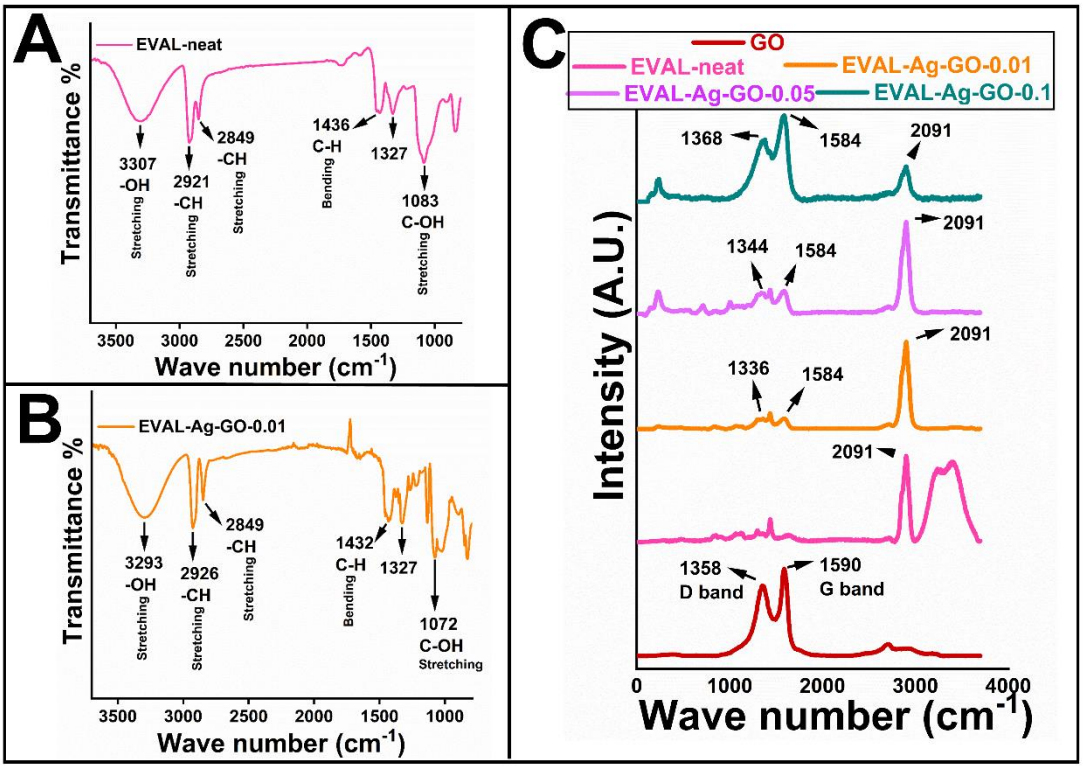

Figure 33: FTIR spectra of **(A)** EVAL-neat and **(B)** EVAL-Ag-GO-0.01. **(C)** Raman spectral analysis of EVAL-Ag-GO system.

The band around 3300 cm^{-1} in EVAL-neat represents the -OH stretching (Cooney et al., 1994) that disappeared in EVAL-Ag-GO matrices. The presence of both Ag^{+} and GO in the EVAL-Ag-GO system interfered with the intramolecular hydrogen bonding of the polymer. A peak around 1430 cm^{-1} was found in EVAL-neat representing the CH_2 bending vibrations (Cooney et al., 1994). Its intensity diminished in EVAL-Ag-GO matrices when the GO content increased and it disappeared in EVAL-Ag-GO-0.1.

The presence of GO in the matrices might have influenced the bending vibrations of -CH. The band around 2900 cm^{-1} in EVAL-neat attributed to -CH stretching vibrations also diminished according to the increase in GO. The peaks around 3500 cm^{-1} represent the -OH stretching vibration in EVAL which got disappeared in EVAL-Ag-GO matrices. The disappearance of the peak in EVAL-Ag-GO matrices might be due to the interaction of Ag^{+} and GO with the -OH and the disruption of intramolecular hydrogen bonding.

4.4.6. Fiber morphology, diameter, and orientation evaluation from SEM analysis of EVAL-Ag-GO system

The appearance of the EVAL matrices according to the Ag^{+} and GO content is shown in Figure 34A. It is clear from the image that Figure 34A, the colour of the matrices was darkening according to an increase in GO content. Here, $AgNO_3$ concentration was the same in all cases. Whereas, the GO concentration varied. The darkening of the matrices was due to the increase in GO content.

The fiber morphology, diameter, and orientation were analyzed from SEM images. The SEM images are shown in Figure 34B. Fiber diameter and orientation analysis were evaluated from the SEM images by subjecting them to ImageJ software analysis. The images indicated that EVAL-neat and EVAL-Ag-GO systems were having bead free fibers (Figure 34B). Figure 34B also shows that the EVAL-neat had thin fibers and EVAL-Ag-GO-0.01 fibers were thicker than EVAL-neat. The fibers of EVAL-Ag-GO-0.05, and EVAL-Ag-GO-0.1 had thick, flat non-uniform fibers. It was evident from the images that the fibers of EVAL-neat were randomly oriented (unaligned fibers or random fibers) and the EVAL-Ag-GO fibers were uniaxially oriented (aligned).

Mayuri et al., Cho et al., and Song et al. have reported in their studies that the incorporation of ionic salts will result in the generation of aligned fibers (Cho et al., 2016; Mayuri and Ramesh, 2016; Song et al., 2011). The ionic salts in the polymer solution will increase the conductivity of the spinning solution (Cho et al., 2016; Mayuri and Ramesh, 2016; Song et al., 2011). According to Song et al., high conductivity will increase the net charge density on the jet surface and might result in stronger jet whipping. However, a large stretching force occurs on the jet under high voltage. So, the repulsive force becomes insignificant compared to this large stretching force. Thus, the stretching of the jet occurs unidirectionally and results in aligned fiber generation (Song et al., 2011). This might also happen due to the highly charged unstable jet, that tries to discharge soon and achieve it via taking a short path (straight path) (Song et al., 2011). Mayuri et al. reported that the incorporation of $AgNO_3$ in the polymer solution will decrease the volatility of the solvent and the jet remains stable (no whipping) throughout its journey to form aligned fibers (Mayuri and Ramesh, 2016). As a result of fiber alignment, unlike the random fibers that fall on a large area of the collector, the aligned fibers are localized on a particular portion (Song et al., 2011).

The fiber orientation analyzed using ImageJ software also indicated that the EVAL-neat had random fibers (Figure 34C). The peaks representing fiber orientation in EVAL-neat were widely distributed indicating the random orientation of the fibers. For the EVAL-Ag-GO system, the peaks representing the angles were concentrated around 80-100º angles. This indicates the system's fiber alignment. The peaks when concentrated at a particular portion or the distribution of the angles are narrow, then the fibers are said to be aligned (Cho et al., 2016).

Fiber diameter was also measured from the SEM images with ImageJ software (Figure 34D). The fiber diameter of the EVAL-Ag-GO system significantly increased than the EVAL-neat. The EVAL-neat had a fiber diameter of 1.3 ± 0.4 µm. Whereas, the fiber diameter of EVAL-Ag-GO-0.01 was 3.5 ± 2 µm. The UV-Visible spectra, FTIR spectra, and XPS analysis have shown that the Ag^{+} was complexed with the -OH of the polymer. This complexation might hold the polymer chains closer and increase the fiber diameter. The fiber diameter has a significant role in cell-material interactions (Liu et al., 2009).

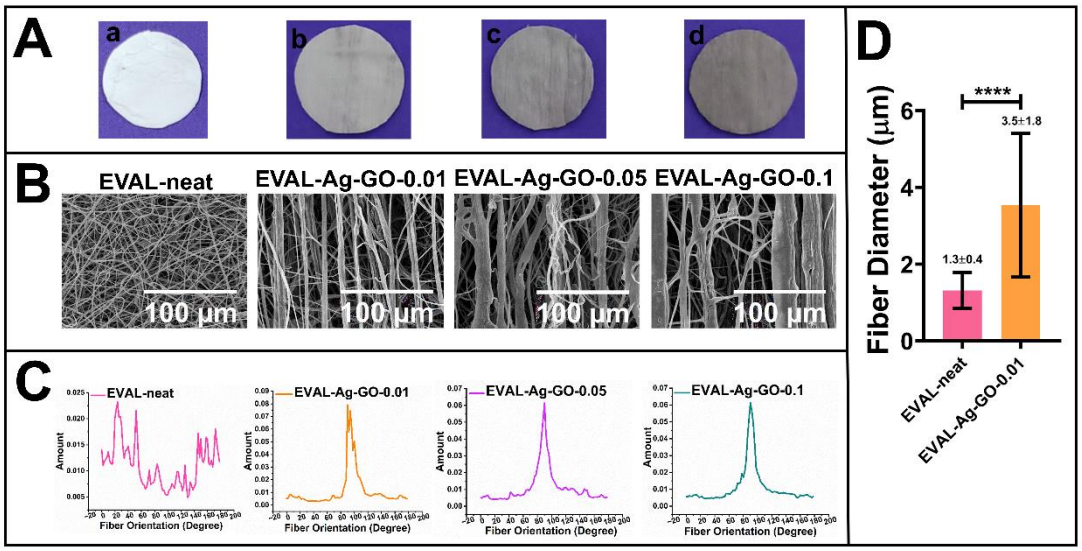

Figure 34: (A) Images of EVAL-Ag-GO matrices: **(a)** EVAL-neat**, (b)** EVAL-Ag-GO-0.01**,** EVAL-Ag-GO-0.05, and **(c)** EVAL-Ag-GO-0.1. **(B)** SEM analysis of EVAL-Ag-GO system, **(C)** Fiber orientation of EVAL-Ag-GO system, **(D)** Fiber diameter analysis of EVAL-Ag-GO system. Scale bar: 100 µm. Statistical significance: **** indicate 'p-value' < 0.0001.

EVAL-Ag-GO-0.05 and EVAL-Ag-GO-0.1 matrices were excluded from the fiber diameter analysis due to the high variation in their fiber structures. These matrices showed fiber fusion and had flat fibers with very large fiber diameters (eg; > 10 µm). GO in EVAL-Ag-GO makes hydrogen bonding with -OH of the polymer and water molecules. GO at concentrations 0.05 and 0.1 % (w/v) might decrease the solvent volatility due to the hydrogen bonding. The wet fibers falling on top of other fibers

would lead to the fusion of fibers (Keirouz et al., 2023). The flow rate of electrospinning was 5 mL/h, which is a fast flow rate. Under such a flow rate solvent evaporation from the jet would not be completed before it reaches the collector. So, the flow rate also contributes to the fiber fusion. The increasing content of GO can also lead to its deposition along the fiber axis and result in flatter ribbon-like fibers (Al-Dhahebi et al., 2020; Ma et al., 2020).

4.4.7. Mechanical property analysis of EVAL-Ag-GO system

Tensile property analysis is a requisite step in developing nerve repair scaffolds. Any nerve repair scaffold must have the same or better tensile properties than a nerve to withstand the *in vivo* mechanical forces (Borschel et al., 2003). The EVAL-Ag-GO system had aligned fibers. So, the mechanical properties of these matrices were evaluated with dumbbells punched out in two directions. The details about dumbbells are given in Figure 35A. During the electrospinning process of the EVAL-Ag-GO system, the fibers fall on the rotating drum so that the fibers are parallel to the drum rotation. The dumbbells punched out in the direction of drum rotation were represented with “L” (Longitudinal). Dumbbells punched perpendicular to drum rotation were represented with “T” (Transverse). The dumbbells were designated as EVAL-Ag-GO-0.01 L and EVAL-Ag-GO-0.01 T. During mechanical property analysis, the direction of tensile load in the longitudinal dumbbells will be in the direction of fiber alignment. Whereas, in transverse dumbbells the direction of tensile load will be perpendicular to the fiber alignment. Since, EVAL-neat had random fibers, the punching direction had no significance. The EVAL-Ag-GO-0.05 and EVAL-Ag-GO-0.1 matrices were

excluded from the mechanical property studies due to their irregularities in fiber diameter and flattening of the fibers.

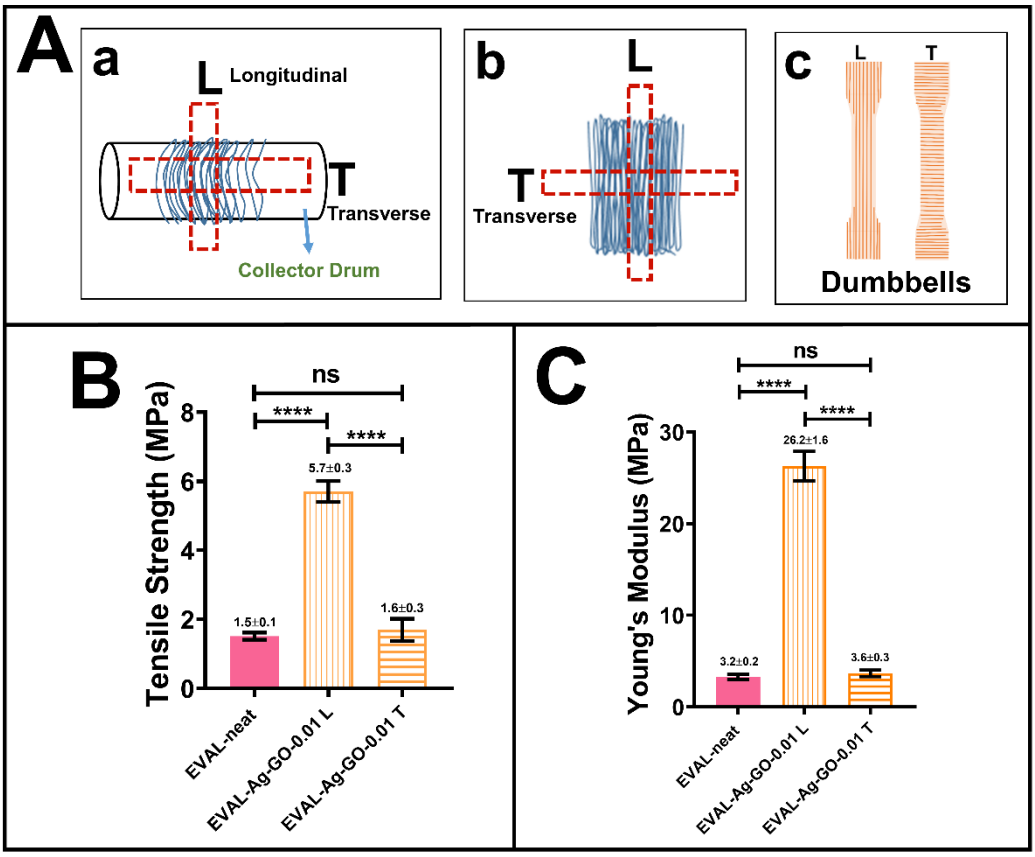

Figure 35: (A) Diagrammatic representation of **(a)** Punching orientation of dumbbells according to the collector drum rotation, **(b)** punching orientation of dumbbells from the matrix, and **(c)** fiber orientation in dumbbells. "L" represents longitudinal and "T" represents transverse. **(B)** Tensile strength of EVAL-Ag-GO-0.01 matrix. **(C)** Young's modulus of EVAL-Ag-GO-0.01 matrix. Statistical significance: **** and ns indicate 'p-value' < 0.0001 and non-significance.

EVAL-Ag-GO-0.01 L and EVAL-Ag-GO-0.01 T had a tensile strength of 6 ± 0.3 and 2 ± 0.3 MPa respectively (Figure 35B). So, the EVAL-Ag-GO-0.01 L had significantly higher tensile strength than the EVAL-Ag-GO-0.01 T. The Young's modulus of EVAL-Ag-GO-0.01 L and EVAL-Ag-GO-0.01 T were 26 ± 2 and 4 ± 0.3 MPa respectively (Figure 35C). Here also, the EVAL-Ag-GO-0.01 L had significantly higher Young's modulus than EVAL-Ag-GO-0.01 T. It is obvious that the longitudinal dumbbells will have significantly higher mechanical properties than the transverse dumbbells. EVAL-

neat had a tensile strength and Young's modulus of 1.5 ± 0.1 and 3.2 ± 0.2 MPa respectively (Figure 35B and C). The significant increase in tensile strength and Young's modulus of longitudinal dumbbells also indicates the fiber alignment of the EVAL-Ag-GO system. The presence of GO also contributes to the improvement of tensile properties. The aligned fibrous membranes from polycarbonate urethane fabricated with the incorporation of GO by Thampi et al. had better tensile properties than the bare material. The applied load will be transmitted to the GO from the matrix at the interface of GO-polymer composites (Thampi et al., 2015).

It is evident from the results that the longitudinal samples have significantly higher tensile properties than the transverse samples. When an aligned fibrous scaffold is used to bridge the proximal and distal stumps of a nerve, the scaffold must be sutured to the nerve stumps in a manner where the aligned fibers must run parallel to the nerve running direction. This would help the axonal sprouts to align and extend perfectly and avoid neuroma formation. The tensile strength (6±0.3 MPa) and Young's modulus (26 ± 2 MPa) of EVAL-Ag-GO-0.01 L samples was in the range of tensile properties obtained for peripheral nerves of animals (Borschel et al., 2003; Menzies et al., 2013; Rydevik et al., 1990).

4.4.8. ICP-OES analysis of EVAL-Ag-GO system

Any substrate with silver has a chance to release it into the surroundings when in contact with a medium. If the release occurs in the body fluids, the interaction of silver with the cells could lead to cytotoxicity. The Ag^+ in the EVAL-Ag-GO system does not exclusively interact with the polymer hydroxyl group, whereas it also interacts with the COOH of GO. So, the Ag^+ can be released into the medium. Therefore, the silver

release from a substrate must be evaluated. Here, the silver content in a matrix and PBS was quantified. The PBS was selected as the extraction medium because of its similarity with the body fluid pH (7.4). The matrix sample and extracts were subjected to ICP-OES analysis.

The silver content in 0.016 g of the EVAL-Ag-GO-0.01 matrix was 358.8 ppm. The silver released from a 0.014 g matrix immersed in PBS for 24 was only 0.207 ppm. However, only 0.230 ppm silver was released from the 0.013 g matrix into the PBS after one week. This indicates that the silver incorporated in the fibers was not completely released into the surrounding media. This interaction and complexation could prevent cytotoxicity by controlling the leaching of the silver from the membranes.

4.4.9. Direct contact test with EVAL-Ag-GO system

The Direct contact test is carried out to evaluate the material toxicity on cells by analyzing the cellular morphology and viability after 24 h interaction with the material. The phase contrast images captured after 24 h of interaction were used for evaluation (Figure 36A (a-d). Negative and positive controls were used along with the test materials (EVAL-neat and EVAL-Ag-GO-0.01). The dark portions in the images are the test and control materials. The cells interacted with EVAL-neat and EVAL-Ag-GO-0.01 retained their actual morphology because the cell membranes were intact (Figure 36A c and d). The cells were viable after interacting with the EVAL-Ag-GO-0.01 matrix. The cells that interacted with the negative control also had intact cell membranes, original morphology, and viability (Figure 36A a). Whereas, the cells that

interacted with the positive control were dead, non-viable, and lost the cell integrity due to the Tin-induced toxicity (Figure 36A b).

4.4.10. MTT assay with EVAL-Ag-GO system

MTT assay evaluates the viability of the cells regarding the mitochondrial activity. Any viable cell with active mitochondria picks up the MTT (Yellow coloured cell permeable substance) from the medium and converts it into formazan (Purple coloured non-permeable substance). The formazan crystals are solubilized and measured by the

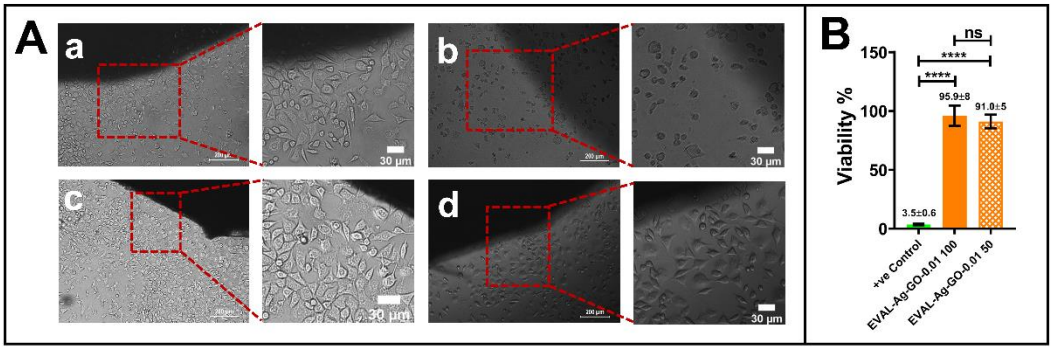

Figure 36: (A) Phase contrast images of Direct contact test **(a)** negative control (Ultra High Molecular Weight Poly Ethylene; UHMWPE), **(b)** positive control (Tin compound incorporated Polyvinyl chloride; Tin-PVC) **(c)** EVAL-neat, and (d) EVAL-Ag-GO-0.01. **(B)** MTT assay. Scale bar: main images are 200 µm and cropped images are 30 µm. Statistical significance: **** and ns indicate 'p-value' < 0.0001 and non-significance.

absorbance at 570 nm to quantify the cell viability. The quantity of formazan crystals directly indicated the viability. The results indicate that more than 90 % of the cells were viable after treatment with the extracts of EVAL-Ag-GO-0.01 (Figure 36B). The cells interacted with the undiluted (100 % extract) and diluted (50 % extract) extracts of EVAL-Ag-GO-0.01 and showed mitochondrial activity. Less cell viability (< 5 %) was observed for the cells that interacted with phenol (positive control).

The Direct contact test and MTT assay prove that the Ag^{+} released from the EVAL-Ag-GO-0.01 matrix is not significant to induce cytotoxicity.

4.4.11. Cell viability assessment of N2a and C6 cell lines with EVAL-Ag-GO system

The cells are subjected to live/dead assay to find the viability of the cells via fluorescent staining. The live/dead stains (Acridine orange; AO and Ethidium bromide; EtBr) are added to the cells (control and test). The live cells pick up AO and appear green in the fluorescent images. Whereas, EtBr enters only in the dead cells whose cytoplasm is disrupted and membrane integrity is lost. The EtBr entered cells fluoresce red. Figure 37 (A and B) show the viability of N2a and C6 cell viability respectively. In all the fluorescent images, the green-coloured cells were abundant. A negligible number of red cells were present. This indicates that the extracts of the matrices were not causing any damage to the cells (N2a and C6 cells). So, the majority of the cells were viable.

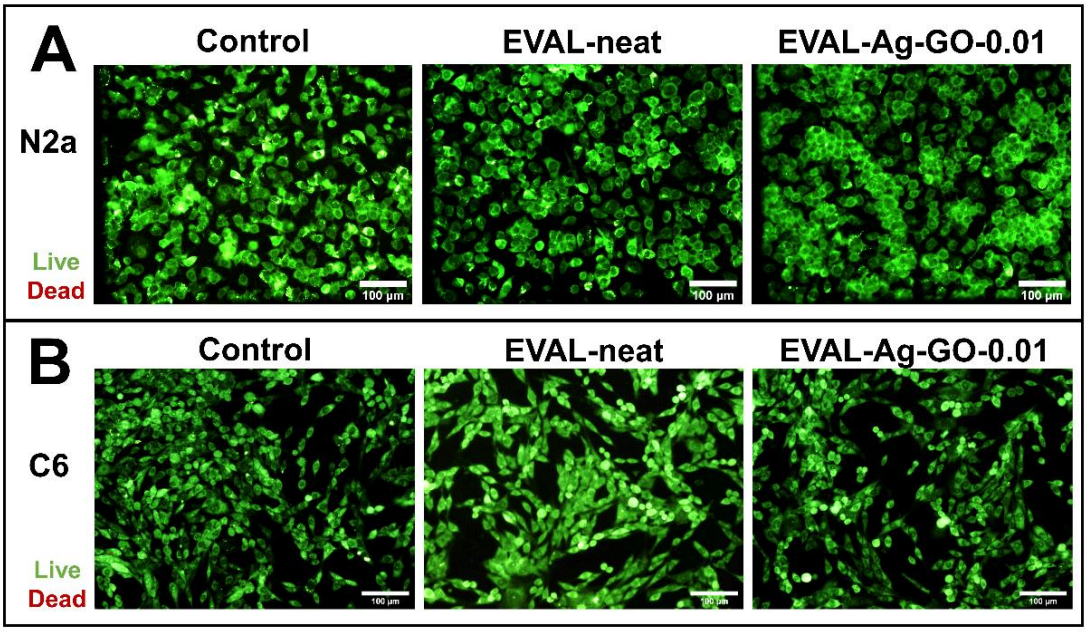

Figure 37: Fluorescence images of Live/dead assay (viability assessment) done on **(A)** N2a cell line and **(B)** C6 cell line after treatment with extracts of EVAL-neat and EVAL-Ag-GO-0.01. Control are untreated cells cultured on TCP surface. Scale bar: 100 µm.

The C6 cell line viability was quantified with flow cytometry (Figure 38B). For counting the live cells, the cells were stained with the FDA, a stain picked up and metabolized only by the live cells. The cells treated with extracts of EVAL-neat and EVAL-Ag-GO-0.01 were subjected to flow cytometry. The cells interacted with EVAL-neat and EVAL-Ag-GO-0.01 extracts showed a viability > 90 %. This also confirms the cytocompatible nature of the matrices.

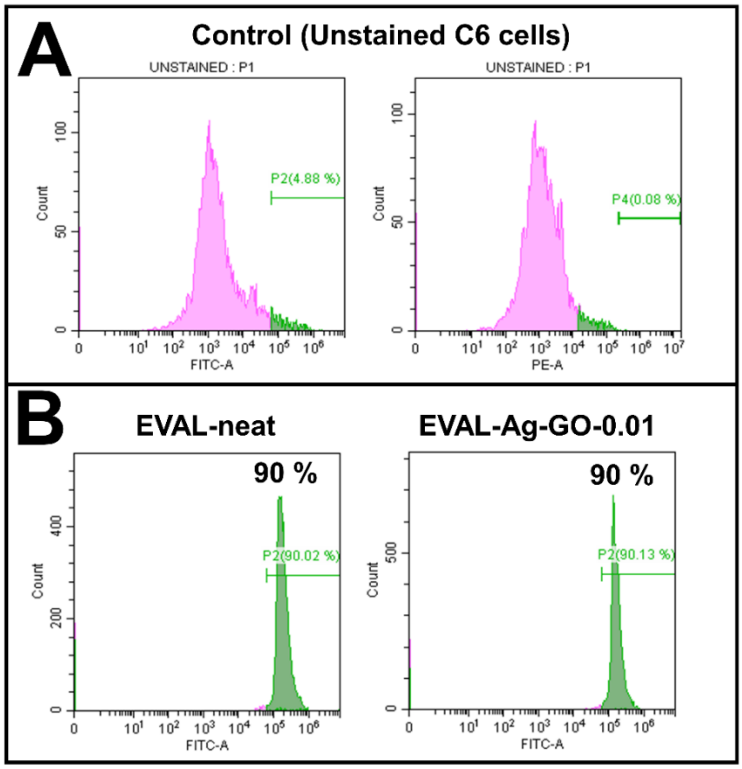

Figure 38: Viability assessment of C6 cell line using flow cytometry: **(A)** Control C6 cells (unstained) and **(B)** Cells stained after treatment with EVAL-neat and EVAL-Ag-GO-0.01 extracts.

4.4.12. Cellular/neurite response of N2a and C6 cell lines on EVAL-Ag-GO system

During natural nerve regeneration, the glial cells (Schwann cells) align and form a tube-like structure called “Bands of Bungner” (Wang et al., 2019). These cells secrete basal lamina. The basal lamina gives guidance cues for the axonal sprouts to reach the

distal stump. For proper nerve regeneration, the cellular and neurite alignment have significant impacts. So, nowadays for constructing a nerve repair scaffold, attempts are made to fabricate it with anisotropic features. The anisotropic features could easily orient the axonal sprouts (neurites) uniaxially (Hoffman-Kim et al., 2010; Leclech and Villard, 2020). Among the anisotropic substrates, aligned fibers are getting more attention in the construction of nerve repair scaffolds, since they resemble extracellular matrix (Cho et al., 2016; Lin et al., 2019; Lü et al., 2017; Orkwis et al., 2020; Thampi et al., 2020; Zou et al., 2016).

In the present study, N2a cell lines were considered for studying the neurite alignment. The neurites that arise from the N2a cells were visualized from F-actin staining. The F-actin is a part of the cytoskeleton and it helps in the extension of neurites. The F-actin is targeted because it guides a cell to adapt shape according to the substrate topography (Leclech and Villard, 2020). So, the staining of F-actin could provide information about the orientation of neurites. Focal adhesions (FAs) are the region where the actin stress fibers originate. The FAs themselves align on and orient along the topographies. The orientation of FAs determines the actin orientation and finally the neurite orientation. So, the orientation of the actin filaments is according to the orientation of FAs (Leclech and Villard, 2020). The overall event results in contact guidance according to the topography.

The neurites of N2a cells cultured on the TCP (control) were oriented in multiple directions (Figure 39A). The TCP surface is a homogenous (isotropic) one. So, the cells adhering to this surface get an opportunity to form their focal adhesion anywhere near the cell. This leads to a neurite extension in many directions. The EVAL-neat had

random fibers and the N2a cells extended their neurites in random orientations (Figure 39B). The fibrous surface of EVAL-neat is not similar to a TCP surface. However, a cell adhered to the randomly oriented fibrous surface has opportunities to form FAs in any fiber. Due to this reason, a cell gives rise to multiple neurites oriented in various directions. As mentioned earlier the neurites orient to a particular direction in which the FAs are formed and actin is oriented. The EVAL-Ag-GO-0.01 matrices had aligned fibers wherein the cells extended the neurites in an aligned manner. The cell adheres to an aligned fiber and is restricted to the fiber. So, the FAs are formed along and in the direction of fiber. This led to the aligned orientation of neurites in EVAL-Ag-GO-0.01 (Figure 39C).

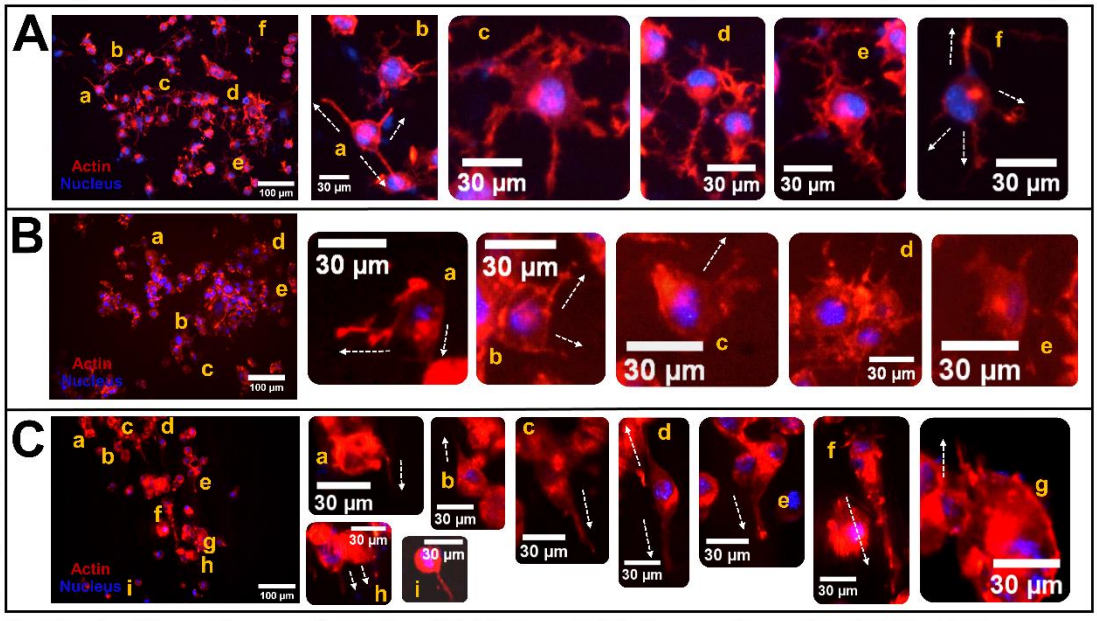

Figure 39: Fluorescence images of F-actin staining of N2a cells cultured on **(A)** control; Tissue culture plate (TCP), **(B)** EVAL-neat, and **(C)** EVAL-Ag-GO-0.01. Scale bar: main images are 100 µm and cropped images are 30 µm.

The Schwann cells play a significant role in nerve regeneration by forming “Bands of Bungner” and secreting basal lamina. So, the aligned arrangement of Schwann cells on a nerve repair scaffold would fasten the nerve regeneration. Regarding this concept,

C6 cells (considered instead of Schwann cells) were cultured on TCP surfaces, EVAL-neat, and EVAL-Ag-GO-0.01 matrices to evaluate cellular orientation. F-actin staining was done to evaluate the cellular arrangement. F-actin orientation determines the morphology and spatial arrangement of a cell.

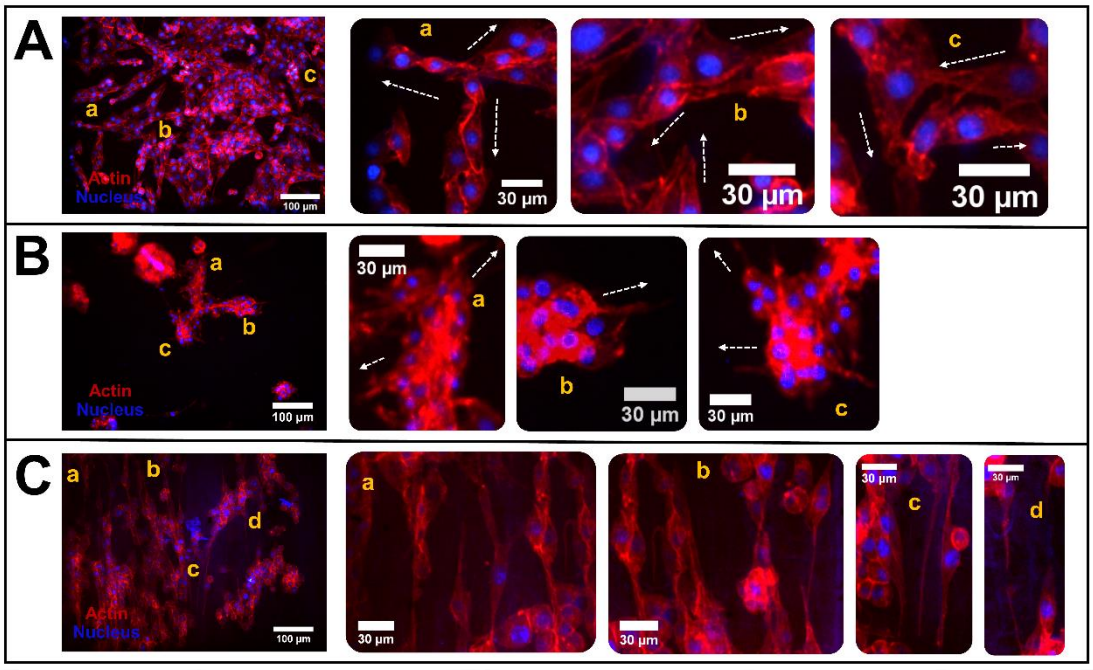

Figure 40: Fluorescence images of F-actin staining of C6 cells cultured on **(A)** control; Tissue culture plate (TCP), **(B)** EVAL-neat and **(C)** EVAL-Ag-GO-0.01. Scale bar: main images are 100 µm and cropped images are 30 µm.

The F-actin staining shows that the cells that adhered to the TCP surface were oriented in multiple directions and spread more on the surface (Figure 40A). As mentioned earlier the TCP surface is homogeneous (isotropic surface) and the cells could form the FAs at any point without any orientation. On such a surface the cells also spread more and attain elliptical morphology. Despite the fibrous nature, the EVAL-neat (random fibers) is more or less similar to the TCP surface. However, when the cells interact with this material, they adhere to the fibers. So, the FAs form on the fibers, and the cells spread along the fibers. This leads to the random orientation of the cells

on randomly oriented fibers of EVAL-neat. Here the cells have a similar elliptical morphology to the cell on the TCP surface (Figure 40B). The C6 cells on EVAL-Ag-GO-0.01 were aligned on the fibers and attained more elliptical morphology with long filopodia (Figure 40C). The aligned appearance of actin fibers indicates that the FAs formed on the fibers are also in an aligned manner.

A similar finding was made by Liu et al. in their study of human dermal fibroblast, where the spatial response of these cells was evaluated by culturing them on polymethyl methacrylate (PMMA). They observed that the fibroblasts plated on flat PMMA films stretched across the surface. The cells plated on the fibers with a lesser diameter (0.16 μm) were more similar to those on the film. When the fiber diameter increased to 0.97 μm and 8.64 μm, the cells spread well, though they became narrower and had well-defined actin fibers oriented along the polymer fibers (Liu et al., 2009). Similarly, Badami et al. showed that the cells on fibers with 2.1 μm (> 1 μm) had a greater aspect ratio showing that they spread mostly along the fiber (Badami et al., 2006). So, these studies suggest that the cell could align on parallel aligned features (aligned fibers or aligned grooves) that have 1 – 5 μm spacing (width or diameter) since this feature can orient the FAs and actin cytoskeleton for the contact guidance (Badami et al., 2006; Liu et al., 2009). Studies have shown that FAs are more than 1 μm size (Badami et al., 2006; Liu et al., 2009). In the present study also one can observe that the fiber diameter has a profound role in the cellular arrangement and filopodial extension. In the present study, the fiber diameter of EVAL-Ag-GO-0.01 is 3.5 ± 2 μm (> 1 μm) (Figure 34D) would support the FAs to align well on the fibers and this matrix could provide better contact guidance than the EVAL-neat.

Cell adhesion was evaluated from the SEM images of N2a and C6 cell-seeded EVAL-Ag-GO-0.01 matrices. The N2a and C6 cells were adhered to the fibers and extended their neurites and filopodia on the fibers (Figure 41A and B). Figure 41B very clearly shows that a C6 cell adhered to and extended its filopodia along the fibers.

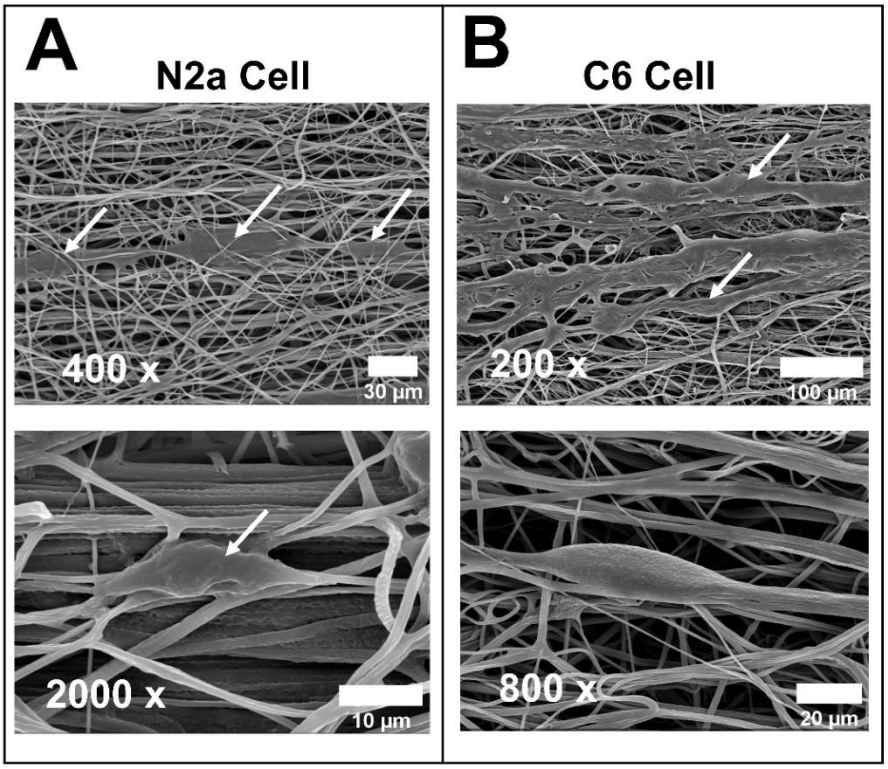

Figure 41: SEM images showing the cell adhesion on EVAL-Ag-GO-0.01 matrix. **(A)** N2a cell line and **(B)** C6 cell line. Scale bar: N2a cells are 30 µm and 10 µm for 400x and 2000x images respectively. C6 cells are 100 µm and 20 µm for 200 x and 800 x respectively.

β III tubulin is known as a neuronal marker since it is exclusively found in neuronal cells and their neurites. So, the fluorescent labeling of β III tubulin with antibodies would help to visualize the neurites and their orientations. The N2a cells were seeded on the EVAL-neat and EVAL-Ag-GO-0.01 matrices and were subjected to immunostaining of β III tubulin. The fluorescent images showed that the neurites on EVAL-neat oriented in multiple directions (Figure 42A) whereas, the neurites in

EVAL-Ag-GO-0.01 oriented in an aligned fashion (Figure 42B). These observations were consistent with that of F-actin staining results of N2a cells (Figure 39B and C).

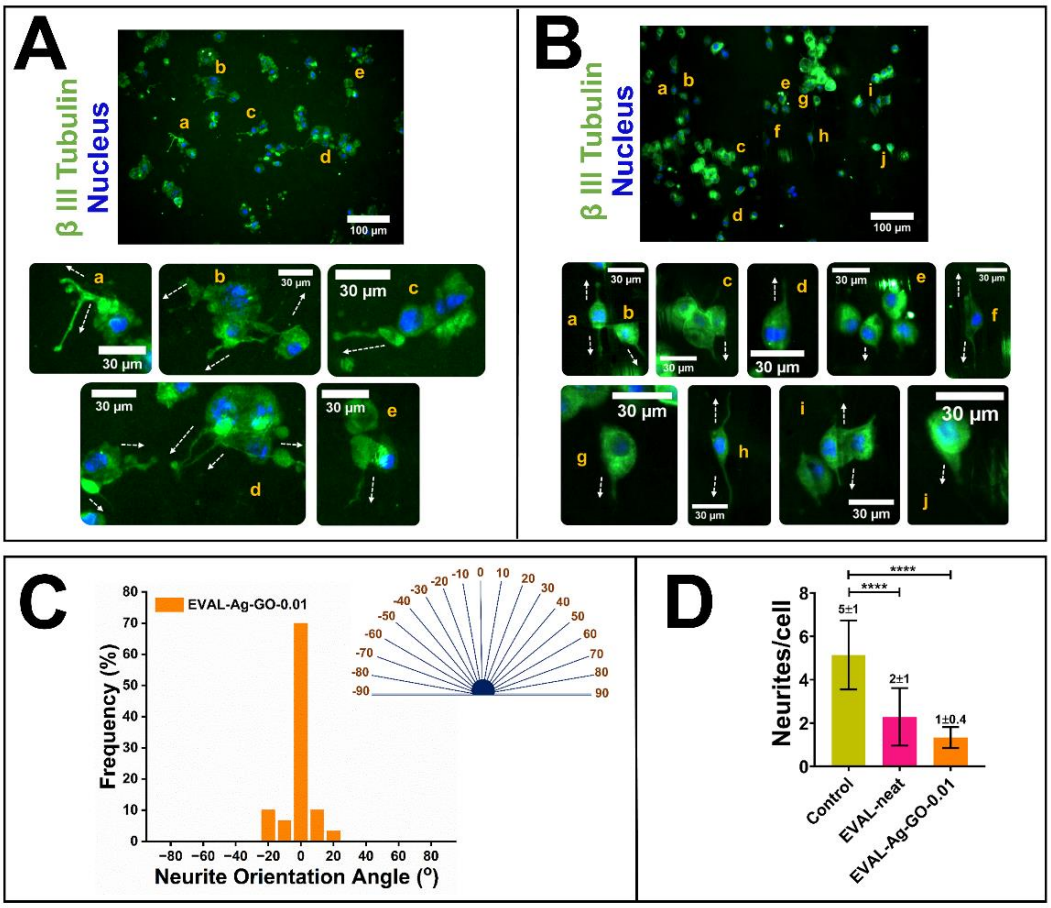

Figure 42: Fluorescence images of immunostained β III tubulin of N2a cells cultured on **(A)** EVAL-neat and **(B)** EVAL-Ag-GO-0.01. **(C)** Quantification of neurite orientation on EVAL-Ag-GO-0.01. **(D)** Neurites per N2a cell on control, EVAL-neat, and EVAL-Ag-GO-0.01. Scale bar: main images are 100 µm and cropped images are 30 µm. Significant difference: **** indicates 'p-value' ≤ 0.0001.

The neurite alignment was substantiated by quantifying the neurite orientations on the EVAL-Ag-GO-0.01 matrix. The results showed that > 70 % of neurites were oriented between -20 and 20 ° angles (Figure 42C). The neurites that arose from a cell also differed among control, EVAL-neat, and EVAL-Ag-GO-0.01 (Figure 42D). The TCP and EVAL-neat provide enough surfaces for the cells to adhere to and form their focal adhesions. So, it is possible to extend many neurites from a single cell. The neurites

per cell in control was 5 ± 1 and EVAL-neat was 2 ± 1. However, the cells on aligned fibers (EVAL-Ag-GO-0.01) have limited opportunities to extend their neurites in many directions. Since they follow the fiber to which they adhere, the N2a cells emanate 1 or 2 neurites. The neurite per cell in EVAL-Ag-GO-0.01 was 1 ± 0.4.

4.5. Spatial response of PC12 cell lines on EVAL-Ag-0.01 and EVAL-Ag-GO-0.01 systems

PC12 cells are small irregularly shaped loosely adherent cells in their undifferentiated stage. When differentiated these cells resemble the sympathetic neurons of the peripheral nervous system. Like the sympathetic neurons, they secrete catecholamines, dopamine, and norepinephrine (Wiatrak et al., 2020). Without nerve growth factor (NGF), they are small, spherical, aggregated, and proliferative. When supplied with NGF, they stop proliferation and differentiate into neuron-like morphology (Mingorance-Le Meur et al., 2009). So, these cell lines are preferred in studies related to neuronal proliferation, differentiation, adhesion, and response to topographical features. Several studies have been done to assess the spatial response of PC12 cells to the topographic cues of various polymeric fibrous substrates (Cho et al., 2016; Lin et al., 2019; Lü et al., 2017; Sumam and Parameswaran, 2023; Thampi et al., 2020; Zou et al., 2016). Here the PC12 cell lines were used to assess the spatial response on the EVAL matrices because the PC12 neurite extension and orientation could resemble a peripheral neuronal extension. The EVAL matrices with aligned fibers (EVAL-Ag-0.01 and EVAL-Ag-GO-0.01) were used to evaluate the PC12 cell response.

Figure 43 shows the immunostaining images of PC12 cells cultured on control (TCP), EVAL-Ag-0.01, and EVAL-Ag-GO-0.01 matrices. The β III tubulin (neuronal marker) was stained with antibodies to evaluate the cell response to topographic cues. The PC12 cells were also cultured on TCP surfaces and considered as control. It is evident from Figure 43 that the neurites extended from the PC12 cells on a TCP surface were oriented in various directions. In contrast, the cells on EVAL-Ag-0.01 and EVAL-Ag-

GO-0.01 surfaces respond well to the topographic cues and are found to be aligned on the fibers. Even in the undifferentiated stage, the PC12 cells have adhered to the fibers of EVAL-Ag-0.01 and EVAL-Ag-GO-0.01 in an aligned fashion. The neurite length was also measured from the β III tubulin-stained images (Figure 44).

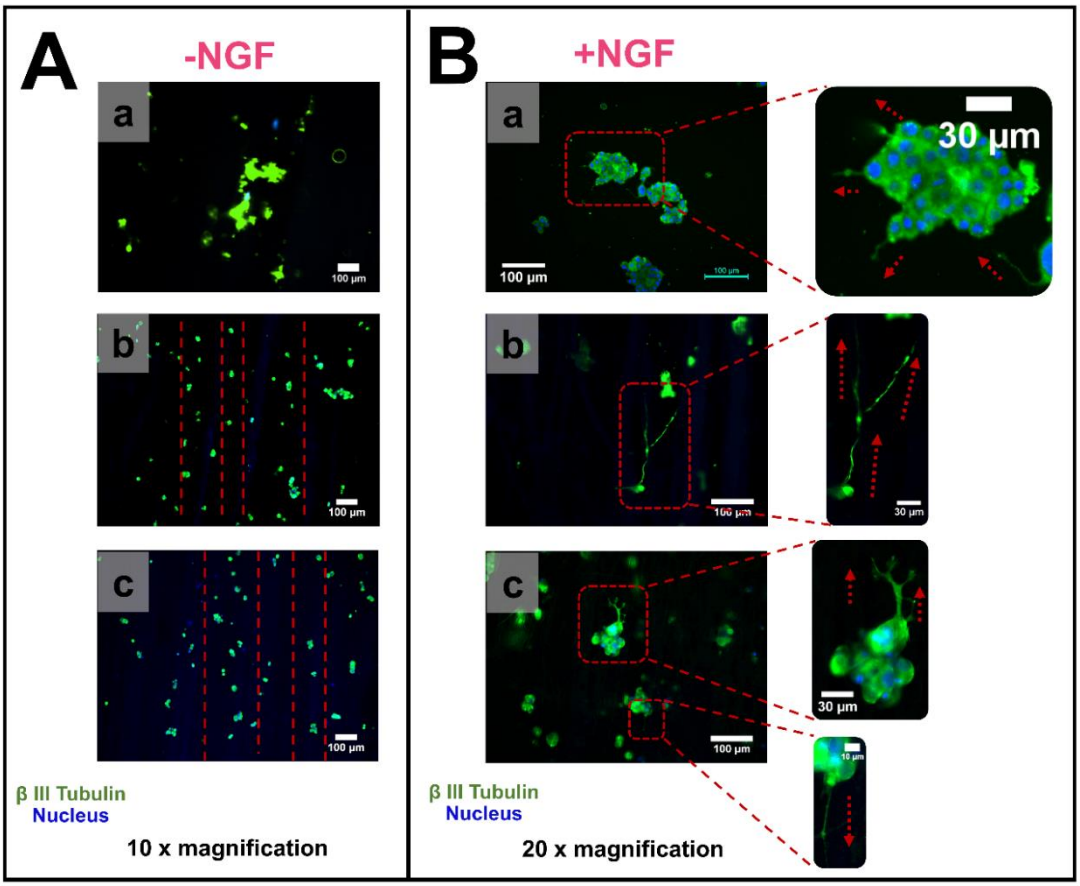

Figure 43: Fluorescence images of immunostained β III tubulin in PC12 cells cultured on **(A)** without NGF (10 x images) and (B) with NGF (20 x images). The images notated with 'a, b, and c' represent control (TCP), EVAL-Ag-0.01, and EVAL-Ag-GO-0.01 respectively. Scale bar: main images are 100 µm and cropped images are 30 µm.

Zou et al. fabricated aligned fibers from PLLA and studied the PC12 cell response on them. Interestingly, they also obtained results similar to this work. They fabricated PLLA fibers via electrospinning with pyrrole codoped with poly(glutamic acid)/dodecyl benzenesulfonic acid sodium (PPy-PLLA). They also observed that the PC12 differentiated on the TCP surface had many neurites directed in multiple orientations and those adhered to aligned fibers ran parallel to the fibers (Zou et al.,

2016). Similar findings were made by Lin et al. on aligned electrospun fibers. They also found directional outgrowth of neurites from PC12 cells on aligned fibers when compared to the TCP surface (Lin et al., 2019). Thampi et al. found that the GO in the polymer composites would create a favorable microenvironment for the development and outgrowth of neurites (Thampi et al., 2020). The wrinkled GO films also make the polymer similar to a soft substrate and induce mechanical stimulus where the neurites can stretch longer (Thampi et al., 2020).

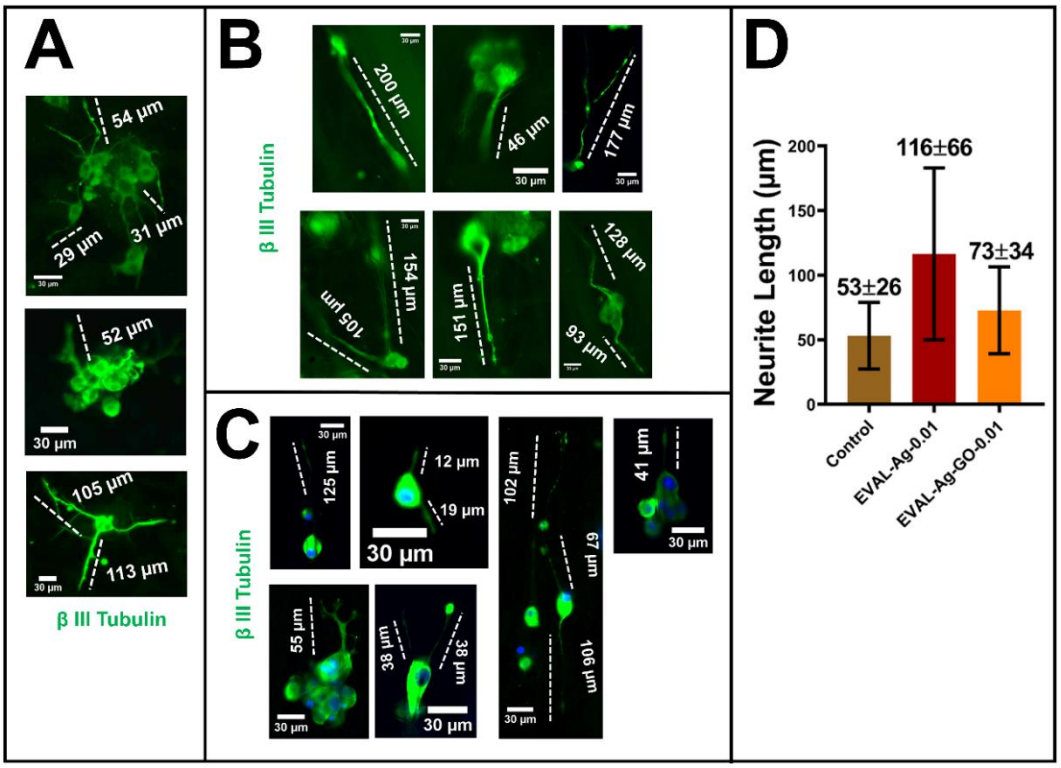

Figure 44: Neurite length of PC12 cells. Neurite length depicted in the fluorescence images showing immunostained β III tubulin in PC12 cells cultured on **(A)** control (TCP), **(B)** EVAL-Ag-0.01, and **(C)** EVAL-Ag-GO-0.01. **(D)** Graphical representation of neurite length of PC12. Scale bar: 30 µm.

CHAPTER 5: SUMMARY AND CONCLUSION

5.1. Summary and Conclusion

The present study aimed to fabricate electrospun matrices with aligned fibers that could provide contact guidance for the cells and neurites to orient them. The neurites and cells depend on topographical cues on substrates to ease their regeneration process in a definite direction. This would prevent neuroma formation due to delay in regeneration and help in a successful neuronal regeneration. Such matrices can be developed into nerve repair scaffolds (NGC/NWs) that could be used instead of nerve autografts in treating nerve injuries. Several FDA-approved NGC/NWs are available. However, a substrate similar to an autograft in many aspects is still lacking. One of the peculiarities necessary in an NGC/NWs is topographical cues to guide the regenerating neurites (axonal sprouts) to outgrow in an aligned fashion and reach their destiny via contact guidance. Electrospun fibers could provide such topographical cues. The alignment of the fibers in the matrices provides orientation for the cells and neurites via contact guidance. For constructing an NGC/NWs, a substrate must also promote cell adhesion, growth, proliferation, migration, differentiation, etc, besides the fiber alignment. Based on the previously mentioned facts, the entire work was planned based on the objectives:

1. To fabricate electrospun matrices incorporated with silver ions and/or graphene oxide.
2. To evaluate the physico-chemical properties of the matrices.
3. To evaluate the cell-material interactions *in vitro*.
    - Evaluation of cytotoxic effects of the matrices *in vitro.*

- Evaluation of guided neurite extension based on cell and neurite response on fibers of the matrices.

EVAL was the polymer that was considered for the matrix fabrication via electrospinning. The biocompatibility of EVAL is already known for its suitability in promoting neuronal cultures. The dissolution in nontoxic solvents and ease of electrospinnability made it more convenient. Three different systems, namely EVAL-GO, EVAL-Ag, and EVAL-Ag-GO were fabricated from EVAL using electrospinning. EVAL-GO system was fabricated with EVAL incorporated with graphene oxide (GO), EVAL-Ag system with $AgNO_3$, and EVAL-Ag-GO system with $AgNO_3$ and GO.

The $AgNO_3$ incorporated systems (EVAL-Ag and EVAL-Ag-GO) had aligned fibers. The fiber alignment was confirmed from SEM images, fiber orientation analysis of these systems using ImageJ software, and tensile property analysis. The fiber alignment in these matrices was due to the presence of Ag^+ in the EVAL solution. The presence of Ag^+ in the solution increased the conductivity of the solution in the EVAL-Ag and EVAL-Ag-GO systems when compared to the EVAL-neat. The EVAL-Ag and EVAL-Ag-GO solutions showed significantly high solution conductivity compared to EVAL-neat. An increase in solution conductivity reduced the jet whipping under high voltage and increased the jet stretching. High solution conductivity also increased the tendency of polymer solution to discharge fast. So, the jets consider a straight path to discharge and it led to the collection of aligned fibers on the collector. The significant increase of EVAL-Ag solution viscosity according to the increase in $AgNO_3$ content indicated the interaction of Ag^+ with the -OH group of the polymer. In EVAL-Ag and

EVAL-Ag-GO systems, the complexation of Ag^+ with the -OH of the polymer was then confirmed from the UV-Visible, XPS, and FTIR analysis.

The complexation significantly increased the fiber diameter in these systems when compared to EVAL-neat. The fibers in the EVAL-Ag system were mostly bundled due to the fusion of the splay which occurs as a result of increased solution conductivity. Such a fiber bundling was less in the EVAL-Ag-GO-0.01 matrices. Whereas, the EVAL-Ag-GO-0.05 and EVAL-Ag-GO-0.1 matrices showed fiber fusion rather than bundling. So, the EVAL-Ag-GO-0.05 and EVAL-Ag-GO-0.1 had fiber diameters > 10 μm. The EVAL-Ag-0.01 and EVAL-Ag-GO-0.01 also had significantly higher fiber diameters than the EVAL-neat.

The tensile properties also indicated that the EVAL-Ag-0.01 and EVAL-GO-0.01 had significantly higher tensile properties than the EVAL-neat. The Longitudinal dumbbells showed better tensile properties than the transverse dumbbells. The results indicated that the Longitudinal dumbbells had better tensile properties than the animal peripheral nerves. The betterment in tensile properties of these longitudinal dumbbells were because the fiber orientation was parallel to the tensile loading. When a nerve repair scaffold with aligned fibers is bridging a proximal and distal stump, the fiber orientation must be parallel to the nerve axis. So, the better tensile properties of Longitudinal dumbbells of EVAL-Ag-0.01 and EVAL-Ag-GO-0.01 would be favorable in developing an NGC/NWs that would not be damaged in daily *in vivo* mechanical forces.

EVAL-Ag-0.01 and EVAL-Ag-GO-0.01 matrices were noncytotoxic and guided the cells and neurites via contact guidance in an aligned manner. The F-actin staining (N2a,

and C6 cells) and β III tubulin immuno staining (N2a and PC12 cells) revealed the cellular and neurite response on the aligned fibers. The fluorescent staining images showed that FAs of the cells and neurites were on the fibers and were oriented along the fibers. So, the cells and neurites were showing an aligned arrangement. So, these results suggest that the EVAL-Ag-0.01 and EVAL-Ag-GO-0.01 matrices were suitable for developing NGC/NWs.

When compared to the EVAL-Ag and EVAL-Ag-GO systems. The EVAL-GO system had random fibers, that were not suitable for neurite or cellular alignment. Moreover, this system had a fiber diameter which was significantly lesser than the EVAL-neat. The fiber diameters of EVAL-GO matrices were at submicron size (< 1 μm). The submicron-sized fibers affected the C6 cellular adhesion and their morphology because these cells were prevented from spreading and attaining their morphology. Several studies have shown that the FAs have a size of 1 – 2 μm and it is difficult for a fiber with submicron size to support FAs and cell spreading. These matrices had better tensile properties compared to EVAL-neat and were also noncytotoxic. However, these matrices were not suitable for cellular and neurite alignment and could not perform well if they are developed as an NGC/NWs.

In conclusion, among the three systems (EVAL-GO, EVAL-Ag, and EVAL-Ag-GO) based on cellular and neurite-aligned orientation via contact guidance provided by the topographic cues, EVAL-Ag-0.01 and EVAL-Ag-GO-0.01 matrices showed similar performances. So, EVAL-Ag-0.01 and EVAL-Ag-GO-0.01 matrices will be considered for further studies to develop a nerve repair scaffold (NGC/NWs). More

mechanical, *in vitro*, and *in vivo* studies are necessary to determine that either EVAL-Ag-0.01 or EVAL-Ag-GO-0.01 is suitable for developing an NGC/NWs.

5.2. Future Perspectives

The future perspectives of the present study are listed below:

1. Gene expression: The difference between EVAL-Ag-GO-0.01 and EVAL-Ag-0.01 is the presence of GO. So, the effect of GO on the spatial responses of cells would be easily assessed by using gene expression studies *in vitro*. The Schwann cells play an important role in nerve regeneration by forming Bands of Bungner and secrete basal lamina. They also differentiate into myelinating cells during regeneration. Evaluating the gene expression and protein expression of myelin-associated proteins concerning the interaction of GO would help to determine whether EVAL-Ag or EVAL-Ag-GO is better in performance as an NGC/NWs.
2. Implantation studies in small animals could determine the dimensions of the matrices when used as NGC/NWs.

REFERENCES

Abzan N, Kharaziha M and Labbaf S (2019) Development of three-dimensional piezoelectric polyvinylidene fluoride-graphene oxide scaffold by non-solvent induced phase separation method for nerve tissue engineering. *Materials & Design* 167: 107636.

Al-Dhahebi AM, Gopinath SCB and Saheed MSM (2020) Graphene impregnated electrospun nanofiber sensing materials: a comprehensive overview on bridging laboratory set-up to industry. *Nano Convergence* 7(1): 27.

Alon N, Miroshnikov Y, Perkas N, et al. (2014) Substrates coated with silver nanoparticles as a neuronal regenerative material. *International Journal of Nanomedicine* 9(Suppl 1): 23–31.

Anderson M, Shelke NB, Manoukian OS, et al. (2015) Peripheral Nerve Regeneration Strategies: Electrically Stimulating Polymer Based Nerve Growth Conduits. *Critical Reviews in Biomedical Engineering* 43(2–3): 131–159.

Arras MML, Grasl C, Bergmeister H, et al. (2012) Electrospinning of aligned fibers with adjustable orientation using auxiliary electrodes. *Science and Technology of Advanced Materials* 13(3). Taylor & Francis: 035008.

Aucejo S, Marco C and Gavara R (1999) Water effect on the morphology of EVOH copolymers. *Journal of Applied Polymer Science* 74(5): 1201–1206.

Badami AS, Kreke MR, Thompson MS, et al. (2006) Effect of fiber diameter on spreading, proliferation, and differentiation of osteoblastic cells on electrospun poly(lactic acid) substrates. *Biomaterials* 27(4): 596–606.

Bashur CA, Dahlgren LA and Goldstein AS (2006) Effect of fiber diameter and orientation on fibroblast morphology and proliferation on electrospun poly(D,L-lactic-co-glycolic acid) meshes. *Biomaterials* 27(33): 5681–5688.

Borschel GH, Kia KF, Kuzon WM, et al. (2003) Mechanical properties of acellular peripheral nerve. *The Journal of Surgical Research* 114(2): 133–139.

Bozkurt A, Brook GA, Moellers S, et al. (2007) In vitro assessment of axonal growth using dorsal root ganglia explants in a novel three-dimensional collagen matrix. *Tissue Engineering* 13(12): 2971–2979.

Bunge RP (1994) The role of the Schwann cell in trophic support and regeneration. *Journal of Neurology* 242(1): S19–S21.

Burger C, Hsiao BS and Chu B (2006) NANOFIBROUS MATERIALS AND THEIR APPLICATIONS. *Annual Review of Materials Research* 36(Volume 36, 2006). Annual Reviews: 333–368.

Burnett MG and Zager EL (2004) Pathophysiology of peripheral nerve injury: a brief review. *Neurosurgical focus* 16(5). American Association of Neurological Surgeons: 1–7.

Buskermolen ABC, Ristori T, Mostert D, et al. (2020) Cellular Contact Guidance Emerges from Gap Avoidance. *Cell Reports. Physical Science* 1(5): 100055.

Chhabra A, Ahlawat S, Belzberg A, et al. (2014) Peripheral nerve injury grading simplified on MR neurography: As referenced to Seddon and Sunderland classifications. *The Indian Journal of Radiology & Imaging* 24(3): 217–224.

Chiacchiaretta M, Bramini M, Rocchi A, et al. (2018) Graphene Oxide Upregulates the Homeostatic Functions of Primary Astrocytes and Modulates Astrocyte-to-Neuron Communication. *Nano Letters* 18(9): 5827–5838.

Chiono V and Tonda-Turo C (2015) Trends in the design of nerve guidance channels in peripheral nerve tissue engineering. *Progress in neurobiology* 131. Elsevier: 87–104.

Cho M, Kim S-H, Jin G, et al. (2016) Salt-Induced Electrospun Patterned Bundled Fibers for Spatially Regulating Cellular Responses. *ACS Applied Materials & Interfaces* 8(21): 13320–13331.

Chou H, Wu C, Lin F, et al. (2014) Interactions between silver nanoparticles and polyvinyl alcohol nanofibers. *AIP Advances* 4: 087111–1~10.

Çiplak Z, Karabudak Yildiz N and Çalimli A (2014) Investigation of Graphene/Ag Nanocomposites Synthesis Parameters for Two Different Synthesis Methods. *Fullerenes, Nanotubes and Carbon Nanostructures* 23: 361–370.

Cooney TF, Wang L, Sharma SK, et al. (1994) Raman spectral study of solid and dissolved poly(vinyl alcohol) and ethylene-vinyl alcohol copolymer. *Journal of Polymer Science Part B: Polymer Physics* 32(7): 1163–1174.

Corey JM, Lin DY, Mycek KB, et al. (2007) Aligned electrospun nanofibers specify the direction of dorsal root ganglia neurite growth. *Journal of Biomedical Materials Research Part A* 83A(3): 636–645.

Daeschler SC, So KJW, Feinberg K, et al. (2025) A functional tacrolimus-releasing nerve wrap for enhancing nerve regeneration following surgical nerve repair. *Neural Regeneration Research* 20(1): 291.

Deitzel JM, Kleinmeyer J, Harris D, et al. (2001) The effect of processing variables on the morphology of electrospun nanofibers and textiles. *Polymer* 42(1): 261–272.

Evans GR (2001) Peripheral nerve injury: a review and approach to tissue engineered constructs. *The Anatomical Record* 263(4): 396–404.

Fang X, Guo H, Zhang W, et al. (2020) Reduced graphene oxide-GelMA-PCL hybrid nanofibers for peripheral nerve regeneration. *Journal of materials chemistry. B* 8.

Feles S, Overath C, Reichardt S, et al. (2022) Streamlining Culture Conditions for the Neuroblastoma Cell Line SH-SY5Y: A Prerequisite for Functional Studies. *Methods and Protocols* 5(4): 58.

Ferraria A, Carapeto A and Rego AM (2012) X-ray photoelectron spectroscopy: Silver salts revisited. *Vacuum* 86.

Ferreira CL, Valente CA, Zanini ML, et al. (2019) Biocompatible PCL/PLGA/Polypyrrole Composites for Regenerating Nerves. *Macromolecular Symposia* 383(1): 1800028.

Gan Y, Bai S, Hu S, et al. (2016) Reaction mechanism of thermally-induced electric conduction of poly(vinyl alcohol)–silver nitrate hybrid films. *RSC Advances* 6(61): 56728–56737.

Gaudin R, Knipfer C, Henningsen A, et al. (2016) Approaches to peripheral nerve repair: generations of biomaterial conduits yielding to replacing autologous nerve grafts in craniomaxillofacial surgery. *BioMed research international* 2016. Hindawi.

Ghafaralahi S, Ebrahimian-Hosseinabadi M and Zargar A (2018) Poly (glycerol-sebacate)/poly (caprolactone)/Graphene nanocomposites for nerve tissue engineering. *Journal of Bioactive and Compatible Polymers* 33: 088391151879391.

Gnavi S, Fornasari BE, Tonda-Turo C, et al. (2015) The Effect of Electrospun Gelatin Fibers Alignment on Schwann Cell and Axon Behavior and Organization in the Perspective of Artificial Nerve Design. *International Journal of Molecular Sciences* 16(6): 12925–12942.

Grinsell D and Keating CP (2014) Peripheral nerve reconstruction after injury: a review of clinical and experimental therapies. *BioMed research international* 2014. Hindawi.

Guroff G (1985) PC12 Cells as a Model of Neuronal Differentiation. In: Bottenstein JE and Sato G (eds) *Cell Culture in the Neurosciences*. Boston, MA: Springer US, pp. 245–272. Available at: https://doi.org/10.1007/978-1-4613-2473-7_8 (accessed 11 May 2024).

Haider A, Haider S and Kang I-K (2018) A comprehensive review summarizing the effect of electrospinning parameters and potential applications of nanofibers in biomedical and biotechnology. *Arabian Journal of Chemistry* 11(8): 1165–1188.

Hall JE and Guyton AC (2011) *Guyton and Hall Textbook of Medical Physiology*. 12th ed. Philadelphia, Pa: Saunders/Elsevier.

Hansora DP, Shimpi NG and Mishra S (2015) Graphite to Graphene via Graphene Oxide: An Overview on Synthesis, Properties, and Applications. *JOM* 67(12): 2855–2868.

He Z, Xie L, Song S, et al. (2010) The impact of silver modification on the catalytic activity of iodine-doped titania for *p*-chlorophenol degradation under visible-light irradiation. *Journal of Molecular Catalysis A: Chemical* 319(1): 78–84.

Heath CA and Rutkowski GE (1998) The development of bioartificial nerve grafts for peripheral-nerve regeneration. *Trends in biotechnology* 16(4). Elsevier: 163–168.

Hoffman-Kim D, Mitchel JA and Bellamkonda RV (2010) Topography, Cell Response, and Nerve Regeneration. *Annual review of biomedical engineering* 12: 203–231.

Hoffmann LF, Martins A, Majolo F, et al. (2022) Neural regeneration research model to be explored: SH-SY5Y human neuroblastoma cells. *Neural Regeneration Research* 18(6): 1265–1266.

Houshyar S, Bhattacharyya A and Shanks R (2019) Peripheral Nerve Conduit: Materials and Structures. *ACS Chemical Neuroscience* 10(8): 3349–3365.

Hsiao M-C, Liao S-H, Yen M-Y, et al. (2010) Preparation of Covalently Functionalized Graphene Using Residual Oxygen-Containing Functional Groups. *ACS Applied Materials & Interfaces* 2(11). American Chemical Society: 3092–3099.

Hu Y, Zhang H, Wei H, et al. (2022) Scaffolds with anisotropic structure for neural tissue engineering. *Engineered Regeneration* 3(2): 154–162.

Huang H-D, Ren P-G, Chen J, et al. (2012) High barrier graphene oxide nanosheet/poly(vinyl alcohol) nanocomposite films. *Journal of Membrane Science* s 409–410: 156–163.

Huang Z, Jiang H, Peidang L, et al. (2014) Continuous synthesis of size-tunable silver nanoparticles by green electrolysis method and multi-electrode design for high yield. *J. Mater. Chem. A* 3.

Huang Z-M, Zhang Y-Z, Kotaki M, et al. (2003) A review on polymer nanofibers by electrospinning and their applications in nanocomposites. *Composites Science and Technology* 63(15): 2223–2253.

Huber AB, Kolodkin AL, Ginty DD, et al. (2003) Signaling at the growth cone: ligand-receptor complexes and the control of axon growth and guidance. *Annual Review of Neuroscience* 26: 509–563.

Ikram R, Jan BM and Ahmad W (2020) An overview of industrial scalable production of graphene oxide and analytical approaches for synthesis and characterization. *Journal of Materials Research and Technology* 9(5): 11587–11610.

Ishibe K, Tamatsu Y, Miura M, et al. (2011) Morphological study of the vasa nervorum in the peripheral branch of human facial nerve. *Okajimas Folia Anatomica Japonica* 88(3): 111–119.

Jiang H, Qian Y, Fan C, et al. (2020) Polymeric Guide Conduits for Peripheral Nerve Tissue Engineering. *Frontiers in Bioengineering and Biotechnology* 8: 582646.

Jin G-Z, Kim M, Shin US, et al. (2011) Neurite outgrowth of dorsal root ganglia neurons is enhanced on aligned nanofibrous biopolymer scaffold with carbon nanotube coating. *Neuroscience Letters* 501(1): 10–14.

Kalil K and Dent EW (2005) Touch and go: guidance cues signal to the growth cone cytoskeleton. *Current Opinion in Neurobiology* 15(5). Neuronal and glial cell biology / New technologies: 521–526.

Kameoka J, Orth R, Yang Y, et al. (2003) A scanning tip electrospinning source for deposition of oriented nanofibres. *Nanotechnology* 14(10): 1124.

Kang N-U, Lee S-J and Gwak S-J (2022) Fabrication Techniques of Nerve Guidance Conduits for Nerve Regeneration. *Yonsei medical journal* 63: 114–123.

Kang Y, Liu J, Wu J, et al. (2017) Graphene oxide and reduced graphene oxide induced neural pheochromocytoma-derived PC12 cell lines apoptosis and cell cycle alterations via the ERK signaling pathways. *International Journal of Nanomedicine* 12: 5501–5510.

Kanjwal MA and Ghaferi AA (2022) Graphene Incorporated Electrospun Nanofiber for Electrochemical Sensing and Biomedical Applications: A Critical Review. *Sensors* 22(22). 22. Multidisciplinary Digital Publishing Institute: 8661.

Kehoe S, Zhang XF and Boyd D (2012) FDA approved guidance conduits and wraps for peripheral nerve injury: A review of materials and efficacy. *Injury* 43(5): 553–572.

Keirouz A, Wang Z, Reddy VS, et al. (2023) The History of Electrospinning: Past, Present, and Future Developments. *Advanced Materials Technologies* 8(11): 2201723.

Kenawy E-R, Layman JM, Watkins JR, et al. (2003) Electrospinning of poly(ethylene-co-vinyl alcohol) fibers. *Biomaterials* 24(6): 907–913.

Kim SW and Choi HM (2015) Enhancement of thermal, mechanical, and barrier properties of ethylene vinyl alcohol copolymer by incorporation of graphene nanosheets: effect of functionalization of graphene oxide. *High Performance Polymers* 27(6). SAGE Publications Ltd STM: 694–704.

Kim Y-K, Han SW and Min D-H (2012) Graphene oxide sheath on Ag nanoparticle/graphene hybrid films as an antioxidative coating and enhancer of surface-enhanced Raman scattering. *ACS applied materials & interfaces* 4(12): 6545–6551.

Kumar R, Rashid J and Barakat MA (2015) Zero valent Ag deposited TiO2 for the efficient photocatalysis of methylene blue under UV-C light irradiation. *Colloids and Interface Science Communications* 5: 1–4.

Le HN, Thai D, Nguyen TT, et al. (2023) Improving safety and efficiency in graphene oxide production technology. *Journal of Materials Research and Technology* 24: 4440–4453.

Leach JB, Brown XQ, Jacot JG, et al. (2007) Neurite outgrowth and branching of PC12 cells on very soft substrates sharply decreases below a threshold of substrate rigidity. *Journal of Neural Engineering* 4(2): 26–34.

Leclech C and Villard C (2020) Cellular and Subcellular Contact Guidance on Microfabricated Substrates. *Frontiers in Bioengineering and Biotechnology* 8: 551505.

Li W, Song J, Wang C, et al. (2019) Facile synthesis of cubic Ag/Ag2O composites and its shape-dependent photo-catalytic activity examination. *Journal of Materials Science: Materials in Electronics* 30(6): 5366–5374.

Liao C-C, Wang C-C, Shih K-C, et al. (2011) Electrospinning fabrication of partially crystalline bisphenol A polycarbonate nanofibers: Effects on conformation, crystallinity, and mechanical properties. *European Polymer Journal* 47(5): 911–924.

Lin C-Y, Luo S-C, Yu J-S, et al. (2019) Peptide-Based Polyelectrolyte Promotes Directional and Long Neurite Outgrowth. *ACS Applied Bio Materials* 2(1): 518–526.

Litowczenko J, Maciejewska BM, Wychowaniec JK, et al. (2019) Groove-patterned surfaces induce morphological changes in cells of neuronal origin. *Journal of Biomedical Materials Research Part A* 107(10): 2244–2256.

Liu X, Hao M, Chen Z, et al. (2021) 3D bioprinted neural tissue constructs for spinal cord injury repair. *Biomaterials* 272: 120771.

Liu Y, Ji Y, Ghosh K, et al. (2009) Effects of fiber orientation and diameter on the behavior of human dermal fibroblasts on electrospun PMMA scaffolds. *Journal of Biomedical Materials Research Part A* 90A(4): 1092–1106.

Lü X, Yang F, Huang Y, et al. (2017) Role of integrin in influencing differentiation of PC12 cell grown on PLLA-aligned nanofiber: a mRNA–microRNA–protein integrative study. *Regenerative Biomaterials* 4(2): 89–96.

Luo L (2002) Actin Cytoskeleton Regulation in Neuronal Morphogenesis and Structural Plasticity. *Annual Review of Cell and Developmental Biology* 18(Volume 18, 2002). Annual Reviews: 601–635.

Ma H, Zhang H, Wang D, et al. (2020) Structure and performance analysis of flatter ribbon-like electrospun poly(L-lactic acid)/graphene oxide nanofiber webs. *Journal of Engineered Fibers and Fabrics* 15. SAGE Publications Ltd STM: 1558925020952924.

Ma J, Li Y, Yin X, et al. (2016) Poly(vinyl alcohol)/graphene oxide nanocomposites prepared by in situ polymerization with enhanced mechanical properties and water vapor barrier properties. *RSC Advances* 6(55). The Royal Society of Chemistry: 49448–49458.

Magaz A, Li X, Gough JE, et al. (2021) Graphene oxide and electroactive reduced graphene oxide-based composite fibrous scaffolds for engineering excitable nerve tissue. *Materials Science and Engineering: C* 119: 111632.

Mamun A, Blachowicz T and Sabantina L (2021) Electrospun Nanofiber Mats for Filtering Applications—Technology, Structure and Materials. *Polymers* 13(9): 1368.

Marcano DC, Kosynkin DV, Berlin JM, et al. (2010) Improved Synthesis of Graphene Oxide. *ACS Nano* 4(8). American Chemical Society: 4806–4814.

Mayuri PV and Ramesh P (2016) Fabrication and characterization of silver nanoparticle impregnated uniaxially aligned fibre yarns by one-step electrospinning process. *Journal of Materials Science* 51(5): 2739–2746.

Mayuri PV, Bhatt A, Joseph R, et al. (2016) Effect of photografting 2-hydroxyethyl acrylate on the hemocompatibility of electrospun poly(ethylene-co-vinyl alcohol) fibroporous mats. *Materials Science & Engineering. C, Materials for Biological Applications* 60: 19–29.

Meinel AJ, Germershaus O, Luhmann T, et al. (2012) Electrospun matrices for localized drug delivery: current technologies and selected biomedical applications. *European Journal of Pharmaceutics and Biopharmaceutics: Official Journal of Arbeitsgemeinschaft Fur Pharmazeutische Verfahrenstechnik e.V* 81(1): 1–13.

Menzies CH, Lauto A, Mirto LV, et al. (2013) A nested-lumen nerve graft design for neuroengineering. *Journal of Biomimetics Biomaterials and Tissue Engineering*: 2–8.

Mi H-Y, Jing X and Turng L-S (2015) Fabrication of porous synthetic polymer scaffolds for tissue engineering. *Journal of Cellular Plastics* 51(2). SAGE Publications Ltd STM: 165–196.

Ming J, Sun D, Wei J, et al. (2020) Adhesion of Bacteria to a Graphene Oxide Film. *ACS Applied Bio Materials* 3(1). American Chemical Society: 704–712.

Mingorance-Le Meur A, Mohebiany AN and O'Connor TP (2009) Varicones and Growth Cones: Two Neurite Terminals in PC12 Cells. *PLoS ONE* 4(2): e4334.

Mit-uppatham C, Nithitanakul M and Supaphol P (2004) Effects of Solution Concentration, Emitting Electrode Polarity, Solvent Type, and Salt Addition on Electrospun Polyamide-6 Fibers: A Preliminary Report. *Macromolecular Symposia* 216(1): 293–300.

Mohammadi S, Shafiei SS, Asadi-Eydivand M, et al. (2017) Graphene oxide-enriched poly(ε-caprolactone) electrospun nanocomposite scaffold for bone tissue engineering applications. *Journal of Bioactive and Compatible Polymers* 32(3). SAGE Publications Ltd STM: 325–342.

Muheremu A and Ao Q (2015) Past, present, and future of nerve conduits in the treatment of peripheral nerve injury. *BioMed research international* 2015. Hindawi.

Orkwis JA, Wolf AK, Shahid SM, et al. (2020) Development of a Piezoelectric PVDF-TrFE Fibrous Scaffold to Guide Cell Adhesion, Proliferation, and Alignment. *Macromolecular Bioscience* 20(9): 2000197.

Papadimitriou L, Manganas P, Ranella A, et al. (2020) Biofabrication for neural tissue engineering applications. *Materials Today Bio* 6: 100043.

Pham Q, Sharma U and Mikos A (2006) Electrospinning of Polymeric Nanofibers for Tissue Engineering Applications: A Review. *Tissue engineering* 12: 1197–211.

Puhl DL, Funnell JL, D'Amato AR, et al. (2020) Aligned Fingolimod-Releasing Electrospun Fibers Increase Dorsal Root Ganglia Neurite Extension and Decrease Schwann Cell Expression of Promyelinating Factors. *Frontiers in Bioengineering and Biotechnology* 8: 937.

Qian Y, Song J, Zhao X, et al. (2018) 3D Fabrication with Integration Molding of a Graphene Oxide/Polycaprolactone Nanoscaffold for Neurite Regeneration and Angiogenesis. *Advanced Science* 5(4): 1700499.

Qing H, Jin G, Zhao G, et al. (2018) Heterostructured Silk-Nanofiber-Reduced Graphene Oxide Composite Scaffold for SH-SY5Y Cell Alignment and Differentiation. *ACS Applied Materials & Interfaces* 10(45). American Chemical Society: 39228–39237.

Rahman M, Mahady Dip T, Padhye R, et al. (2023) Review on electrically conductive smart nerve guide conduit for peripheral nerve regeneration. *Journal of Biomedical Materials Research Part A* 111(12): 1916–1950.

Ranjan P, Agrawal S, Sinha A, et al. (2018) A Low-Cost Non-explosive Synthesis of Graphene Oxide for Scalable Applications. *Scientific Reports* 8(1). Nature Publishing Group: 12007.

Rashid TU, Gorga RE and Krause WE (2021) Mechanical Properties of Electrospun Fibers—A Critical Review. *Advanced Engineering Materials* 23(9): 2100153.

Rattana, Chaiyakun S, Witit-anun N, et al. (2012) Preparation and characterization of graphene oxide nanosheets. *Procedia Engineering* 32. ISEEC: 759–764.

Resmi R, Parvathy J, Saravana RP, et al. (2021) Biosynthesized Nanosilver from Alginate Dialdehyde: An In Vitro Evaluation. *ChemistrySelect* 6(43): 12007–12017.

Robinson AJ, Pérez-Nava A, Ali SC, et al. (2021) Comparative analysis of fiber alignment methods in electrospinning. *Matter* 4(3). Elsevier: 821–844.

Rodrigues AF, Newman L, Lozano N, et al. (2018) A blueprint for the synthesis and characterisation of thin graphene oxide with controlled lateral dimensions for biomedicine. *2D Materials* 5(3). IOP Publishing: 035020.

Rosa V, Xie H, Dubey N, et al. (2016) Graphene oxide-based substrate: physical and surface characterization, cytocompatibility and differentiation potential of dental pulp stem cells. *Dental Materials: Official Publication of the Academy of Dental Materials* 32(8): 1019–1025.

Rydevik BL, Kwan MK, Myers RR, et al. (1990) An in vitro mechanical and histological study of acute stretching on rabbit tibial nerve. *Journal of Orthopaedic Research: Official Publication of the Orthopaedic Research Society* 8(5): 694–701.

Sangsanoh P, Israsena N, Suwantong O, et al. (2017) Effect of the surface topography and chemistry of poly(3-hydroxybutyrate) substrates on cellular behavior of the murine neuroblastoma Neuro2a cell line. *Polymer Bulletin* 74(10): 4101–4118.

Sarker MD, Naghieh S, McInnes AD, et al. (2018) Regeneration of peripheral nerves by nerve guidance conduits: Influence of design, biopolymers, cells, growth factors, and physical stimuli. *Progress in neurobiology* 171. Elsevier: 125–150.

Scaccini L, Mezzena R, De Masi A, et al. (2021) Chitosan Micro-Grooved Membranes with Increased Asymmetry for the Improvement of the Schwann Cell Response in Nerve Regeneration. *International Journal of Molecular Sciences* 22(15): 7901.

Sharma N, Tomar S, Shkir Mohd, et al. (2021) Study of Optical and Electrical Properties of Graphene Oxide. *Materials Today: Proceedings* 36. National Conference on Advanced Functional Materials 2019: 730–735.

Sherwood L (2010) *Human Physiology from Cells to Systems*. Cengage Larning. Available at: http://repository.unipa.ac.id/xmlui/handle/123456789/629 (accessed 12 March 2024).

Simitzi C, Ranella A and Stratakis E (2017) Controlling the morphology and outgrowth of nerve and neuroglial cells: The effect of surface topography. *Acta Biomaterialia* 51: 21–52.

Song B, Cui W and Chang J (2011) Study on the effect of inorganic salts on the alignment of electrospun fiber. *Journal of Applied Polymer Science* 122(2): 1047–1052.

Song H and Poo M (2001) The cell biology of neuronal navigation. *Nature Cell Biology* 3(3). Nature Publishing Group: E81–E88.

Sumam P and Parameswaran R (2023) Neuronal cell response on aligned fibroporous electrospun mat generated from silver ion complexed ethylene vinyl alcohol copolymer. *Journal of Biomedical Materials Research Part B: Applied Biomaterials* 111(4): 782–794.

Sun D, Chang C, Li S, et al. (2006) Near-Field Electrospinning. *Nano Letters* 6(4). American Chemical Society: 839–842.

Sunderland SS (1990) The anatomy and physiology of nerve injury. *Muscle & Nerve* 13(9): 771–784.

Surendranath M, Rajalekshmi R, Ramesan RM, et al. (2022) UV-Crosslinked Electrospun Zein/PEO Fibroporous Membranes for Wound Dressing. *ACS Applied Bio Materials* 5(4): 1538–1551.

Teo WE and Ramakrishna S (2006) A review on electrospinning design and nanofibre assemblies. *Nanotechnology* 17(14): R89–R106.

Teo WE, Kotaki M, Mo XM, et al. (2005) Porous tubular structures with controlled fibre orientation using a modified electrospinning method. *Nanotechnology* 16(6): 918.

Terenghi G (1999) Peripheral nerve regeneration and neurotrophic factors. *The Journal of Anatomy* 194(1). Cambridge University Press: 1–14.

Thampi S, Muthuvijayan V and Parameswaran R (2015) Mechanical characterization of high-performance graphene oxide incorporated aligned fibroporous poly(carbonate urethane) membrane for potential biomedical applications. *Journal of Applied Polymer Science* 132.

Thampi S, Nandkumar AM, Muthuvijayan V, et al. (2017) Differential Adhesive and Bioactive Properties of the Polymeric Surface Coated with Graphene Oxide Thin Film. *ACS Applied Materials & Interfaces* 9(5). American Chemical Society: 4498–4508.

Thampi S, Thekkuveettil A, Muthuvijayan V, et al. (2020) Accelerated Outgrowth of Neurites on Graphene Oxide-Based Hybrid Electrospun Fibro-Porous Polymeric Substrates. *ACS Applied Bio Materials* 3(4). American Chemical Society: 2160–2169.

Torigoe K, Tanaka HF, Takahashi A, et al. (1996) Basic behavior of migratory Schwann cells in peripheral nerve regeneration. *Experimental Neurology* 137(2): 301–308.

Tortora GJ and Derrickson BH (2018) *Principles of Anatomy and Physiology*. John Wiley & Sons.

Wach RA, Adamus-Wlodarczyk A, Olejnik AK, et al. (2020) Carboxymethylchitosan hydrogel manufactured by radiation-induced crosslinking as potential nerve regeneration guide scaffold. *Reactive and Functional Polymers* 152: 104588.

Wahab H, Xu G, Jansing C, et al. (2015) Signatures of different carbon bonds in graphene oxide from soft x-ray reflectometry. *X-Ray Spectrometry* 44.

Wang D-Y and Huang Y-Y (2008) Fabricate coaxial stacked nerve conduits through soft lithography and molding processes. *Journal of Biomedical Materials Research. Part A* 85(2): 434–438.

Wang HB, Mullins ME, Cregg JM, et al. (2010) Varying the diameter of aligned electrospun fibers alters neurite outgrowth and Schwann cell migration. *Acta Biomaterialia* 6(8): 2970–2978.

Wang J, Zheng W, Chen L, et al. (2019) Enhancement of Schwann Cells Function Using Graphene-Oxide-Modified Nanofiber Scaffolds for Peripheral Nerve Regeneration. *ACS Biomaterials Science & Engineering* 5(5): 2444–2456.

Wang X, Zhang K, Zhu M, et al. (2008) Continuous polymer nanofiber yarns prepared by self-bundling electrospinning method. *Polymer* 49(11): 2755–2761.

Wang X, Liu X, Yuan H, et al. (2018) Non-covalently functionalized graphene strengthened poly(vinyl alcohol). *Materials & Design* 139: 372–379.

Weiss P (1945) Experiments on cell and axon orientation in vitro; the role of colloidal exudates in tissue organization. *The Journal of Experimental Zoology* 100: 353–386.

Wiatrak B, Kubis-Kubiak A, Piwowar A, et al. (2020) PC12 Cell Line: Cell Types, Coating of Culture Vessels, Differentiation and Other Culture Conditions. *Cells* 9(4): 958.

Wong S-C, Baji A and Leng S (2008) Effect of fiber diameter on tensile properties of electrospun poly(ε-caprolactone). *Polymer* 49(21): 4713–4722.

Wu Y, Xiang Y, Fang J, et al. (2019) The influence of the stiffness of GelMA substrate on the outgrowth of PC12 cells. *Bioscience Reports* 39(1): BSR20181748.

Xie J, Liu W, MacEwan MR, et al. (2014) Neurite Outgrowth on Electrospun Nanofibers with Uniaxial Alignment: The Effects of Fiber Density, Surface Coating, and Supporting Substrate. *ACS Nano* 8(2): 1878–1885.

Xue W, Shi W, Kong Y, et al. (2021) Anisotropic scaffolds for peripheral nerve and spinal cord regeneration. *Bioactive Materials* 6(11): 4141–4160.

Yang D, Lu B, Zhao Y, et al. (2007) Fabrication of Aligned Fibrous Arrays by Magnetic Electrospinning. *Advanced Materials* 19(21): 3702–3706.

Yang F, Murugan R, Ramakrishna S, et al. (2004) Fabrication of nano-structured porous PLLA scaffold intended for nerve tissue engineering. *Biomaterials* 25(10): 1891–1900.

Yang F, Murugan R, Wang S, et al. (2005) Electrospinning of nano/micro scale poly(l-lactic acid) aligned fibers and their potential in neural tissue engineering. *Biomaterials* 26(15): 2603–2610.

Yang X, Ye Y, Liu J, et al. (2023) Graphene oxide as a multi-functional additive for compatilizer, enhancer, and barrier in ethylene vinyl alcohol copolymer/aramid pulp composites. *RSC Advances* 13(7). The Royal Society of Chemistry: 4746–4753.

Yen C, Chang T and Kakinoki H (1990) Studies on the preparation and properties of conductive polymer. I. Novel method to prepare metalized plastic from metal chelate of poly(vinyl alcohol). *Journal of Applied Polymer Science* 40(1–2): 53–66.

Yi S, Xu L and Gu X (2019) Scaffolds for peripheral nerve repair and reconstruction. *Experimental neurology* 319. Elsevier: 112761.

Young TH, Lin CW, Cheng LP, et al. (2001) Preparation of EVAL membranes with smooth and particulate morphologies for neuronal culture. *Biomaterials* 22(13): 1771–1777.

Zhang D, Yao Y, Duan Y, et al. (2020) Surface-Anchored Graphene Oxide Nanosheets on Cell-Scale Micropatterned Poly(D , L -lactide- *co* -caprolactone) Conduits Promote Peripheral Nerve Regeneration. *ACS Applied Materials & Interfaces* 12(7): 7915–7930.

Zhang K, Zheng H, Liang S, et al. (2016) Aligned PLLA nanofibrous scaffolds coated with graphene oxide for promoting neural cell growth. *Acta Biomaterialia* 37: 131–142.

Zhao J, Liu H and Xu L (2016) Preparation and formation mechanism of highly aligned electrospun nanofibers using a modified parallel electrode method. *Materials & Design* 90: 1–6.

Zong X, Ran S, Fang D, et al. (2003) Control of structure, morphology and property in electrospun poly(glycolide-*co*-lactide) non-woven membranes via post-draw treatments. *Polymer* 44(17): 4959–4967.

Zou Y, Qin J, Huang Z, et al. (2016) Fabrication of Aligned Conducting PPy-PLLA Fiber Films and Their Electrically Controlled Guidance and Orientation for Neurites. *ACS Applied Materials & Interfaces* 8(20): 12576–12582.

ANNEXURES

LIST OF PUBLICATIONS

1. Sumam P and Parameswaran R (2023) Neuronal cell response on aligned fibroporous electrospun mat generated from silver ion complexed ethylene vinyl alcohol copolymer. *Journal of Biomedical Materials Research Part B: Applied Biomaterials* 111(4): 782–794.
2. Sumam Prima, P. R. Anil Kumar, Parameswaran Ramesh. Aligned fibroporous generated from silver ion and graphene oxide incorporated ethylene vinyl alcohol copolymer as a potential biomaterial for peripheral nerve repair. (Under communication).
3. Sumam P and Parameswaran R (2023) Neurite extension on graphene oxide incorporated electrospun ethylene vinyl alcohol copolymer matrices. (Under preparation).

BIODATA

Name	**:**	Prima S.
Permanent Address	**:**	Kochuveedu, Mayyanad, P.O., Kollam, 691303, Kerala, India.
Date of Birth	**:**	15/11/1991
Educational Qualifications	**:**	**2018 – 2024:** Ph.D. Scholar at Sree Chitra Tirunal Institute for Medical Sciences and Technology, Division of Polymeric Medical Devices, Biomedical Technology Wing, Thiruvananthapuram, Kerala, India. **2012 – 2014:** Master of Science in Zoology, Department of Zoology, Fatima Mata National College, Kollam, Kerala, India. **2009 –2012:** Bachelor of Science in Zoology, Department of Zoology, Sree Narayana College, Kollam, Kerala, India.